Analysis and inhibition of oncogenic RET-dependent signalling

Thesis

ANALYSIS AND INHBITION OF ONCOGENIC RET-DEPENDENT SIGNALLING

Elisa Sala

A thesis submitted to the Open University of London for the degree of Doctor in Philosophy

January 2007

Istituto Nazionale per lo Studio e la Cura dei Tumori,
Via Venezian 1, 20133 Milan, Italy

Università Milano-Bicocca
Piazza dell'Ateneo Nuovo 1, 20126, Milan, Italy

Abstract:

The aim of this PhD project is to analyse the RET-dependent signalling pathway and to block it with small molecule inhibitors, thus promoting innovative approaches to cure papillary thyroid carcinoma (PTC).

The first goal was to determine the three-dimensional structure of RET catalytic domain to obtain detailed knowledge of the target molecule. The Baculovirus expression system and purification procedure was optimised to produce high amount of recombinant protein (rRET) to perform biochemical characterization and crystallization attempts. rRET was active and properly folded, thus resulting a suitable reagent for inhibitors screening and crystallization experiments.

The crystallization screening was performed using rRET (complete kinase domain) and three other constructs, in which different deletions were introduced. No crystals were obtained after many attempts in two independent laboratories.

Concurrently, the members of 2-indolinone family, a promising class of compounds studied with molecular modelling, were screened in an ELISA-based assay to identify the best inhibitor of RET. SU5416 demonstrated an efficient inhibition of RET and was further analysed both *in vitro* and cellular systems, showing good specificity and selectivity. In animal model SU5416 blocked RET phosphorylation, indicating feasible pharmacological properties also in *in vivo* system.

Since B-RAF hyperactivation leads to transformation of thyroid cells, we also used siRNA technology to investigate whether B-RAF represented a target for selective treatment and tested a new inhibitor that showed activity in B-RAF positive melanoma cell lines, in B-RAF and RET/PTC thyroid models. The current study demonstrated that B-RAF inhibition by siRNA and small molecule inhibitor determined re-expression of thyroid specific proteins, thus indicating a restoring of the differentiation process, and block of the proliferation.

This work has proposed the rational identification of RET and B-RAF inhibitors by analysing their signalling pathway. These results raise the possibility that PTC could be treated effectively with small molecule inhibitors.

INDEX

1 INTRODUCTION

1.1 Overview about protein kinases and their role in cancer

1.1.1 The kinome

Ever since the discover nearly 50 years ago that reversible phosphorylation regulates the activity of glycogen phosphorylase, there has been intense interest in the role of protein phosphorylation in regulating protein function. The completion of the human genome sequence now allows the identification of almost all human protein kinases, representing 1.5- 2.5% of all eukaryotic genes. Most protein kinases belong to a single superfamily containing a eukaryotic protein kinase (ePK) catalytic domain.

In addition, forty atypical protein kinases have been identified. These proteins retain the catalytic activity even if they have lost the sequence similarity to the ePK domain and their close homologs.

All known 518 kinases have been classified into a hierarchy of groups, families and subfamilies primarily by sequence comparison of their catalytic domain, aided by the knowledge of sequence similarity and domain structure outside of the catalytic domain, known biological functions and similar classification of the yeast, worm and fly kinomes [1]. A scheme of this relationship is shown below.

Family comparison shows that the major kinase groups and most kinase families are shared among metazoans and many are also found in yeast, reflecting the breadth of conserved functions mediated by kinases.

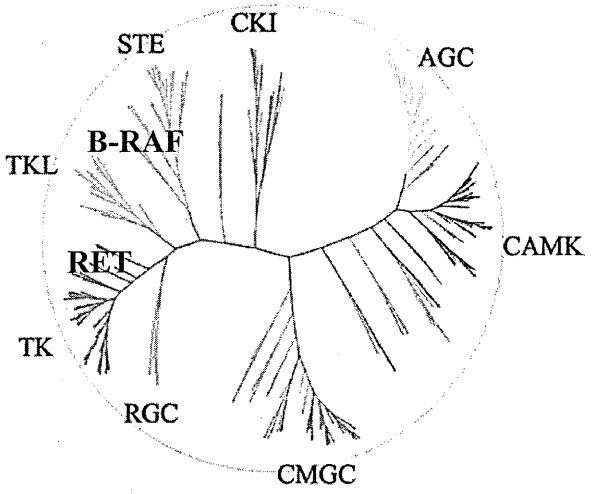

Figure 1.1.1 Kinome tree [1] RET and B-RAF belong to TK and TKL family, respectively.

Indeed, comparison of the yeast (*Saccaromyces Cerevisiae*) kinome with those of worm (*Caernorhabditis Elegans*), fruit fly (*Drosophila Melanogaster*) and human demonstrates the presence of at least 97 kinases shared with higher organisms. Conversely, only in the common ancestor of worm, fly and human there are additional 94 subfamilies, including tyrosine kinase and tyrosine kinase-like groups, that are specific for metazoans and required for the signaling functions and the sophisticated control of the development, differentiation and intercellular communication [2]. 18 families found only in fly and human and not in worm might encode more recent functions that developed after their divergence from nematode lineage. Within these coelomate- specific families there is a preponderance of kinases associated with immunity, cell cycle control, neurobiology and morphogenesis. The human genome has approximately twice as many kinases as those of fly or worm; accordingly, most kinase families have twice as many human members as they have in worm or fly, even if this expansion is not uniform [1]. The human expansion of many of these families can be traced both to large duplications of multigene loci and to local tandem duplications of smaller loci often containing just one gene. For instance, each of the four human

epidermal growth factor receptors (EGFR) maps close to one of HOX clusters in *D. Melanogaster*, implying that the proposed double duplication of that cluster early in vertebrate evolution created the EGFR family from a single ancestral EGFR gene [3].

Most protein kinases act in a network of kinases and other signaling effectors, and are modulated by autophosphorylation and phosphorylation by other kinases. Other 83 domains, in addition to the catalytic domain, have been identified in 258 of the 518 kinases. These domains regulate the biochemical activity, determine the subcellular localization of the corresponding kinase and link it to other signaling molecules. Comparison of members of the same family demonstrates that the general structure is conserved but some domain shuffling is seen to confer peculiar properties to each kinases. The most common domains mediate interactions with other signaling proteins, for instance 24 kinases contain the SH2 domain that binds to phosphotyrosine residues; other domains link to small guanosine trisphosphatase signaling, lipid signaling and calcium signaling, target the protein to the cytoskelethon or mediate interactions with other proteins or RNA [1]. The presence of these non catalytic domains is crucial in ePKs that have lost their biochemical activity: nearly 10% of all kinase domain appear to be enzimatically inactive. However, these domains are well conserved and likely to maintain the typical kinase domain fold. These have been postulated to act as kinase substrates and scaffolds for assembly of signaling complexes. The inactive kinase domains fall into three main categories: the first is represented by domains that may act as modulators of the other catalytic domains; the second group contains kinases with high similarity to the canonical ePK profile, for instance several receptor tyrosine kinase (RTK) where the inactive kinase may dimerize and act as substrate of another RTK. The third group consists of members exhibiting very weak similarities to the kinase domain profile and may have quite divergent function [1].

1.1.2 Structure of a protein kinase and mechanisms of phosphorylation reaction control

The protein kinase fold is extremely well conserved among serine/threonine and tyrosine kinases and is composed by two lobes. The smaller N-terminal lobe is characterized by a five-stranded β sheet and one prominent α helix, called helix αC. The C-terminal lobe is larger and is predominantly constituted by helices. The two lobes are joined by a polypeptide chain that functions as a hinge. ATP is bound in a cleft between the two lobes and sits beneath a high conserved loop connecting strands β1 and β2.

1.1.2.1 Regulation in serine/ threonine kinase

The three-dimensional structure of cyclic-AMP dependent protein kinase (PKA, shown in Figure 2), the first serine/threonine kinase to be solved by X-ray diffraction [4], has enabled its mechanism of reaction to be clarified.

A

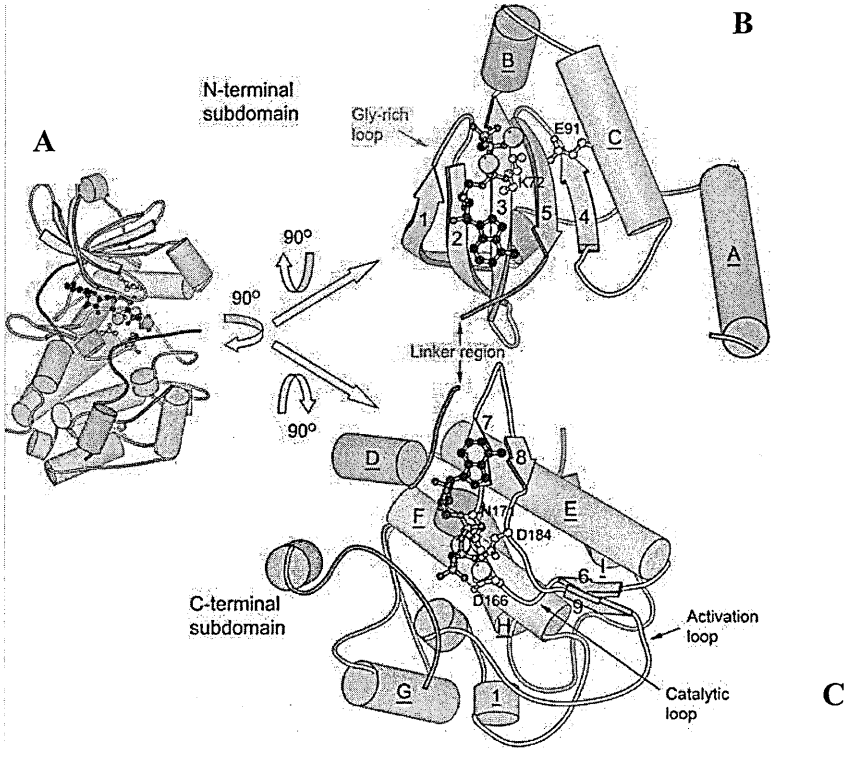

B

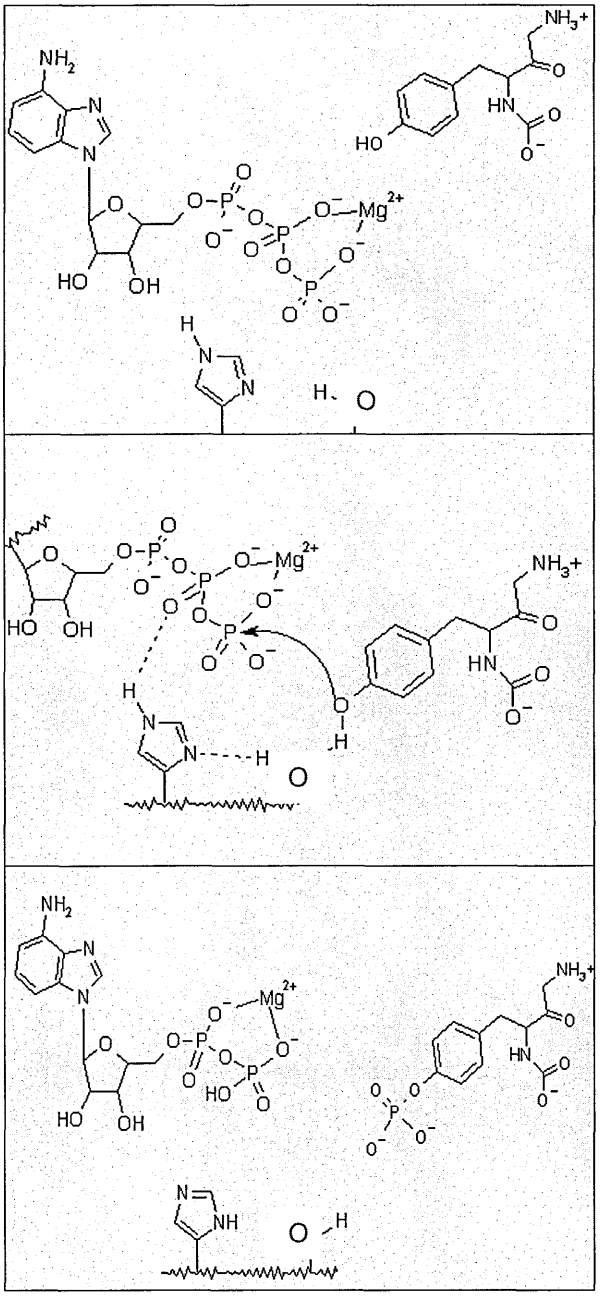

Figure 1.1.2 A: Schematic representation of catalytic subunit of protein kinase A: the most important amino acid involved in its regulation are labelled in ball and sticks. (A) shows the complete structure of PKA, (B) and (C) represent N-terminal and C-terminal. B sheet are ribbon and helices are cylinder. B: Mechanism of phosphorylation reaction, as described in the text.

The adenine of ATP is located in a hydrophobic pocket and the sugar is stabilized by hydrogen bonding; the phosphates γ are involved in the catalysis by interactions with the Lys-72, Mg^{2+} ions and the main chain nitrogen of a glycine-rich loop, a sequence

(Gly-X-Gly-X- Tyr or Phe-Gly) very flexible in absence of ATP that can easily bind small molecule inhibitors. The catalytic Asp 166, invariant in all kinases, is located in the C-terminal lobe in the catalytic loop, and acts as a base to remove a proton from the protein substrate hydroxyl group. The resulting alcoholate (in the case of serine and threonine) or phenolate (in the case of tyrosine) ion is positioned to nucleophilic attack the γ phosphate of ATP. The activation loop begins at the highly conserved DFG motif (Asp-Phe- Gly) with Asp 184. The segment continues with a region that adopts remarkably different conformations between the active and inactive kinase structures. In PKA there is a short β strand followed by a loop containing the autophosphorylation site Thr 197. The segment ends in the region that has a 3_{10} helix structure and includes residues that are important for the peptide substrate recognition. The final residue glutamate 208 is a part of APE (Asp-Pro-Glu) which is conserved in most kinases and is hydrogen bonded to the conserved arginine 280 [5].

The autophosphorylation reaction involves the threonine 197, in the activation loop, that has an important role in the kinase activation. Indeed, the phosphate is placed inside a positive charge cluster, composed by His 87 of N-terminal lobe, Arg 165, Lys 189, stabilizing it. In particular the interaction with Arg 165 promotes the correct orientation and electrostatic environment for the catalytic Asp 166. The activation loop is located in the convenient conformation to allow the peptide substrate recognition, while the interaction of P-Thr 197 with Lys 189 promotes the contact between Asp 184 and activatory Mg^{2+} ion. Finally, the contact with His 87 allows the correct domain-domain interaction, which is also critical for ATP binding. The structural studies has clarified the mechanism of control of PKA, that is very similar to those of other serine/threonine kinase proteins.

Another mechanism of control is the association of other regulatory proteins, e.g. the complex CDK2- cyclin A. CDK2 shows, in the helix corresponding to helix C of PKA, the sequence PSTAIRE, important for the recognition of cyclin A. When cyclin A binds CDK2, the activation loop changes its position and Thr 160 is exposed and available for the phosphorylation. P-Thr 160 stabilizes the positive cluster, disposed in the same line as that of PKA. The phosphorylated complex CDK2- cyclin A is totally active and can promote the activation of downstream substrates [6].

1.1.2.2 Regulation in protein tyrosine kinases

A different model has been proposed for the regulation of protein tyrosine kinases.

This family is composed by two groups of proteins: receptor tyrosine kinase (RTK) and non receptor tyrosine kinase (NRTK). The wide majority of RTKs is a single polypeptide chain, consisting of an extracellular portion, a transmembrane helix and a cytoplasmatic region that contains the catalytic domain. Otherwise, NRTKs are localized in the cytoplasm, after lacking the extracellular portion and the transmebrane-spanning region. In addition to a tyrosine kinase domain, NRTKs possess domains that mediate protein- protein, protein- lipid or protein- DNA interactions. Schematic examples are shown in Figure 1.1.3

A

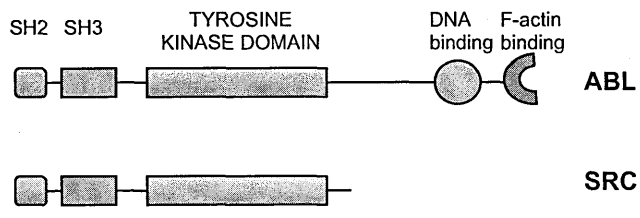

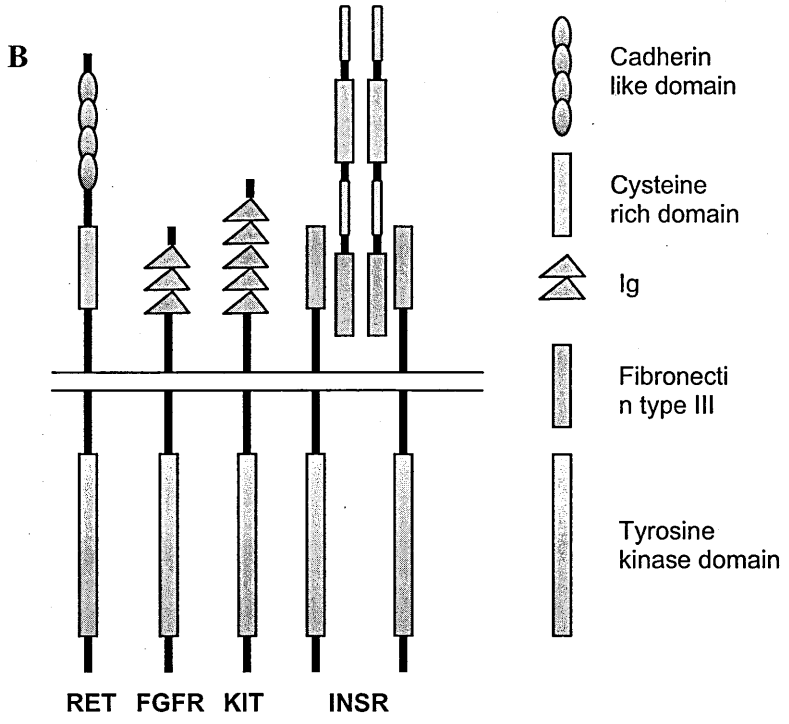

Figure 1.1.3 Examples of NRTKs (A) and RTKs: (B) the most significant domain in both intracellular and extracellular regions are represented.

The mechanism of control of NRTKs is dependent on the presence of tyrosine residues for phosphorylation. For instance, Src has two regulatory tyrosine phosphorylation sites: the first is Tyr 527 in the C-terminal lobe that repress the catalytic activity when phosphorylated by the NRTK Csk. In this case, the interactions between P-Tyr 527 and SH2 domain favors and stabilizes the contact of SH3 domain with a short polyproline type II helix, causing a misalignment of amino acids important for the kinase reaction and the consequent block of the enzymatic activity. Src is activated when the binding of high- affinity ligands disrupts these intramolecular restrains. The second tyrosine (Tyr 416) is located in the activation loop and is autophosphorylated to reach the maximal activity of the kinase [7, 8].

Receptor tyrosine kinases contain between one and three tyrosines in the activation loop that regulate the catalytic activity and the biological function of the proteins. In general,

the autophosphorylation could occur either in *cis*, eg. when the ligand-induced dimerization causes conformational changes that favor intramolecular phosphorylation or in *trans*, when a simple proximity effect provides opportunity to phosphorylate another receptor molecule. Ligand-induced oligomerization triggers the activity of RTKs. Ligand non-covalently binds the extracellular region, favors the dimerization and induces structural rearrangements that activate the autophosphorylation process. Crystal structures of the un-phosphorylated form of insulin receptor kinase (IRK) provide the molecular basis to explain how the catalytic activity is repressed before receptor activation [9]. Crucially, Tyr 1162, in the activation loop, forms hydrogen bonds with conserved aspartic acid and arginine. In addition, the conserved aspartic acid of DFG motif in the beginning of the activation loop, involved in Mg-ATP binding, is not properly positioned for the catalysis. Autophosphorylation of IRK induces a repositioning of the activation loop. This new conformation is stabilized by hydrogen bonds between P-Tyr 1163 and the conserved arginine in the beginning of the activation loop and a backbone amide nitrogen in the latter half of the loop [10]. The analysis of mode of substrate binding to tyrosine kinases has been performed co-crystallizing three-phosphorylated IRK kinase domain with 18-residues peptide containing YMXM motif present also in IRK activation loop. The backbone- backbone interactions between the peptide and the activation loop ensure that only tyrosine residues can conveniently fit into the active site, while the methionine side chains sit into two shallow hydrophobic pockets on the surface of C-terminal lobe [10]. Another model of regulation of tyrosine kinase domain has been proposed by Kuriyan et al (2007). The kinase domain of EGFR is itself responsive to the dimerization of the receptors, converting from an inactive conformation to an active one in response to an increase in the local concentration of the receptor. The fundamental on/off switch utilized by EGFR is the same used by CDK/

cyclin complexes, except that EGFR and its relatives serve as their own "cyclins". In this asymmetric dimer the C-lobe of one kinase domain is juxtaposed against the N-lobe of the other molecule with extensive interactions spanning helix C. The C-lobe takes the relative position in the dimer analogous to that of cyclin in the active CDK/Cyclin complex [11].

Additional mechanisms to control the biological activity of RTKs are the action of phosphatases that temporarily limits the activity of the receptors and the downregulation mediated by endocytosis or ubiquitin-directed proteolysis.

1.1.3 Role of protein kinases in cellular biochemistry and alteration in cancer

Protein kinases regulate several functions during cell life, e.g. cell cycle, apoptosis, migration, differentiation and in multicellular organism control embryonic development, metabolism and the function of the immune system. In particular, PKs are crucial actors in signaling pathways that enable cells to communicate with the environment. It is therefore clear that alterations in the activation of this class of proteins determine a drastic deregulation of cellular biochemistry; consequently, a wide variety of diseases are associated to misregulation of PKs.

In cancer, mutations in signaling pathway have frequently been observed: cancer cells divide inappropriately in respect to environmental context, develop robust anti-apoptotic stimuli and molecular mechanism to escape the immune response [12].

For these reasons, selectively targeting signaling elements altered only in tumour cells represents a promising alternative to cytotoxic agents normally used in therapeutic approaches. Moreover, the results of structural studies have identified the properties of

the ATP binding site in several kinases, giving the basis for a rational design of new drugs that block the enzymatic activity of PKs [13].

1.1.4 Rational drug design on protein kinases as therapeutic intervention in cancer

One approach to inhibit kinases is to find small molecules that immobilize the kinase domain in its inactive state. An example of such an inhibitor of the inactive conformation is represented by Gleveec (STI571) that inserts its pyrimidine and pyridine rings in the ATP binding site of Abl with high specificity. The rest of the molecule is wedged between C helix and the activation loop, locking the kinase in an inactive conformation [14]. Another inhibitor of Abl is PD173955; in this case the compound blocks both active and inactive conformations of Abl, thus improving the potency in anti-kinase effects [15]. Targeting the active conformation could be advantageous because conservation of the correct 3D structure is required for the enzyme functionality and, therefore, this conformation is less tolerant of mutations, which makes it less likely to develop resistance to inhibition.

The alignment of 491 kinases demonstrated that the combination of the amino acids in the ligand binding site was characteristic for each protein kinase or a limited number of PKs. This observation suggested that the selectivity could be reached by interaction between inhibitor and the set of amino acids constituting the ligand binding site.

The interaction between p38 and several chemical entities, such as pyrimidine imidazoles, quinazolines and pyridol-pyrimidines, occurs in a small hydrophobic pocket at the back of the ATP- binding site that ATP does exploit, giving high selectivity for p38 [16]. This indicates that less conserved domains can also be successfully targeted.

Sometimes the presence of a single specific amino acid guarantees the formation of hydrogen bonds that stabilize the interaction with small molecule inhibitors. For

instance, the binding of aspargine 568 to the oxindole ring of SU5402 confers selectivity for fibroblast growth factor receptor 1 (FGFR 1) [17].

Furthermore, it is possible to target the extracellular domain as in the case of HER2 and the monoclonal antibody trastuzumab (Herceptin®, Genentech, San Francisco, CA). Herceptin binds close to the juxtamembrane region of the extracellular domain of the receptor. This may allow engagement with the endocytotic machinery while avoiding receptor dimerization and kinase activation, which would explain its inhibitory effects on receptor signaling [18].

1.1.5 The problem of resistance

The major problem related to targeted therapies is the resistance that cancer cells tend to acquire after prolonged treatment, thus rendering the therapy ineffective. For instance, in patients affected by chronic myeloid leukemia, STI571 produces hematological remission if administrated in appropriate doses in nearly all cases during the chronic phase of the disease and in ≥50% during blast crisis. However, patients in remission frequently relapse and become resistant to further Imatinib treatment. Two different mechanisms of resistance have been identified: the first is Bcr-Abl gene amplification, the second is the acquisition of mutations within the catalytic domain [19]. Indeed, STI571 treatment imposes a potent selection for drug- resistant alleles.

Agents active against these new mutated targets that arise during therapy with first-generation tyrosine kinase inhibitors, are being rapidly developed. For example BMS354825, a dual Src-Abl inhibitor, is active in patients resistant to Imatinib because it binds Abl with less stringent structural requirements [20].

The second generation of kinase inhibitors confirm the potential of mutation- specific anti-cancer therapies, and it is yet to be verified if the combination of first and second

generation inhibitors will delay or avoid resistance [21]. In solid tumors it's important to consider the complexity of intercellular network and the possibility that other normal signaling pathways could compensate for the blocking of oncogenic pathways obtained by chemiotherapic approaches. Therefore, the combination of several inhibitors against different molecular targets could improve the outcome of therapies, compared to single agent treatments [21].

Future researches will focus on the identification of new small molecule inhibitors as well as on the application of known compounds to novel type of cancer.

1.1.6 Papillary thyroid carcinoma: a model for targeted therapies against protein kinases

In this scenario, a good model for specific therapy against protein kinases is represented by papillary thyroid carcinoma. Indeed, alterations in expression and activation of both tyrosine and serine/threonine protein kinases involved in mitogen-activated protein kinase (MAPK) signaling have been proposed as initiating events. These proteins could be considered as targets for small molecule inhibitors, offering a new strategy for the care of thyroid malignancies.

1.2 Papillary, poorly differentiated and anaplastic thyroid carcinomas

1.2.1 Classification

Papillary thyroid carcinoma (PTC) is the most common malignancy of the endocrine system, with an incidence of half million new cases per year. It affects females more frequently than males and while it may occur at any age, the mean age at diagnosis is 40 years. In general, PTCs have favourable prognosis: 80-90% of all patients survive at least 10 years after diagnosis.

World Health Organization classifies PTC into eleven categories, based on morphologic pattern and putative diagnostic implication (WHO: Classification of tumours. Pathology and genetics of tumours of endocrine organs 2004).

- Papillary microcarcinoma (PMC): the term microcarcinoma is usually applied to masses measuring 1 cm or less in diameter. Prognosis is excellent and distant metastases are extremely rare; indeed PMCs are considered to be clinically insignificant, when patients are >19 years old. After Chernobyl disaster an increased incidence of PMCs has been observed in young patients.
- Encapsulated variant: this lesion is totally surrounded by a capsule, characterized by the gross appearance of an adenoma and architectural and nuclear features similar to conventional papillary thyroid carcinoma. This variant represents 10% of cases of PTC and has never been associated to distant metastases, even if some nodal metastases have been observed.

- Follicular variant: this PTC has predominantly follicular pattern of growth; the diagnosis is the same of typical PTC with nodal and not distant metastases. The lesion is frequently infiltrative.
- The macrofollicular variant: this tumour exhibits secretory activity, like hyperplastic nodules.
- The solid variant: occurring prevalently in children, especially after strong exposure to ionising radiation, these tumours are typified by sheets of cancer cells with evident features of PTC.
- Diffuse sclerosing variant: this type of PTC presents dense sclerosis, extensive solid foci, squamous metaplasia and massive lymphocytic infiltration. This tumour frequently metastasises in lung, and the survival rate is lower than those of conventional PTCs.
- Oncocytic variant: it is associated with autoimmune thyroiditis and usually affects women. It's composed of oncocytic cells with classic nuclear features.
- The Warthin-like variant: this PTC resembles the salivary gland tumour and overexpresses the Retinoblastoma protein (Rb) and E2F-1 transcription factor.
- The tall cell variant: affecting older men, this tumour is associated to a poorer prognosis than other variants. Extrathyroid extension and vascular invasion are common; the papillae are well formed and covered by tall cells.
- Columnar cell variant: this variant shows the presence of nuclear stratification in association with clear cytoplasm
- Cribiform morular variant: Found in young women with sporadic or familial mutations of adenomatous poliposis coli (APC) gene, this PTC is encapsulated with a cribiform pattern. The follicles are without colloid and there are papillary

formations of tall cells. Strong protein expression and genetic aberrations of β-catenin have been observed.

Poorly differentiated thyroid carcinomas are another class of thyroid malignancies that have a survival rate intermediate between PTCs and anaplastic carcinoma. Cells have molecular features characteristic of PTC with a trabecular or solid growth pattern. E-cadherin expression is suppressed and mutations in β-catenin are reported in many studies.

Finally, undifferentiated thyroid tumours arise as anaplastic transformation of well differentiated papillary carcinoma. The mass grow quickly and bulky neck mass that invades adjacent structures, often causes hoarseness, dysphagia and dyspnoea. Microscopically, there are two main categories: squamoid pattern with occasional focal keratinisation and a mixed pattern composed by giant cells like osteoclasts and spindle cells resembling sarcoma. Fortunately, this tumour is rare; it occurs in patients older then 65 years and there is no effective treatment: death usually ensues within one year (reviewed in [22]).

1.2.2 Epidemiology

Thyroid carcinoma comprises approximately 1% of all malignancies. In Europe and United States of America about three out of 100,000 people develop a thyroid malignancy, but significant regional differences exist. Generally, thyroid cancer is more common in women that in men.

Papillary thyroid carcinoma (PTC) is the most common malignant in countries with sufficient iodine diet and comprises up to 80% of all thyroid malignancies; it prevalently occurs in the third to fifth decade of life.

Other thyroid cancers are less frequent: for instance, follicular thyroid carcinoma (FTC) represents 10-20% of all thyroid malignancies and arises in regions with insufficient iodine diet during fifth and sixth decade, while undifferentiated thyroid carcinoma (UTC) accounts for up to 10% in patients beyond the sixth decade [23].

1.2.3 Aetiology

The aetiology of the more common sporadic forms of thyroid cancer that consist of papillary thyroid carcinoma, follicular thyroid carcinoma and poorly and undifferentiated thyroid carcinoma, is not, as yet, well clarified. External radiation is the only exogenous factor that has been clearly correlated with thyroid carcinomas. After Chernobyl disaster (1986) the impact of nuclear fallout on the incidence of thyroid cancer has been demonstrated with an increased number of cases in new people observed between 1986 and 1991 [24].

Other factors under consideration for the aetiology of thyroid carcinoma are iodine excess and deficiency, but further studies are necessary to better understand their role.

1.2.4 Diagnosis

Thyroid cancers are commonly diagnosed in presence of a thyroid nodule. At this stage most patients present lymph node metastases and often distant metastases in lung, bone and brain. The first examination is a fine-needle aspiration cytology to determine the

histological type [25]. In follicular thyroid carcinoma it's possible to measure calcitonin levels to verify whether the nodule is malignant [26]; otherwise, no other tumoral markers give consistent information in diagnosis.

1.2.5 Prognosis

The overall 5 year survival rate in patients with papillary thyroid carcinoma is about 90-95%, the 10 year survival rate is about 80-95%. In follicular thyroid carcinoma survival rate is slightly lower, around 70-95%, compared to PTCs. Finally, most of patients with undifferentiated thyroid carcinoma die within one year after diagnosis [23].

Several factors influence the prognosis of thyroid cancers, such as histological type and subtype, tumour stage, age, gender, differentiation, DNA euploidy, microvessel count, CD97, E-cadherin expression, telomerase activity, capsular and vascular invasion. However, the most important parameters to determine the outcome are primary tumour size, extra thyroidal extension and distant metastases.

A variety of prognostic scoring systems is available, but unfortunately none of them is widely used and is not possible to make a comparison of different studies.

1.2.6 Treatment

Generally, surgery is the treatment of choice. At the first intervention, ultrasound should be performed, to identify the extent and localization of the primary tumour and coexisting nodules, and also to diagnose enlarged cervical lymph nodes. Distant macrometastases should, however, be ruled out, prior to extensive operation.

In papillary thyroid carcinoma, there is a controversy regarding the extent of thyroid gland resection. Total thyroidectomy is commonly recommended in Europe, while in United States partial ablation is preferred [23]. Totally thyroidectomy is advocated because PTCs are often multifocal and the rate of local recurrences is increased after less than total gland removal. During the follow up, measurement of thyroglobulin can be used as marker. By contrast, partial thyroidectomy is chosen because there is no difference in survival as compared to total gland removal, and, if necessary, ablation of thyroid remnant can be accomplished by radioiodine without morbidity.

In follicular thyroid carcinoma, total thyroidectomy is widely accepted as the treatment of choice, while in undifferentiated thyroid carcinomas this approach is desirable but often unfeasible. In this case the goal must be to prevent trachea and oesophagus obstruction by a multidisciplinary therapeutic strategy, consisting of surgery, external radiation and chemotherapy.

As a post-operative treatment in PTCs and FTCs, radioiodine is often used, mainly after total thyroidectomy. Radioiodine has effects in ablation of small thyroid remnants and pulmonal metastases, while bone metastases is less responsive. External radiation can be well indicated for the treatment of bone metastases. In undifferentiated carcinomas and in medullary thyroid carcinoma radioiodine is not useful because tumoral cells don't internalise iodine, while the use of chemotherapy is limited to paclitaxel for UTCs and octreotide for MTCs [23].

1.2.7 Medullary thyroid carcinoma

Medullary thyroid carcinoma represents 5-10% of all thyroid malignancies. It derives from the parafollicular C-cells that produce calcitonin. High levels of calcinotin

secretion serve as a reliable marker for neoplastic tissue diagnosis. Prognosis usually depends on the stage of tumour progression at the time of diagnosis, with a mean 10-year survival of approximately 75%. Familial MTC occurs as part of three different clinical phenotypes: multiple endocrine neoplasia (MEN) type 2A and type B and familial MTC-only syndrome. Activating RET mutations are the underlying cause of these diseases, these mutations mainly occur in the kinase domain, even if mutations in the cystein-rich region in the extracellular portion have been observed. Because of the tendency of MTC to progress and metastatize rapidly, prophylactic thyroidectomy is recommended.[27]

1.3 Molecular alterations of papillary thyroid carcinoma

Several oncogenes, all encoding for important effectors of the MAPK signaling pathway, have been involved in the pathogenesis of PTC. This pathway is normally involved in physiological response to growth factors, while the effects of thyroid-stimulating hormone (TSH, also known as thyrotropin) are mediated by cAMP [28].

The MAPK cascade is activated by the binding of a ligand to its receptor tyrosine kinase; autophosphorylation or trans-phosphorylation of specific residues in the intracellular portion of the receptor enables the recognition of downstream effectors, such as Shc protein that mediates the recruitment of Grb2-SOS complexes and Ras. Ras, in turn, activates components of the Raf family (A-RAF, B-RAF, C-RAF) and then, through MEK1/2 and ERK1/2, the signal reaches the nucleus and cellular response to the initial stimulus is achieved.

A scheme of the reaction is shown in figure 1.3.1

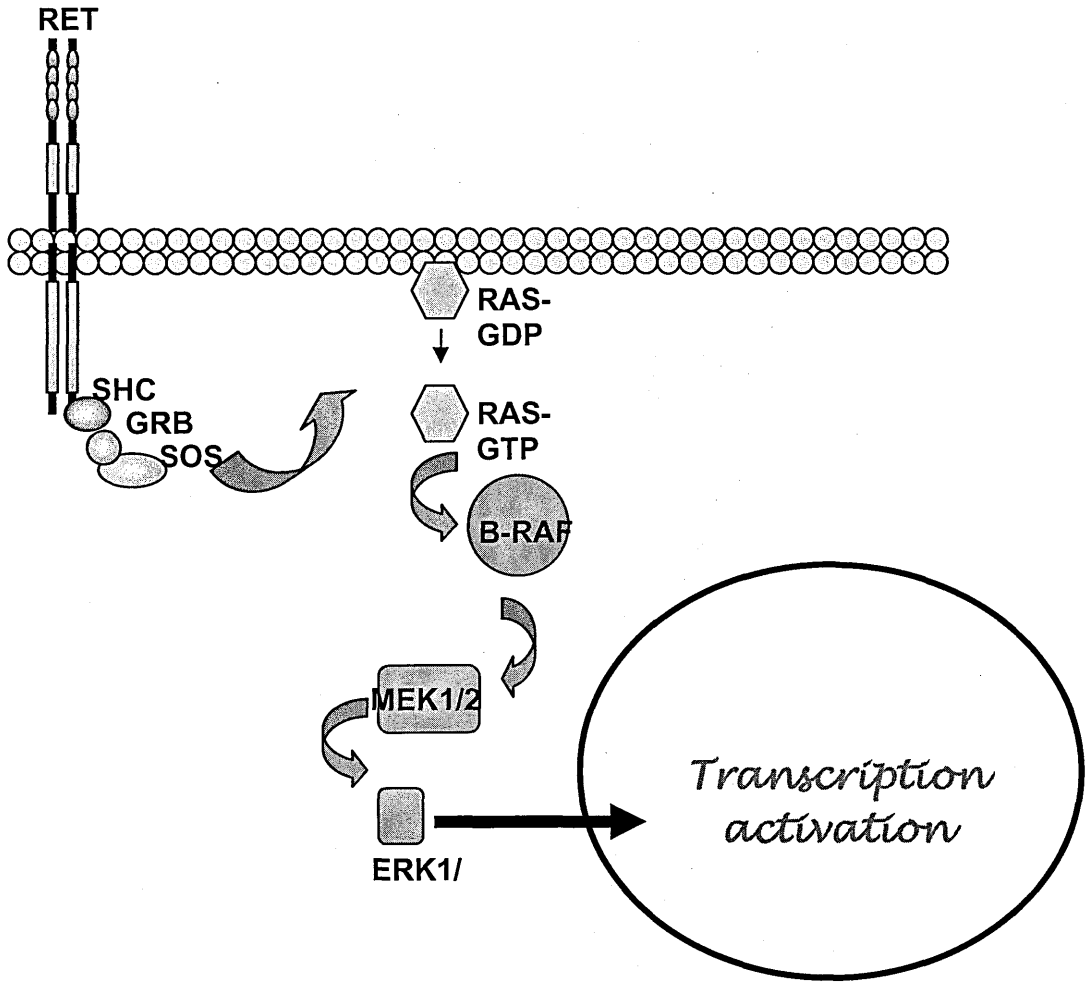

Figure 1.3.1 Schematic representation of MAPK pathway, where RET, RAS and B-RAF are often altered in papillary thyroid carcinoma. Mutations in these genes are mutually exclusive.

In PTCs, genetic alterations occurring in the effectors of the MAPK signaling pathway are mutually exclusive, thus suggesting that the proteins work in tandem along one common signaling cascade and mutations at more than one site do not provide an advantage to cells. *RET*, *NTRK1*, *RAS* and *BRAF* gene mutations are the most common events in PTC. *RET* and *NTRK1* genes encode for dysregulated RTKs that are constitutively activated in PTCs following chromosomal translocation resulting in the generation of fusion proteins. Ras protein is altered in numerous human cancers, including pancreatic, colorectal and lung cancer, and melanoma with point mutations prevalently occur at codons 12, 13 and 61. Finally, B-Raf is a serine/threonine protein

kinase in which the substitution of valine 600 with glutamate, due a single nucleotide transversion, leads to hyperactivation.

1.3.1 Aberrations in *RET* gene

1.3.1.1 Translocation

Chromosomal translocation is the most important genetic alteration, involving *RET* gene.

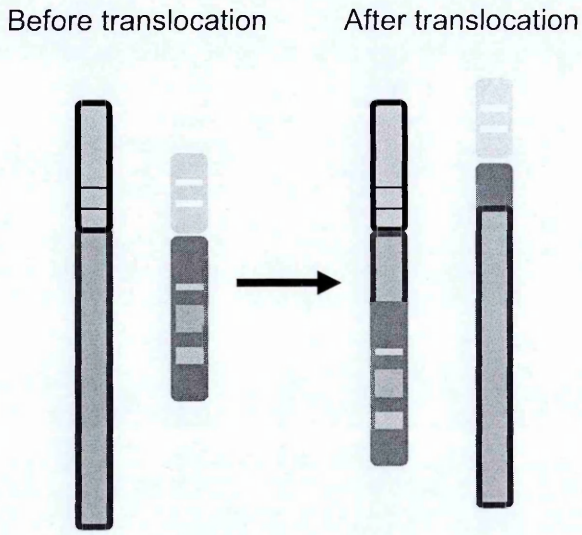

Figure 1.3.2 Schematic representation of chromosomal translocation.

Translocation (Figure 1.3.1) is a chromosomal alteration in which chromosome fragments change their position and as a consequence, genetic sequences, normally distant, are juxtaposed. If the position change involves only one chromosome, intrachromosomal translocation is achieved. Conversely, when two chromosomes are involved, an interchromosomal translocation occurs. In this case, genetic material can move from one chromosome to the other or portions of both chromosomes can invert their position. During translocation, genetic information are never lost; by contrast, as a consequence of this juxtaposition, new genes are generated and new proteins are expressed, termed fusion proteins.

In papillary thyroid carcinomas several fusion proteins encoded by *RET* gene fused with different partner genes are detected. *RET* (rearranged during transfection) gene encodes for a receptor tyrosine kinase. The extracellular portion contains four cadherin-like repeats, a calcium binding site, and a cysteine-rich domain important for the dimerization after ligand-induced stimulation, while the intracellular region contains typical tyrosine kinase domain. RET protein forms a cell-surface protein complex with glycosylphosphatidylinositol (GPI)- anchored co-receptors, designated GDNF family receptor alpha (GFRα), that recognize the glial cell-derived neurotrophic factor family members (GDNF, persephin, artemin, neurturin). When the ligand binds the complex RET- GFRα, dimerization and activation RET occurs. Some tyrosines (e.g. Y1015 or Y1062), crucial for signal transduction, are then phosphorylated with the activation of downstream signalling cascade. During embryogenesis the activation of RET by GDNF is essential for the development of the sympathetic, parasympathetic and enteric nervous system and the kidney, as well as for the differentiation of spermatogonia [29]. Expression of RET is also found in central motor, dopamine and noradrenaline neurons and its function is strictly regulated and limited in embryonic life.

In contrast, *RET* fusion partners are normally ubiquitously expressed. Thus, RET/PTC rearrangements result in the aberrant expression of RET fusion proteins in thyroid cells in childhood and adults, where deregulation of the tyrosine kinase domain can lead to the generation of tumours.

The most common rearrangements at locus 10q11.2 generate *RET/PTC1* and *RET/PTC3* oncogenes, in which the sequence encoding the kinase domain of RET is fused with the sequence for the amino terminal region of H4/D10S170 and Ele1/ARA70 (also designated as RET-fused gene, *RFG*), respectively. Recently, H4/D10S170 has been characterized as a pro-apoptotic protein that loses its regulative domains during the

fusion [30, 31], whereas EleI is a transcriptional co-activator and appears to inhibit the peroxisome proliferator-activated receptor gamma (PPARγ) steroid hormone receptor that also exerts pro-apoptotic function [32]. At present, it is unclear whether the loss of these pro-apoptotic functions executed by H4/D10S170 and EleI could contribute to tumorigenesis in thyroid cells.

Other genes have been identified as involved in the rearrangement at locus 10q11.2, such as *GOLGA5* (also known as *golgin84* or *RFG5*), generating the RET/PTC5 fusion; human transcriptional intermediary factor 1 (*HTIF1*) gene for RET/PTC6; *RFG7* gene for RET/PTC7; *RFG9* gene for RET/PTC9; the glutamic-leucine-lysine-serine-rich protein (*ELKS*) gene causes the ELKS/RET rearrangement; finally, the pericentriolar material 1 (*PCM1*) and the RET finger protein (*RFP*) genes give rise to the PCM/RET and RFP/RET fusions [33].

1.3.1.2 Mechanism of constitutive activation

The RET/PTC2 fusion contains a portion of the regulatory subunit of the PKA serine/threonine kinase (RIα). RIα exists in native form as a dimer of two subunits whose interaction could be stabilized by interchain disulfide bonds. The sequence involved in the rearrangement with *RET* gene retains the information to code for the cysteines, providing the redox environment necessary to form these disulfide bridges [34]. In accordance with the general model of the activation of tyrosine kinase membrane receptors, RET/PTC2 dimerization could explain the observed constitutive tyrosine phosphorylation of this protein. Indeed, all fusion proteins provide an interface of dimerization, essential to obtain the constitutive activation of the kinase domain of RET. For example, in RET/PTC8, the translocated amino termini of Kinectin fused to RET could be folded in coiled coils that facilitate the protein-protein interaction.

Kinectin is a cytoplasmic-oriented vescicle membrane anchored protein that interacts with the molecular motor kinesin, promoting kinesin-dependent organelle movement along the microtubules. The two leucine zipper motifs present in the Kinectin sequence are juxtaposed to the TK domain of RET and are responsible for the ligand-independent activation of the RET TK domain and for its ectopic expression [35].

Furthermore, the subcellullar localisation of the partner proteins could result in the relocation of the RET fusion proteins to the cytoplasm (rather than the cell surface) thus while preventing the interaction of RET with its usual signal transducers, would allow the phosphorylation of other substrates.

1.3.1.3 Oncogenic pathways

The mechanisms by which RET/PTC fusion proteins trigger cellular transformation are only partly known. RET/PTC oncoproteins can activate diverse signalling pathways including the PI3-K/AKT [36, 37], RAS/ERK [38, 39] and PLC-γ [40] pathways. The activation of these pathways has been shown to be important for RET/PTC induced cell transformation. For example, RET/PTC2 mutants unable to activate the PLC-γ pathway or bind to the adaptor molecule SHC, important for the activation of the PI3-K/AKT and RAS/ERK pathways, displayed drastically reduced transforming ability in NIH3T3 cells [40-42]. In the case of RET/PTC1 it has been recently demonstrated that PI-3K pathway is activated by the constitutive interaction between RET/PTC and RAI, a member of Shc family and GAB1, promoting the phosphorylation of the downstream effector Akt [37]. Finally, RET directly phosphorylates tyrosine residues of FAK, ERK1/2, DOK1, the p85 subunit of PI-3K, JNK 1 and 2, p38, and PLC-γ. These data indicate a direct interaction between RET and a broad range of effector molecules that may contribute to tumor pathogenesis [43].

The detection of RET/PTC expression by immunohistochemistry and RT-PCR in occult PTCs provides evidence that RET-PTC fusion proteins expression is an early event in papillary thyroid carcinoma genesis [44]. Two different animal models for PTC have been generated to confirm this role of RET in thyroid malignancies. In the first case, two lines of transgenic mice expressing RET/PTC1 oncogene in the thyroid gland were produced. Thyroid disease with cellular features comparable to human papillary thyroid cancers arose after one month of age in all animals. This finding indicates that RET/PTC1 is not only a biomarker associated with PTC but also the only proven specific event leading to the development of papillary thyroid carcinoma [45]. The same results have been obtained from the animals transgenic for RET/PTC3. Again, transgene expression was controlled by thyroglobulin promoter, that guarantees an organ-specific expression in murine thyroid. These transgenic mice developed thyroid hyperplasia and solid tumour variants of papillary thyroid carcinoma with metastatic spread, similar to those as observed in human cases of thyroid carcinomas in children expressing RET/PTC3. The fact that these tumours are reportedly more invasive than other papillary thyroid carcinomas suggests that RET/PTC3 fusion protein confers this increased malignant phenotype in transformed thyroid cells: the transgenic mice provide an ideal model system to study the genes that distinguish the variants of papillary thyroid carcinoma as well as the pathways controlling follicular cell differentiation [46]. In conclusion, tumour development in RET/PTC transgenic mice provides support for the theory that thyroid specific fusion proteins can initiate malignant transformation of thyroid follicular epithelium.

Inhibition of the constitutive activity of RET could be a way to block the development of thyroid cancer: the demonstration that the expression of oncogenic variants alone is sufficient to transform NIH3T3 fibroblasts indicates how RET accounts for multiple

mechanisms leading to the transformed phenotype, thus making it a potential therapeutic target [47, 48]. The presence of the same portion of RET in all fusion proteins implies that the same drug may be used against all RET/PTC oncoproteins.

1.3.1.4 Small molecule inhibitors of RET

In recent years, numerous small molecule compounds, developed as inhibitors of other kinase targets, have been identified as RET inhibitors. These compounds belong to different chemical classes: pyrazolo-pyrimidines (PP1, PP2), aniloquinazolines (ZD6474), indolocarbazoles (CEP-701, CEP-751), the 2-indolinones (RPI).

PP1 (4-amino-1-*tert*-butyl-3-(p-methylphenyl) pyrazolo[3,4-d]pyrimidine) and PP2 (4-amino-5-(4-chlorophenyl)-7-(t-butyl) pyrazolo[3,4-d]pyrimidine) have been described as selective Src family kinase inhibitors [49].

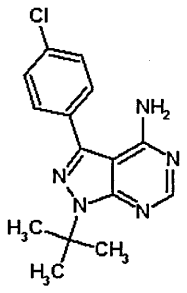

PP2

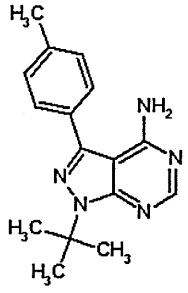

PP1

However, these compounds are also active against other kinases including RET. In *in vitro* kinase assays, PP1 and PP2 have been shown to have IC_{50} values of approximately 50 nM and 100 nM, respectively [50-52]. PP1 and PP2 inhibited cell growth of NIH3T3 cells transformed with RET/PTC3 of RET/PTC1, as well as the human PTC cell lines, TPC-1 and FB2, expressing RET/PTC1 [50, 51]. Moreover, PP1 was effective in

reducing tumour size in nude mice that had been injected with NIH3T3-RET/PTC3 cells.

Crystallographic and mutational studies have allowed an insight into the structural basis for the specificity of pyrazolo-pyrimidines. The crystal structure of PP1 bound to Hck revealed that the methylphenyl group inserts into the selectivity pocket adjacent to the ATP binding site [49]. In addition, the gatekeeper residue has been identified by mutational analysis, as a critical structural determinant controlling the binding of PP1 to kinases. Src-family kinases contain a small threonine residue at the gatekeeper position, explaining their sensitivity to PP1 [53]. The presence of a large gatekeeper residue was associated with a decreased potency of PP1, while kinases with small residues were more sensitive to PP1 inhibition. RET possesses a valine residue at the gatekeeper position (aa 804 of full length RET), which is small enough to allow pyrazolo-pyrimidine compounds to bind. Indeed, when valine 804 is substituted with a methionine or leucine, RET becomes resistant to PP1 and PP2 [54]. These RET gatekeeper mutations (V804M or V804L) have been identified in some patients affected by sporadic and familial medullary thyroid carcinoma (MTC) [54] and will certainly be relevant in deciding treatment regimes in the future, given the correlation between large gatekeeper residues and inhibitor resistance [55]. As pyrazolo-pyrimidine compounds are not specific for RET it is possible that the clinical application of these compounds may generate unwanted side-effects. However, it is also possible that selectivity profile of these compounds could be advantageous in terms of hitting multiple signal transduction pathways involved in tumour formation. For example, the inhibition of PDGFR and c-Src could prevent vascular remodelling and restenosis controlled by these kinases, respectively [56].

ZD6474 ([N-(4-bromo-2-fluorophenyl)-6-methoxy-7-[(1-methylpiperidin-4-yl)methoxy]-quinazolin-4-amine) is a selective inhibitor of the VEGFR and EGFR tyrosine kinases [57].

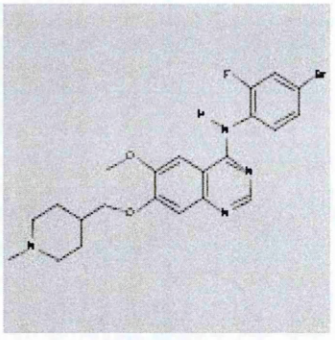

In preclinical studies, ZD6474 has been shown to inhibit VEGF-dependent tumour angiogenesis and EGFR-dependent tumour cell growth and survival in numerous solid tumour model systems [58-60]. The targeting of two key tumour-promoting pathways by a single agent has stimulated much interest in ZD6474. In phase I clinical trials, ZD6474 demonstrated low toxicity and good oral bioavailability [61]. Phase II clinical trials are ongoing to assess the efficacy of ZD6474 as a monotherapy or in combination with certain chemotherapies for the treatment of non small cell lung cancer and metastatic breast carcinoma [62, 63]. ZD6474 has also been demonstrated to inhibit RET, with an IC_{50} of 100 nM in an *in vitro* kinase assay [64]. Five micromolar ZD6474 completely arrested growth of RET/PTC transformed cells after 24h of treatment. Cell cycle analysis showed that ZD6474 caused an increase in the G_0G_1 and sub-G_1 fractions, indicating an arrest in G_1 and pro-apoptotic activity. In nude mice injected with NIH3T3-RET/PTC3 cells, the daily treatment with 1 mg of ZD6474 completely arrested tumour development [64]. In addition, ZD6474 has recently been shown to be effective at inhibiting oncogenic forms of RET in an *in vivo* Drosophila model system [65]. These data indicate that ZD6474 may be an effective treatment for RET-dependent carcinomas and clinical trials are merited. As with PP1 and PP2, mutation of the

gatekeeper residue desensitizes RET to ZD6474, presenting a possible mechanism for the development of resistance [54]. However, the activity of ZD6474 on multiple tumour-promoting pathways, may reduce this risk.

CEP-701 and CEP-751 are synthetic derivatives of the indolocarbazole K252a.

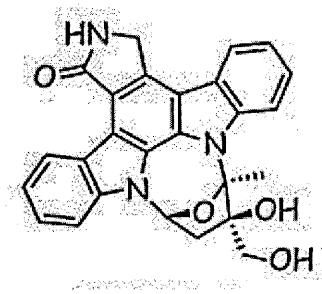

These compounds showed inhibitory activity on RET in an autophosphorylation assay with an IC_{50} of 50 nM, and in a proliferation assay obtaining complete growth cessation and significant cell loss at 100 nM [66]. Cell cycle analysis indicated that CEP-701 and CEP-751 arrested cell growth without inducing apoptosis. In nude mice bearing subcutaneous MTC cell xenografts only CEP-751 and its pro-drug CEP-2563 suppressed tumour growth, while CEP-701 was ineffective. CEP-2563 has undergone phase I clinical trials as monotherapy in patients with refractory solid tumours and showed an acceptable toxicity profile [67]. CEP-701 has also been used as a monotherapy to treat refractory AML expressing activating FLT3 mutations [68]. Recent evidence has pointed to the potential value of these compounds in combination therapy. CEP-751 augmented the anti-tumour activity of Irinotecan, a topoisomerase I poison, in a pre-clinical model of MTC [69]. It will be interesting to see if indolocarbazoles have clinical efficacy against PTC harbouring RET fusion tyrosine kinases.

The 2-indolinone derivatives were the first small molecules identified as selective RET inhibitors [70]. In particular, RPI-1 (1,3-dihydro-5,6-diemthoxy-3-[(4-

hydroxyphenyl)methylene)-2H-indol-2-one) inhibited cell proliferation and reverted the transformed phenotype in cells expressing RET/PTC1 [70, 71]. RPI-1 induced an accumulation of cells at the G_2-phase of the cell cycle that was mediated by the cyclin-dependent kinase inhibitor, p21WAF1, and related to a decrease in activation of AKT and JNK2 [72]. This cellular response was controlled by the decrease in phosphorylation of the multifunctional docking site Tyr1062, and SHC binding [41, 73]. RPI-1 has been identified as a reversible, ATP competitive kinase inhibitor by biochemical studies, which is supported by the findings of structural studies of another 2-indolinone derivative complexed with FGFR-1 [17].

1.3.2 Aberrations in NTRK gene

The second gene involved in papillary thyroid carcinogenesis is TRK gene that encodes for nerve growth factor receptor. As occurs for *RET* gene, the main genetic aberration is translocation.

Indeed, the *TRK* family of oncogenes results from a genetic fusion of the 3' end of *NTRK1* to the 5' end of different partner genes. A paracentric inversion of chromosome 1 joins the 5' end of the gene coding for tropomyosin to *NTRK1* [74]. Similarly, *TRK-T1* results from the paracentric inversion of chromosome 1 joining the 5' end of *TPR* to the 3' end of *NTRK1*. Different rearrangements involving these same two genes generate *TRK-T2* and *TRK-T4*, while *TRK-T3* results from the translocation of chromosomes 1 and 3 that fuses the genes *TFG* (TRK fused gene) and *NTRK* [75-77].

NTRK1- related translocations are found less frequently than the rearrangements that involve *RET* gene, with a reported incidence of 0-12% in patients with PTC [78]. Although the NTRK1 protein is known to function as a receptor for nerve growth factor, little is understood about its pathological role in the genesis of human papillary thyroid

carcinoma. Some evidences suggest that it may be important for cancer development in a manner analogous to RET/PTC. *In vitro*, the *TRK-T1* oncogene transforms NIH3T3 cells, even if it's unable to promote growth in soft agar or nude mice when it was transfected into rat epithelial thyroid cell line PC C13 [79]. Transgenic mice encoding the human *TRK-T1* have been generated: the oncogene was expressed under control of thyroglobulin promoter to obtain a tissue targeted expression. The development of differentiated carcinomas in these mice supports a direct role for *TRK-T1* in the thyroid tumorigenesis [80].

1.3.3 Aberrations in *RAS* gene

RAS genes code for the members of a super-family of ubiquitously expressed signal transduction intermediates that are crucial for cell growth and differentiation. Four mammalian RAS proteins (H-RAS, N-RAS, K-RASA/B) are guanine nucleotide binding proteins with intrinsic low level GTPase activity, which transduce signals generated by activation of growth factor plasma membrane receptors or G protein-coupled receptors to downstream effector pathways. Many cellular responses to RAS are transduced through ERK MAPKs pathway, resulting from sequential activation of RAF, MEK and p42-44 MAPK. Moreover, RAS can also activate the PI3K pathway, JUN N-terminal kinase (JUNK) and p38 kinase.

RAS is frequently mutated in tumours. Point mutations affecting the guanosine triphosphate GTP binding domain (codons 12/13) or GTPase domain (codon 61) determine the substitution of specific amino acid residues that lock p21RAS in the active GTP bound form by decreasing GTP hydrolysis rate or enhancing the GTP binding affinity [81]. Despite of the large number of studies on *RAS* oncogene, the mechanisms by which hyperactive RAS causes cell transformation are not well

understood yet: mutated RAS is not sufficient alone to induce transformation and secondary events, such as gene amplification, are required.

A possible explanation of its role in the cancerogenesis could be that RAS mutations may predispose cells to accumulate other genetic abnormalities. Indeed, RAS over-expression has been observed to generate genetic instability and chromosomal aberrations in several cell lines, for instance rat mammary carcinoma cells, rat prostatic tumour cells and in PCCL3 rat thyroid cells [82].

PCCL3 cells are derived from rat thyroid follicular cells and are dependent on TSH for growth; they also retain differentiated properties as they trap iodide, express thyroglobulin, thyroid peroxidase and the TSH receptor in TSH dependent manner.

Saavedra et al. [82] set up a conditional system to express $HRAS^{V12}$ under control of tetracycline to analyse RAS contribution in genetic instability. To compare RAS activity with other effectors, also MEK1, RET/PTC1, RET/PTC3 and $RAC1^{V12}$ were stably transfected in PCCL3 cells. Over-acute expression of RAS causes formation of micronuclei (small nuclear-like structures which contain chromosomes or chromosome fragments that arise during mitosis as result of chromosomal missegregation). This process was mediated by MAPK pathway activation because the induction of MEK1 expression results in an increased number of micronuclei, while $RAC1^{V12}$ which signals through SEK-JNK or SEK-p38MAPk had no effects. Acute expression of RET fusion protein did not induce micronucleation, either. Micronuclei are generally believed to form either by disruption of the mitotic spindle, leading to the loss of a whole chromosome (aneugenic event) or by induction of double strand DNA breaks with loss of a portion of the chromosome (clastogenic event). RAS induces micronuleation with both mechanisms, suggesting that the development of chromosomal abnormalities occurs within the first few cell cycles after activation. In conclusion, this study

demonstrated that RAS mutations predispose thyrocytes to large scale genomic abnormalities, promoting a transformed phenotype.

In thyroid, activating RAS mutations have been identified in benign neoplasms but are more prevalent in malignant follicular tumours and are often associated to poorly differentiated phenotype [28]. Although this point is still controversial, some experimental evidence demonstrate that RAS could play an important role in the dedifferentiation process in tumoral cells, for example, by suppressing thyroid-specific gene expression. Missero and co-workers [83] showed that the activation of RAF-MEK-ERK by RAS inhibits TTF-1 transcriptional activity, through direct TTF-1 phosphorylation by ERK observed both *in vitro* and *in vivo*, while the other well characterized signal pathways, such as PI3K, RAL GDS, Rac, Rho pathways were not effective. TTF-1 is a transcription factor that belongs to the Nkx-2 class of homeodomain-containing proteins that function as regulator of regional specification, cell fate determination and organ morphogenesis during embryonic development. In adults, TTF-1 positively controls thyroglobulin (Tg), thyroperoxidase (TPO), thyroid-stimulating hormone receptor and sodium-iodide simporter (NIS). Rat thyroid cell line FTRL5 was transfected with thyroid-specific promoters driving the expression of CAT reporter gene and with a plasmid expressing oncogenic forms of RAS. The authors [83] used V12-RAS and other mutant forms to measure the TTF-1 transcriptional activity inhibition to identify which signalling pathway is mainly involved in TTF-1 inhibition. They observed that only V12S35 RAS mutant, that signals through RAF-MEK-ERK blocks significantly TTF-1 transcriptional activity. The confirmation of these results was achieved using RAF BxB, a constitutively activated form of RAF capable of strong activation of ERK, obtaining an arrest of TTF-1, and MEK inhibitors, such as PD98059 and UO126, partially restoring TTF-1 activity. Furthermore, they identified a mutant

unable to activate ERK but able to interfere with TTF-1 activity, suggesting that also a RAF-independent pathway participates in repression of thyroid specific gene transcription.

1.3.4 Aberrations in *B-RAF* gene

RAF protein family is constituted by three proteins A-RAF, B-RAF and C-RAF that share a common architecture with three conserved regions: CR (Conserved Region) 1 and 2 at the N-terminal and CR3 in the kinase domain. RAF proteins are serine threonine kinases important in MAPK signalling because they are directly activated by RAS and phosphorylate MEK. The main differences between these three proteins are related to distribution in human tissues and to the regulation mechanism. Therefore, A-RAF is expressed in urogenital organs, while B-RAF is produced in two forms with alternative splicing in neuronal tissue and C-RAF is ubiquitously expressed.

C-RAF has six important phosphorylation sites: Ser 259 and Ser 621 are involved in 14-3-3 protein binding when RAF is phosphorylated in Ser 259 and avoids the interaction with RAS. When RAS-RAF-MAPK pathway must be activated, PP2A protein phosphatase A removes phosphate group from Ser 259, 14-3-3 protein leaves RAF that is recruited to the plasma membrane by RAS. In the N-terminal region, phosphorylation at the Ser 338 and Tyr 341 (essential for the catalytic activity, as well as phosphorylation in Ser 494 and Thr 491 in the activation segment) determines the activation of C-RAF, by disrupting the interaction between the activation segment and the glycine rich region. In B-RAF protein the most important phosphorylation site is represented by Ser 445, while the presence of aspartate 448, negatively charged, increases twelve fold the activity of B-RAF compared to that of C-RAF [84].

Crystal structures of wild type B-RAF and V600E mutant in complex with BAY43-9006 have been analysed: both forms adopt similar conformation in the presence of the inhibitor that spans the length of interfacial cleft between N and C-lobes. Numerous interactions, described as follows, stabilize the binding of BAY43-9006 to B-RAF: the distal pyridyl ring occupies the ATP binding pocket, interacting with three aromatic amino acids in hinge region, P loop and DFG motif; the lipophilic trifluoromethyl phenyl ring inserts into a hydrophobic pocket constituted by αC and αE helices. The urea group forms two hydrogen bonds with the catalytic Glu 500 and Asp 593 in the DFG motif. A similar interaction was observed in Abl in complex with STI571 [15]. More generally, all structures of B-RAF resemble that of Abl in inactive conformation, because the position of N and C lobes, αC helix and DFG motif in the two proteins are super-imposable. BAY 43-9006 contributes to block B-RAF in the inactive conformation, in which inverted DFG motif orients the adjacent segment of activation loop towards the P-loop in N-lobe, while the amino acids between Gly 595 and Val 600 constitute an array of hydrophobic interactions with the P-loop residues. While the activation segment and DFG motif remain in an unfavourable position to bind ATP, other amino acids crucial for the reaction in the catalytic sites are correctly positioned as in an active kinase. Therefore, only a change in DFG motif/ activation segment is required for the conversion to the active state [85].

B-RAF is frequently mutated in human cancers, including melanomas (30-60% of cases), colorectal cancer (5-20%) and papillary thyroid carcinoma (30-50% of cases). The most frequent alteration is a tranversion that substitutes thymidine nucleotide with adenine with the consequent change in amino acid sequence. Indeed, mutated B-RAF presents glutamate in 600 position instead of valine, causing constitutive activation.

Structural studies have determined how different mutations deregulate the activity of B-RAF. In particular, three groups of mutants have been classified. The first comprises mutants with high activity in which V600E, K601E or G469A substitutions mimic the conformational changes induced by activation segment phosphorylation. The second group is represented by mutants with intermediate activity that have a sub optimal catalytic efficiency due to the interference of mutated amino acid during the interaction between P loop and phosphate group of ATP. Finally, in the third group of mutants, amino acids conserved in the catalytic site are lost and the activity is impaired [85].

The role of B-RAF in thyroid tumorigenesis has been studied in PCCL3 rat thyroid cell lines. Mitsutake et al [86] demonstrated that conditional BRAF V600E expression, under control of doxocyclin inducible system, decreases the dependence from thyrotropin for growth and impairs the synthesis of characteristic thyroid proteins such as sodium iodine simporter (NIS), thyroglobulin (Tg) and Pax8. As previously reported for RAS oncoprotein, BRAF also causes genetic instability, inducing micronuclei and mitotic bridge formation. This is in contrast to RET/PTC1 and RET/PTC 3 which do not generate such abnormalities. A possible explanation for this difference may be the different levels of MAPK activation induced by BRAF and RET/PTC. Activated ERK plays a direct role in chromosomal segregation and mitosis, and phosphorylation and de-phosphorylation steps are needed for orderly progression. The constitutive activation of MAPK by RAS or B-RAF mutants may disrupt one step and deregulates the entire process. RET/PTC evokes less intense ERK phosphorylation because it can signal through many other effectors, therefore genetic instability is less frequent in RET/PTC positive cells.

Two novel mutational events in *B-RAF* gene have recently been identified in papillary thyroid carcinoma cells: a chromosomal rearrangement encoding for 170KDa AKAP9-

BRAF fusion protein and an insertion of three nucleotides named B-RAF599 ins. AKAP9-BRAF results from a paracentric inversion of chromosome 7 inv(7)(q21-22q34) since *BRAF* gene is located on chromosome 7q34 and *AKAP9* (A-kinase anchor protein 9) on 7q21-q22. The wild-type AKAP9 is a protein capable of binding the type II regulatory subunit (RII) of protein kinase A as well as other signalling proteins, anchoring them to the centrosome and the Golgi apparatus; its localization is prevalently perinuclear. The AKAP9/BRAF fusion protein is, however, preferentially located in cytoplasm. As a result of the chromosomal inversion, B-RAF loses the regulatory conserved regions at the N-terminal and has 6-fold higher activity than wild type protein. Also its transforming ability, evaluated by NIH3T3 focus formation assay, is increased in comparison with wild type and V600E mutant. *In vivo* the tumorigenicity is confirmed by tumour growth in nude mice two weeks after the injection.

Similar to chromosomal alterations involving the *RET* gene, AKAP9-BRAF rearrangement is associated with a recent history of radiation exposure, confirming that paracentric inversion represents a common genetic mechanism of radiation- associated thyroid carcinogenesis [87]. In a 66 year old patient affected by PTC classical variant, a heterozigous in-frame insertion (GTT) has been identified at position 1795, predicting the insertion of a valine residue in position 599. B-RAF V599 ins has been biochemically characterized with kinase assay and focus assay in NIH3T3 cells to evaluate its transforming ability. B-RAF V599 ins showed similar catalytic activity on MEK phosphorylation to B-RAF V600E and higher than that of wild-type B-RAF. In focus formation assay, a significant number of transformation foci grew in plates of NIH3T3 cells transfected with B-RAF V599 ins and B-RAF V600E. These results confirmed that B-RAF V599 ins mutation confers to the protein a gain of function that determines deregulated activity. This alteration has been reported both in PTCs and in

non thyroidal tumours. It is a rare event because it requires a nucleotide triplet insertion exactly between two codons, an event statistically far less probable than a simple base substitution [88].

1.3.5 Minor genetic alterations in PTCs

Other genetic alterations have been identified in papillary thyroid carcinoma.

MET protein is a transmembrane receptor with tyrosine kinase activity, its ligand HGF/SF is a powerful mitogen for epithelial cells. MET is frequently overexpressed in human cancers, including PTC. Increased transcription of the *MET* gene is modulated by RET and RAS in primary tumors and is frequently associated with tissue hypoxia, an event often more pronounced at the tumor periphery. The clinico-pathologic consequence of elevated MET expression is unclear at present [89, 90].

Phosphatase and tensin homolog (*PTEN*) is a tumor suppressor gene mapped at chromosome 10q22-23. PTEN is a protein phosphatase and exerts its tumor suppressor effect by antagonizing TK activity, through PI3K and the AKT/ PKB pathways. Hemizygous deletions have been found in 10-20% of adenomas and carcinomas, but rarely in PTCs [91].

1.4 Correlation between genetic alterations and clinical behaviour of the tumour

Several studies have been performed in order to relate genetic mutations in *RET*, *RAS* and *B-RAF* genes to clinical behaviour of the tumour. Results were not exhaustive but there was a general agreement of an association of the *RAS* and *B-RAF* mutations to a less differentiated phenotype and poor prognosis.

To this aim, Adeniran et al [92] analysed 97 samples of papillary thyroid carcinoma carrying *RET/PTC*, *RAS* and *B-RAF* mutations. They performed morphologic assessments scoring nine microscopic features, namely, nuclear enlargement, irregularity of nuclear contour, chromatin clearing, nuclear overlapping, nuclear grooves, nuclear pseudoinclusions, tumour fibrosis, psammona bodies and inflammatory response. The study confirmed the presence of mutations previously reported in the literature (*B-RAF* 42%, *RET/PTC* 18%, *RAS* 15%, no mutation 25%) and the absence of overlap between these mutations.

There were, however, correlations between specific mutations and clinicopathologic features. B-RAF mutations occurred in tumours of older patients who generally had stage III and IV of the disease, while RET/PTC was mainly present in younger people. RAS mutation was prevalent in females and generated tumour of larger size. Moreover, among all papillary carcinomas, the majority was represented by classic variant with RET/PTC and B-RAF mutations, while RAS-positive tumours were all follicular variant, 6% with only *B-RAF* alteration was tall variant, an aggressive form of PTC. The frequency of extra-thyroidal extensions was significantly higher in B-RAF positive tumours, RET/PTC showed lymph node metastasis. Significant differences in the occurrence of microscopic features were found between the groups of papillary thyroid carcinoma. RAS-positive tumours had low prevalence of all microscopic features, while in RET/PTC tumours they were more frequent. Tumours with B-RAF mutations showed a high level of chronic inflammation. Summarizing this work, B-RAF mutations, normally found at all levels of progression from microcarcinomas to poorly differentiated PTCs, could be associated with an aggressive phenotype and the advanced stage of disease. RET/PTC is more common in pediatric patients, often with external radiation history, and even if it is significantly associated with lymph node metastasis,

most of these neoplasms are stage I or II, indicative of a good prognosis. Finally, RAS tumors are prevalently of the follicular variant and their genotype is closer to those of follicular thyroid carcinoma. Their stage at presentation is intermediate between the more advanced B-RAF positive tumors and mostly early stages of tumors harboring RET/PTC.

Another interesting group of studies published in 2004 tried to identify the major mutational events occurring in the Chernobyl area, following the nuclear accident, to clarify the role of external radiation in thyroid tumorigenesis in both children and adults. A lower frequency of B-RAF mutations (12%) has been observed in children than in adults, and 41% of these tumors carried RET/PTC rearrangements. This could reflect the nature of the aetiological agent since ionizing radiation is particularly effective in inducing DNA double-strand breaks rather than point mutations. The presence of B-RAF positive cases could, however, represent a normal background incidence since it is usually rare in sporadic childhood carcinoma, although the major event in adult. Therefore, it is possible that the route to thyroid carcinogenesis involving a B-RAF mutation may have a longer latency period than that involving chromosomal rearrangement. Additional long-term studies are necessary to obtain more information on this aspect [93]. Another subset of young patient samples has been detected with FISH procedure [94] to verify the distribution of RET/PTC positive cells in tumours. FISH (Fluorescence *in situ* hybridization) was performed using yeast artificial chromosome (YAC) DNA probes, specific for a sequence in RET gene and a distal sequence; both probes are labelled with digoxigenin-11-dUTP and biotin-16-dUTP that gives red green signal at confocal laser scanning microscope. Cell nuclei exhibiting a rearranged *RET* gene showed a split FISH signal in red and green in addition to an

overlapping signal, whereas normal cells showed two overlapping signals. Seventy two percent of 32 post-Chernobyl cases showed RET rearrangement in some of the tumour cells. Statistical analysis confirmed a non-homogeneous distribution with subclones of tumour cells with or without any RET rearrangement. This observed genetic heterogeneity in RET/PTC alteration can be explained in two different ways: either *RET/PTC* rearrangement was the first event and new clones emerged later, or *RET/PTC* rearrangement is a late event in radiation-induced thyroid carcinogenesis. The majority of PTCS harbour clones of cells with a RET rearrangement, indicating that RET is crucial for the generation and maintenance of the tumour, perhaps through paracrine interaction with negative cells.

To further validate that RET/PTC rearrangement is the major event in childhood thyroid carcinoma, [95] demonstrated that the percentage of B-RAF positive childhood thyroid carcinoma was low both in non-Chernobyl area (Japan 3.4%) and in Ukraine (0%). These percentages are lower than those of adulthood PTC where B-RAF mutations are detected in 30-50% of cases. By contrast, RET/PTC rearrangement occurred in 35% of cases in Ukrainian population and in 3.2% in Japanese children. One case with B-RAF transversion presented typical characteristics of poorly differentiated follicular carcinoma, that could be likely considered a progression of papillary carcinoma to a more dedifferentiated status. Consistent with this result, other data reported in literature confirmed that poorly differentiated and anaplastic carcinomas with B-RAF mutation can arise from well differentiated papillary carcinoma [96].

In conclusion, RET/PTC rearrangement is the most important mutational event in childhood carcinoma and is frequently associated to radiation exposure, while B-RAF transversion is prevalently present in adult patients and often causes dedifferentiated status.

The investigation of B-Raf mutation in primary tumours and in matched lymph nodes metastases revealed that B-RAF mutation was present in all metastases but only in 62% of primary tumours. Possible explanations include PTC multicentricity or because the primary lesion that had B-RAF mutation was too small to be identified in SSCP (Single strand conformational polymorphism) at the RNA level. Interestingly, a new mutation was found in 3/8 metastases, originating from a deletion of three nucleotides with the consequent loss of Lysine (K) in position 601 while preserving the B-RAF V600E substitution and the translation frame. This new mutation may be seen as a cumulative additional secondary genetic event crucial for cells to acquire metastatic ability in some circumstances. Therefore, B-RAF mutation is frequently present in lymph nodes metastases, supporting the correlation between B-RAF 1799 T-A transversion and more advanced clinical stage and aggressive tumour behaviour [97].

As with the B-RAF transversion, RAS mutations are in general associated with histological features and clinicopathologic parameters indicative of aggressive behaviour, reflecting the strong link between RAS mutations and poorly or undifferentiated thyroid tumours, as demonstrated by Garcia-Rostan et al. [98]. In their study, RAS mutations were present in 8.2% of well differentiated carcinomas –both papillary and follicular variants- in 55.2% of poorly differentiated carcinomas and 51.7% of undifferentiated carcinoma, thus supporting a significant prevalence in less differentiated phenotypes. By contrast, no association was observed between RAS mutation and morphological features or sex and age or presence of lymph modes metastases, as reported in other papers [99].

RAS mutational status was strongly correlated with tumour related death, indicating that RAS mutation analysis may provide a tool to identify those thyroid tumours which, apart from fatal but rare undifferentiated carcinoma, could be associated with patient

death. Therefore, treatment of RAS-positive thyroid cancer with therapeutic agents that target RAS, such as farnesyl transferase inhibitors, could be of benefit to patients with poorly differentiated and undifferentiated carcinoma.

2 AIM OF THE THESIS

2.1 Analysis and inhibition of RET-dependent signalling

As previously described, a large part of mutations found in PTCs patients lead to hyperactivation of protein kinases, such as RET or B-RAF proteins. The aim of this PhD project is to analyse the RET-dependent signalling pathway and to block it with small molecule inhibitors, thus promoting innovative approaches to cure PTC. The success of STI571 (Imatinib) in chronic myeloid leukaemia and ZD1839 (Gefitinib) in non- small cell lung cancer to block aberrant tyrosine kinases, provide a paradigm to study the application of targeted treatment to thyroid cancer, that is prevalently related to a single gene alteration.

The usual way to identify new lead compounds is to test a large number of chemical entities against the target in a simple and time-saving assay to select molecules active at submicromolar concentrations, that could be further modified to improve their biochemical characteristics, such as specificity, selectivity, solubility. This random approach can be rationalized when a computational model of the protein is available to enable the analysis of simulated binding between the target protein and potential inhibitors. In this model, libraries can be virtually screened and only the best fitting molecules will be tested in biological assays. If the *in vitro* assay confirms the results obtained by molecular modelling, modifications can be introduced, firstly at the virtual level and then chemically to improve the binding to the protein. Once a promising compound(s) has been identified that inhibits kinase activity at a submicromolar range and induces cell cycle arrest or apoptosis in appropriate cellular systems, further validation can then be performed in animal models to evaluate its activity *in vivo* in more complex system.

To successfully identify an active and selective inhibitor, a good structural model and a reproducible assay is essential.

2.2 Outline of proposed project

In the absence of a three-dimensional structure of RET, other kinase domains were used as templates for a RET model calculation. RET model was produced in the laboratory led by Prof. Leonardo Scapozza at the University of Génève and was based on the structural characteristics of Abl kinase domain in the inactive conformation and IRK kinase domain in active conformation.

The first goal of this project was to determine the three-dimensional structure of RET catalytic domain and obtain detailed knowledge of the target molecule. The expression system and purification procedure was then optimised to produce high amount of recombinant protein to perform biochemical characterization and crystallization attempts.

At the same time, using virtual modelling, members of the 2-indolinone derivatives family were screened. Results were confirmed using *in vitro* assays and the biological and pharmacological properties of submicromolar amounts of inhibitor were investigated. Although several small molecule inhibitors have been reported in literature as active on RET, the advantage of studying 2-indolinone derivatives is related to wide knowledge of this chemical class and to clinical trials *in fieri* in numerous solid tumours. Since the pharmacological parameters have already been set, once it has been demonstrated that an indolinone compound represents an effective blocker of RET, then they could be rapidly administrated to RET-positive PTC patients. Since B-RAF hyperactivation leads to transformation of thyroid cells, we also used siRNA technology to investigate whether B-RAF represented a target for selective treatment and, if so, test

a new inhibitor that showed activity in B-RAF positive melanoma cell lines, in B-RAF and RET/PTC thyroid models. Blocking RAF activity may be a logical site to interfere with the effects also of RET/PTC and RAS oncoproteins in thyroid cells.

3 RESULT

3.1 Expression, purification and characterization of RET catalytic domain

3.1.1 Introduction

In the first part of my PhD project, I expressed the catalytic domain of RET in Baculovirus, then purified and characterized it using conventional biochemical techniques. The goal was the production of a suitable reagent with which to start crystallization analyses and use in inhibitor screening. The biochemical characterization of rRET is essential to verify its enzymatic properties and physical state.

3.1.1.1 Baculovirus expression system

The Baculovirus expression system provides a versatile and reliable system for the production of recombinant proteins in insect cells. Although many different viruses belong to the Baculovirus family, the most widely used is Autographa Californica multiple capsid nucleopolyhedrovirus (AcMNPV) which can be propagated in Spodoptera Frugiperda (Sf), Trichoplusia Ni (Tn) insect cell lines.

Virus genes are expressed in early, late and very late phases of infection: the early and late genes are largely related to the production of viral particles which then bud from the infected cell thus spreading infection to other cells. The very late genes that encode for polyhedrin and p10 are required for the production of the occlusion bodies containing the virus particle in the nucleus of the host cell. Both of these genes are under the

control of strong promoter, but can be deleted from the virus genome without interfering with the production of infectious virus particles. As consequence, foreign genes can substitute the *polyhedrin* and *p10* sequences to derive expression vector [100].

Several strategies have been followed to make recombinant Baculovirus. The first one used linearized viral DNA and removed the *LacZ* gene reporter and part of viral genome using restriction enzymes and the resulting recombinant viral particles were non infectious and could be recognized by plaque assay. The major difficulty, however, was to distinguish recombinant plaques from wild type [101]. The second attempt involved the direct ligation of foreign genes in a multiple cloning site *ad hoc* inserted in viral genome. In this case, high insertion efficiency was observed although specific infectivity of the virus was low [102]. Finally, an *in vivo* transposition method was developed in which a foreign gene was moved from a donor plasmid to a cloned Baculovirus DNA, such that the foreign gene was controlled by the *polyhedrin* promoter. Since E. Coli clones containing the recombinant Bacmid DNA acquired antibiotic resistance and lost a LacZ marker, they could be quickly selected and distinguished. Viral DNA was isolated from positive bacterial clones and used to transfect insect cells and produce recombinant virus. This method did not require any plaque assay for the selection of recombinant virus; however, the virus stock may be, nevertheless, polyclonal [103, 104].

The Bac' N Blue system was used in the current study. In this system the transposition of the gene of interest from a donor plasmid to viral DNA occurs *in vitro*, and a plaque assay is necessary after the transfection in order to recognize recombinant viruses.

The advances in Baculovirus studies have permitted the development of this system to produce virion displays, (similar to bacterial phage displays), which can be screened

against a complex library of molecules. Foreign proteins were inserted into the Baculovirus envelope fusion protein (GP67) at a site between the signal peptide and the mature protein and displayed on the virus particle surface [105].

An important limitation of Baculovirus-Sf9 expression system using insect cells is, however, their inability to produce the complex biantennary N-linked oligosaccaride sidechain(s) containing penultimate galactose and terminal sialic acid residues frequently present in cell surface proteins, and more, generally in mammalian proteins. A transgenic lepidopteran insect cell line was, therefore, set up to overcome the glycosylation problem: these cell lines were stably transfected with foreign gene encoding N-glycan processing activity. Baculovirus infection led to the production of protein of interest with terminally β-galactosylated n-glycans [106]. The Baculovirus genome could also be modified to express protein in mammalian cells. The addition of the *Cytomegalovirus immediate early enhancer and promoter* (pCMV) and *p10 promoter* replaced the *polyhedrin* promoter, making possible the simultaneous expression of the protein in insect and mammalian cells [107].

The second problem related to the Baculovirus- Sf9 expression system is that the yield of recombinant protein is often low. Cotransfection with Baculovirus expressing chaperon proteins (assist in the folding and modification of newly synthesized proteins) increased the yield [106]. An alternative approach was the introduction of various DNA elements to the virus: for example, the addition of *Baculovirus homology region 1 (hr1)* and *hr3* sequence regions to the viral genome increased luciferase production [108]. The cell lysis observed three to five days after infection of Sf9 cells by Baculovirus may be due to the promotion of increased proteolytic activity and other environmental factors that can determine degradation of any recombinant protein with its consequent low yield. In help circumvent this, a Baculovirus with reduced lysis capability was isolated

by random mutagenesis. This mutant produced a high level of well folded luciferase but with less degradation as compared to the parental virus [109]. In all cases, the Baculovirus expression system has the major advantages the possibility of the production of several types of proteins and the relative ease with which they can be produced on a large-scale production for further studies. Recently, cells from insect larvae were used as a host for protein production, especially in Asian countries such as China, Japan and India. Protein expression levels in Baculovirus infected larvae can be very high, reducing costs for large-scale production.

3.1.2 Materials and methods

3.1.2.1 Cells and media

Sf-9 cells were purchased from Invitrogen and cultured at 27°C in SF-900 II medium supplemented with 5% Fetal Bovine Serum, 100 µg/ml gentamycin, 100 U/ml penicillin, 2 mM glutamine and 0.1% Pluronic-F68. Cells were maintained in adherent culture and passaged at confluence. After approximately 25 passages a new batch of cells was thawed. For infections, the culture was adapted to suspension growth in spinner-flasks (Bellco) and kept at a cell density below $2x10^6$ cells/ml.

3.1.2.2 Buffers, antibodies and inhibitors

All solutions were freshly prepared and filtered. For anionic exchange chromatography: Buffer A contained 50 mM Tris-HCl, pH 6.5, 20 mM NaCl and protease inhibitors (PI) while Buffer B consisted of 50 mM Tris-HCl, pH 6.5 and 2 M NaCl, plus PI. For affinity chromatography Buffer C contained 50 mM Tris-HCl, pH 8, 250 mM NaCl, 20 mM β-mercaptoethanol, 30 mM imidazole, 10% glycerol and PI was used. The antibodies used were: anti-HisG (Invitrogen), anti-phosphotyrosine clone 4G10 (Upstate) and anti-phospho-RET^{Y905} (Cell Signaling), that recognizes phosphorylated tyrosine 905 in the RET activation loop. Protease inhibitors Leupeptin, Aprotinin and Pepstatin A were purchased from Sigma-Aldrich and used at 1 µg/ml final concentration. PP1 and PP2, RET small molecule inhibitor, were purchased from Calbiochem.

3.1.2.3 Generation of recombinant virus

A hybrid Baculovirus transfer vector ($pHis^E$) was obtained by importing an EcoRV-KpnI fragment of pBlueBacHis2 (Invitrogen), containing the 6-Histidine tag, into the pBlueBac4.5 plasmid (Invitrogen) that has the SV40 polyA signal for mRNA stabilization. RET kinase domain cDNA (nucleotide 2293-3255 of transcript variant 1; GeneBank accession no. **NM_000323**) was PCR-amplified with specific primers, RET-F (GGTACCTATGGAGAACCAGGTCTCC) and RET-R (TACTTGGACCTTGCGGCGGTCTAGA) and cloned into the $pHis^E$ vector in KpnI/XbaI sites. Sequencing of the cloned insert confirmed that no mutations were introduced. Mutant V804M RET was obtained from wild-type RET plasmid by site-directed mutagenesis using the QuikChange kit (Stratagene), according to manufacturer's instructions, with the following mutagenic primers: sense, GGCCCGCTCCTCCTCATCATGGAGTACGCCAAATACGGC, and antisense, GCCGTATTTGGCGTACTCCATGATGAGGAGGAGCGGGCC (the nucleotide corresponding to the missense mutation is underlined). Homologous recombination of the plasmid with Bac-N-Blue viral DNA (Invitrogen) generated β-galactosidase-expressing, recombinant Baculovirus particles. Selection and verification of recombinant viral clones was performed according to manufacturer's manual. A single RET-positive recombinant clone was expanded and used for RET expression. Viral titer was calculated for each batch of virus by plaque assay. Briefly, Sf9 cells were seeded in 10-cm cell culture dishes at $6x10^6$/dish and infected with 1 ml virus dilutions, ranging from 10^{-4} to 10^{-10}. Infected cells were then overlayed with 1.25% sterile agarose containing 75 μg/ml X-Gal. After approximately 10 days at 27°C, blue plaques appeared, representing single recombinant particles. The titer (pfu/ml) was calculated as follows:

number of plaques/virus dilution.

3.1.2.4 Infection and extraction of Sf9 cells

Log-phase growing Sf9 cells ($2x10^6$ cells/ml) were infected at a multiplicity of infection (MOI) = 5 and incubated for 72 hours in a spinner-flask, after which the cells were collected by centrifugation, and the cell pellet washed with cold PBS and kept at –80°C until needed. In a typical experiment, cell pellet corresponding to $2x10^9$ cells was thawed on ice and resuspended in clarification buffer, 50mM TrisHCl pH 6.5, 20mM NaCl, protease inhibitors (10^9 cells in 50ml of clarification buffer). After 60 minutes, the suspension was sonicated twice on ice and the cell lysate was cleared by ultracentrifugation at 15,000 g for 20 minutes and the supernatant loaded on the column.

3.1.2.5 Chromatography

All chromatographic steps were controlled by the ÄKTA-FPLC system (Amersham) and carried out at 4°C. Total cell lysate was loaded on a 120-ml anion-exchange column (DEAE-sepharose Fast Flow resin, packed in a XK-26 column [Amersham]). The capture buffer was 50mM TrisHCl pH 6.5, 20mM NaCl, the elution buffer was 50mM TrisHCl pH 6.5, 2M NaCl; in order to obtain a greater resolution we chose a linear gradient 0-20% elution buffer in 4CV. Then, the positive fractions were loaded on a Pro-Bond (Invitrogen) nickel ion affinity resin (15 ml). In this case the capture buffer is 50mM TrisHCl pH 8, 250mM NaCl, 20mM β-mercaptoethanol, 30mM imidazole, glycerol 10%, while the elution buffer is 50mM TrisHCl pH 8, 250mM NaCl, 20mM β-mercaptoethanol, 200mM imidazole, glycerol 10%; the gradient consists of two steps 0-

10% of elution buffer in 3CV and 10-15% in 2CV and a linear fragment 15-100% in 8CV.

3.1.2.6 SDS-PAGE

Samples from the various purification steps were resolved on 10% SDS-polyacrylamide gels. Proteins were either stained with Coomassie brilliant blue or silver nitrate, or transferred to a nitrocellulose membrane and analyzed by western blotting with anti-HisG or anti-phosphoRET antibody. For silver staining, the gel was fixed 5 minutes in 7% acetic acid and 40 minutes in 50% methanol, washed with water, incubated 15 minutes in staining solution (0.2 g $AgNO_3$ dissolved in 80 mM NH_4OH and 0.18 N NaOH), washed again and finally submerged in developing solution (0.005% citric acid and 0.02% formaldehyde) for 2-15 minutes or until the bands were visible.

3.1.2.7 Analytical gel filtration

Positive fractions from affinity chromatography were concentrated using Vivaspin devices (Vivascience) at 2000 g. The concentrated sample was loaded on a Sephacryl-S200 HR Column (Amersham) and separated at 0.1 ml/min in Buffer E containing 50 mM Tris-HCl, pH 8, 1 M NaCl, 10 mM β-mercaptoethanol. Eluted fractions were analyzed in western blot with anti-histidine antibody.

3.1.2.8 Circular dichroism

Three hundred microgram of rRET was used in circular dichroism analysis. rRET was concentrated in 100ul of 50mM TrisHCl pH 8, 250mM NaCl, 10mM β-mercapto-ethanol.

3.1.2.9 Light scattering

The light scattering test was performed with Dyna Pro-99-e50, using rRET in the following conditions: 5 mg/ml in 30mM TrisHCl pH 7.5, 150mM NaCl, 5mM DTT.

3.1.2.10 Peptide synthesis

The peptides ARDIYRASYYRKGGCAMLPVK, SRDVYEEDSYVKRSQGRIPVK and MARTTSQLYDAVPIQSSVVL were prepared following the solid-phase Fmoc amino acid chemistry [110] on a HMP (p-Hydroxymethyl phenoxymethyl polystyrene) resin (1.10 mmol/g) (Applied Biosystems, (Foster City, CA, USA). The chain assembly was performed automatically using a 431 A (Applied Biosystems) peptide synthesizer and Fmoc-protected amino acids activated with a mixture of 2-(1-benzotriazol-1-yl)-1,1,3,3–tetramethyluronium hexafluorophosphate (HBTU), N-Hydroxybenzotriazole (HOBt) and N-ethyldiisopropylamine (DIEA). Peptide resin cleavage and deprotection was achieved following the procedure of King et al. [111]. The crude peptides (50-100 mg in 10 ml water) were purified using a preparative Reverse Phase HPLC-column (prepNova-Pak HR C18, 6 μm, 25x10 mm, Waters, Milford, MA, USA) at 12 ml/min. The purity of peptides was > 95% by analytical Reverse Phase-HPLC on a 5 μm, C18 Symmetry300 column, 4.6x250 mm (Waters).

3.1.2.11 Radioactive kinase assay

Substrate phosphorylation was performed in 50 mM TrisHCl, pH 7.5, 1 mM $MnCl_2$, 5 mM $MgCl_2$, 30 μM [γ^{33}P]ATP (specific activity 1000 dpm/pmol) purified RET (60 ng) and either poly(Glu_4Tyr) (0.1 mg/ml), enolase (2 μg) or peptides as substrates, in a total volume of 30 μl. The reactions were terminated at the indicated times as previously described [112]. In the case of peptide phosphorylation, 25 μl of the incubation mixture were spotted onto P81 phosphocellulose paper, which was then processed as described elsewhere [113]. For enolase phosphorylation and rRET autophosphorylation, the samples were subjected to SDS/PAGE and incorporated ^{33}P was analyzed by a Packard InstantImager. Kinetic constants were determined by GraphPad Prism software fitting the data directly to Michaelis-Menten equation using non-linear regression

3.1.2.12 Non-radioactive kinase assay

Purified RET -rRET- (100 ng) was incubated with or without ATP (30 μM) in kinase buffer (25 mM Hepes, pH 7, 1 mM $MnCl_2$, 5 mM $MgCl_2$) for 15 minutes at 30°C. The autophosphorylation reaction was stopped with Laemli buffer and the sample was run on SDS-PAGE and developed with anti-phospho-RET and anti-HisG antibodies.

The ELISA kinase assay was performed as described by Gunby et al [114] with some modifications. Briefly, 96-well microtiter plates were coated overnight with peptide substrate and washed. The reaction mixture was prepared in 100 μl with 40 ng of pure RET and 300 μM ATP in kinase buffer and added to the coated wells. After 15 minutes incubation at 30°C the plate was washed 3 times with wash buffer (0.05% Tween in PBS) and incubated with anti-phosphotyrosine antibody and HRP-conjugated anti-mouse secondary antibody. Color was developed by addition of TMB substrate and stopped with 0.18 M H_2SO_4. Absorbance was read at 450 nm with Victor microplate

reader (PerkinELmer). Plastic absorbance was read at 570 nm and subtracted. Background signal was determined by including a no-ATP control and subtracted. All experiments were done in triplicate and repeated at least three times. The K_M for ATP was calculated using GraphPad Prism software as the concentration required to reach half-maximal activity. Inhibitors were pre-incubated at room temperature with the enzyme for 10 minutes before the reaction was started by the addition of ATP. Data were always normalized against a vehicle control and analyzed by GraphPad software.

3.1.3 Results

3.1.3.1 Expression and purification

The catalytic domain of RET was produced using the Baculovirus expression system. The construct represented the wild type sequence encoding the kinase domain and contained the active site, the ATP-binding pocket, the activation loop with regulatory functions and an amino-terminal His-tag to enable the purification. The amino acid sequence of the recombinant protein is shown below:

MPRGS***HHHHHH***GMASMTGGQQMGRDLYDDDDKDRWIRPRDLQLVPMENQVSVDA
FKILEDPKWEFPRKNLVLGKTLGEGEFGKVVKATAFHLKGRAGYTTVAVKMLKENAS
PSELRDLLSEFNVLKQVNHPHVIKLYGACSQDGPLLLIVEYAKYGSLRGFLRESRKVGP
GYLGSGGSRNSSSLDHPDERALTMGDLISFAWQISQGMQYLAEMKLVHRDLAARNILV
AEGRKMKISDFGLSRDVYEEDSYVKRSQGRIPVKWMAIESLFDHIYTTQSDVWSFGVL
LWEIVTLGGNPYPGIPPERLFNLLKTGHRMERPDNCSEEMYRLMLQCWKQEPDKRPVF
ADISKDLEKMMVKRRDYLDLAAV

The His tag (labeled in bold in the sequence) is composed of six amino acids that can coordinate nickel ions during affinity chromatography. An Enterokinase cleavage site (DDDDKD) is present in the vector plasmid to permit the removal of this tag after purification. The RET sequence (underlined) starts at MEN and finishes at the LAA sequence; the remaining amino acids belong to the expression vector.

The resultant protein will have a predicted molecular weight of 41.9 kDa and a theoretical isoelectric point of 8. It contains several cysteine residues that may cause

aggregation. The analysis of its primary structure reveals the following amino acid composition (Table 3.1)

AMINO ACID		%
Alanine	A	5,2
Arginine	R	7,1
Aspargine	N	2,7
Aspartic acid	D	7,1
Cysteine	C	0,8
Glutamic acid	E	6,3
Glutamine	Q	3,5
Glycine	G	8,2
Histidine	H	3,5
Iso-leucine	I	3,8
Leucine	L	10,9
Lysine	K	6,8
Methionine	M	4,4
Phenilalanine	F	3,3
Proline	P	4,9
Serine	S	6,8
Threonin	T	2,7
Tryptophane	W	1,9
Tyrosine	Y	3,5
Valine	V	6,5

Table 3.1 Amino acid composition of rRET

```
P11362|FGFR1_HUMAN      AKSIPLRRQVTVSADSSASMNSG-VLLVRPS-RLSSSG-TPMLAGVSEYELPEDPRWELP 474
P21802|FGFR2_HUMAN      TKRIPLRRQVTVSAESSSSMNSN-TPLVRITTRLSSTADTPMLAGVSEYELPEDPKWEFP 477
P07949|RET_HUMAN        HKFAHKPPISSAEMTFRRPAQAFPVSYSSSGARRPSLDSMENQVSVDAFKILEDPKWEFP 720
                         *        :..     . ::  .       * .*       ..*. ::: ***:**:*
                                  gly rich loop
                              β1              β2              β3                  αC
P11362|FGFR1_HUMAN      RDRLVLGKPLGEGCFGQVVLAEAIGLDKDKPNRVTKVAVKMLKSDATEKDLSDLISEMEM 534
P21802|FGFR2_HUMAN      RDKLTLGKPLGEGCFGQVVMAEAVGIDKDKPKEAVTVAVKMLKDDATEKDLSDLVSEMEM 537
P07949|RET_HUMAN        RKNLVLGKTLGEGEFGKVVKATAFHLKG--RAGYTTVAVKMLKENASPSELRDLLSEFNV 778
                        *..*.***.**** **:** * *. :.       ..*******.:*: .:* **:**:::

                                                                      kinase insert
                                  β4          β5          αD
P11362|FGFR1_HUMAN      MKMIGKHKNIINLLGACTQDGPLYVIVEYASKGNLREYLQARRPP--------GLEYCYN 586
P21802|FGFR2_HUMAN      MKMIGKHKNIINLLGACTQDGPLYVIVEYASKGNLREYLRARRPP--------GMEYSYD 589
P07949|RET_HUMAN        LKQVN-HPHVIKLYGACSQDGPLLLIVEYAKYGSLRGFLRESRKVGPGYLGSGGSRNSSS 837
                        :* :. * ::*:* ***:***** :*****. *.** :*:  *          * . . .

                                                        catalytic loop
                                      αE                              β7      β8
P11362|FGFR1_HUMAN      PSHNPEEQLSSKDLVSCAYQVARGMEYLASKKCIHRDLAARNVLVTEDNVMKIADFGLAR 646
P21802|FGFR2_HUMAN      INRVPEEQMTFKDLVSCTYQLARGMEYLASQKCIHRDLAARNVLVTENNVMKIADFGLAR 649
P07949|RET_HUMAN        LDHPDERALTMGDLISFAWQISQGMQYLAEMKLVHRDLAARNILVAEGRKMKISDFGLSR 897
                         .:  *. ::  **:* ::*:::**:***. * :********:**:*.. ***:****:*

                        activation loop  P+1 loop
```

```
                                        αEF                 αF
P11362|FGFR1_HUMAN      DIHHIDYYKKTTNGRLPVKWMAPEALFDRIYTHQSDVWSFGVLLWEIFTLGGSPYPGVPV 706
P21802|FGFR2_HUMAN      DINNIDYYKKTTNGRLPVKWMAPEALFDRVYTHQSDVWSFGVLMWEIFTLGGSPYPGIPV 709
P07949|RET_HUMAN        DVYEEDSYVKRSQGRIPVKWMAIESLFDHIYTTQSDVWSFGVLLWEIVTLGGNPYPGIPP 957
                        *: . * * * ::**:****** *:***::** **********:***.****.****:*

                          αG                  αH                 αI
P11362|FGFR1_HUMAN      EELFKLLKEGHRMDKPSNCTNELYMMMRDCWHAVPSQRPTFKQLVEDLDRIVALTSNQEY 766
P21802|FGFR2_HUMAN      EELFKLLKEGHRMDKPANCTNELYMMMRDCWHAVPSQRPTFKQLVEDLDRILTLTTNEEY 769
P07949|RET_HUMAN        ERLFNLLKTGHRMERPDNCSEEMYRLMLQCWKQEPDKRPVFADISKDLEKMMVKRRDYLD
1017
                        *.**:*** ****::* **::*:* :* :***:  *.:**.* :: :**::::.   :

P11362|FGFR1_HUMAN      LDLSMP-----------------LDQYSPSFPDTRSSTCSSGEDSVFSHEPLPEEPCLPR 809
P21802|FGFR2_HUMAN      LDLSQP-----------------LEQYSPSYPDTRSS-CSSGDDSVFSPDPMPYEPCLPQ 811
P07949|RET_HUMAN        LAASTPSDSLIYDDGLSEEETPLVDCNNAPLPRALPSTWIENKLYGMSDPNWPGESPVPL
1077
                        *  * *                  ::  ... * : .*   ...   :*    * *. :*
```

Figure 3.1.1 Similarity search demonstrated high identity with FGFR1 and FGFR2. The asterisks indicate the identity (the same amino acid presents in the position), while the dots indicate the positivity. α-helics and β-sheet are labelled in green and yellow, respectively. The catalytic loop sequence is red, while the activation loop is blue. The kinase insert is underlined. In FGFR1 sequence, the amino acids M451 and E764 labelled in pink represent the start and the end of the construct crystallized by Mohammadi and co-workers [17]; in RET sequence the start and the end of our construct are brown, M699 and A1020, respectively.

A similarity search performed by BLAST program (Expasy) revealed 52% of identity and 68% of positivity with fibroblast growth factor receptor 1 (FGFR1), and 51% identity and 68% of positivity with fibroblast growth factor receptor 2 (FGFR2) in the kinase domain. The alignment above (Figure 3.1.1) shows the exact position of each amino acid of all three proteins. It should be noted that RET presents a kinase insert sequence 8 amino acids longer than FGFR1 and this could represent a problem for crystallization because of the augmented mobility of the region.

Some biochemical properties of the protein product were defined before the purification was commenced. The optimum buffer to purify our protein (TrisHCl, $NaHPO_3$), was identified. A buffer of 50mM TrisHCl pH 6.5 was chosen for binding of rRET in anionic exchange chromatography using DEAE-Sepharose Fast flow resin while 50mM TrisHCl pH 8 was used for Pro-bond nickel ion affinity resin in the affinity

chromatography. β-mercapto-ethanol was added to the buffers for affinity chromatography to prevent the formation of disulfide bridges between cysteine residues. The stability of rRET, with or without freezing it and in different conditions was determined: the rRET protein was stable for one week after defrosting at 4°C in the chosen buffer. Protease inhibitors (Leupeptin, Apoprotin, Pepstatin A) were added to all buffers to prevent degradation.

An example of purification process optimized to produce rRET was described below.

Sf9 cells with infected with a high titer suspension of recombinant Baculovirus ($5x10^8$ pfu/ml) at the ratio of 1 million cells infected with 20 µl of virus (corresponding to a multiplicity of infection of 10). After 72h of infection, the cells were harvested and lysed on ice for one hour, clarified and then sonicated. with a clarification buffer. Suspension was centrifuged at 15000g for 20 minutes and the resulting supernatant added to a 16XK-DEAE sepharose Fast flow column to perform the first step of purification. Western blotting with anti-His allowed the positive fractions to be identified and the positive fraction was collected at the time point shown below in Figure 3.1.2.

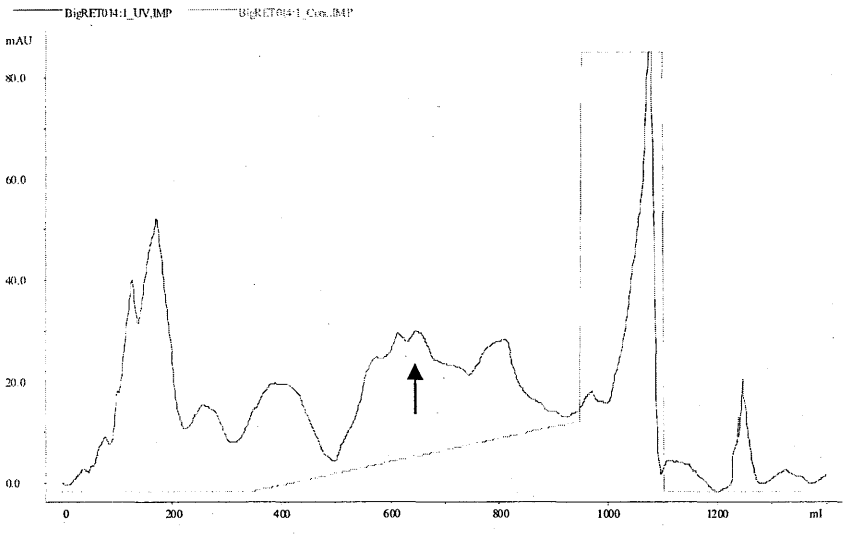

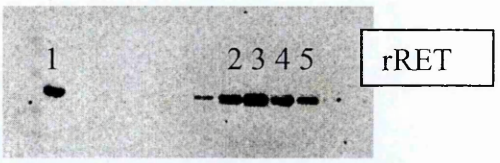

Figure 3.1.2 Chromatogram of anion exchange chromatography. The arrow indicates the peaks containing rRET eluated from 16XK-DEAE sepharose Fast flow column. Western blot with anti-His antibody was performed to identify the positive fractions. In the lane 1 total lysated was loaded, samples 2-5 corresponded to fractions under the peak indicated by he arrow.

The positive fractions were collected and loaded on Pro-bond nickel ion resin for the affinity chromatography. The positive fractions were identified by silver staining and were collected at the time point(s) shown below in Figure 3.1.3.

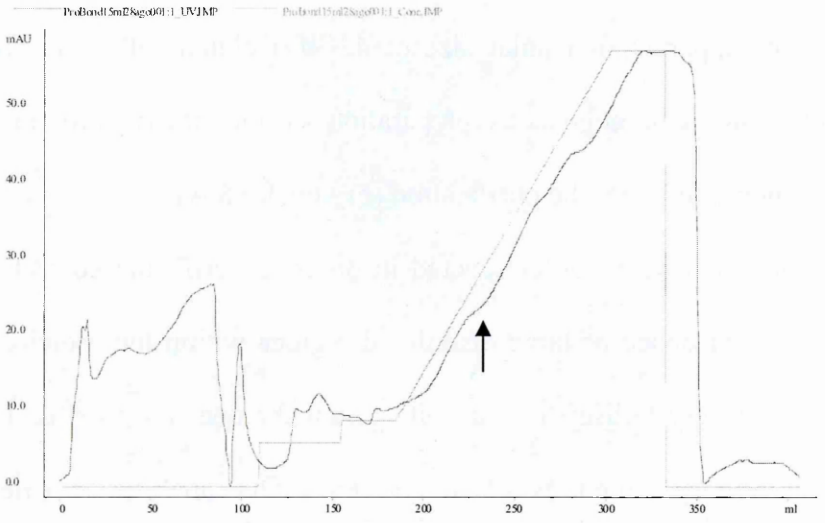

Figure 3.1.3 Chromatogram of Ni-NTA affinity chromatography. The rRET eluted when the imidazole in the buffer solution reached the concentration of 80mM in the column and the collection point is arrowed. The arrow indicates the peak in which rRET eluates

We identified the positive fractions by silver nitrate-stained gel, we collected, pooled and froze them. A sample from each preparation was quantified by Bradford assay and tested in ELISA.

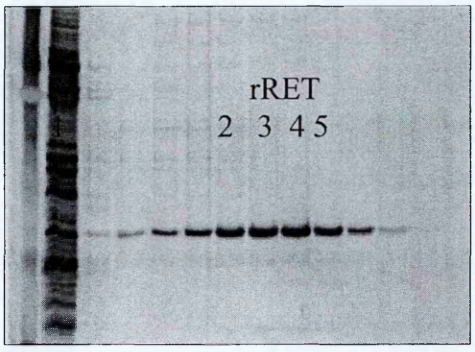

Figure 3.1.4 The silver nitrate stained gel shows the fractions of linear gradient and indicates the high purity of our preparation. In the lane 1 a sample from the positive fractions of DEAE pooled together was loaded; lane 2-5 are representative of the fractions corresponding to the elution peak. The absence of important contaminants indicates the high purity of our preparation.

3.1.3.2 Biochemical characterization

A single peak of apparent molecular size of 42 kDa eluted following analytical gel filtration, indicating a homogeneous preparation of monomeric protein. rRET was totally unphosphorylated after the purification (Figure 3.1.5 A).

Circular dichroism analysis was conducted in order to verify the correct folding and study the possible presence of large disordered regions within the protein, which may impair its ability to crystallise. Indeed, with this technique it's possible to determine secondary and tertiary structures of the proteins. Our analysis revealed a profile compatible with secondary structures that are typical of tyrosine kinase domains (Figure 3.1.5 B).

A

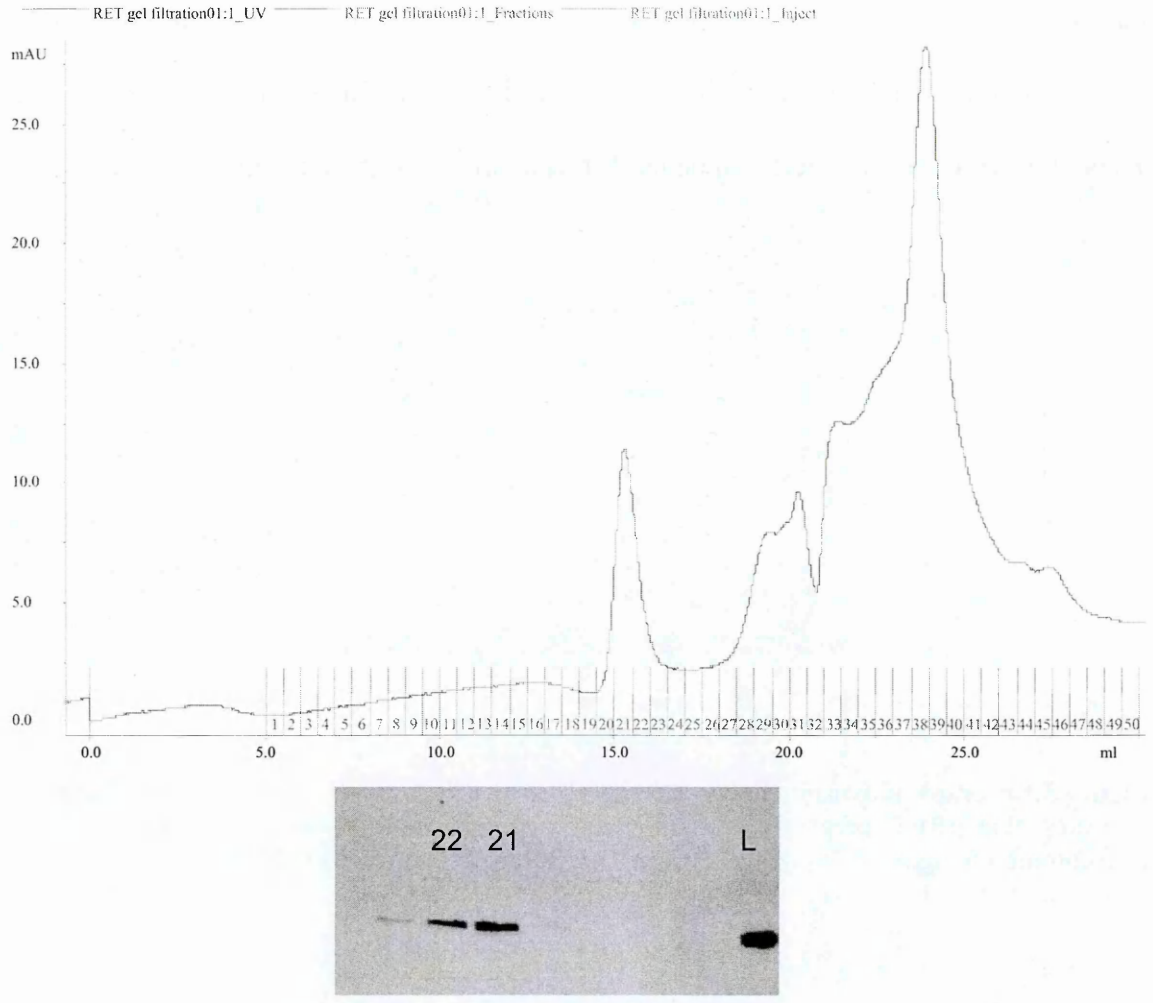

B

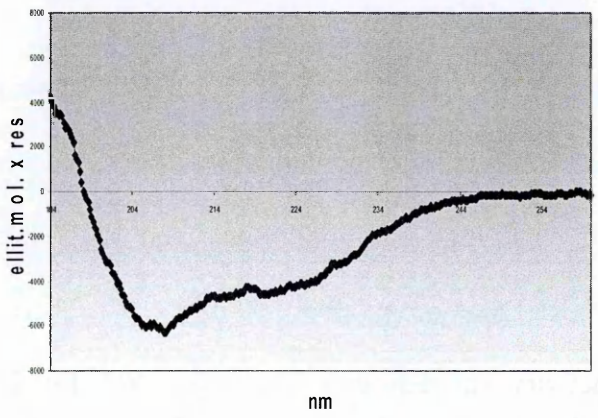

Figure 3.1.5 A Gel filtration column and western blot with anti-His antibody of the fractions corresponding to the peak of 42KDa. B Circular dichroism spectrum of rRET. The profile corresponds to mixed α+β secondary structure of, as expected for a properly folded tyrosine kinase domain.

Furthermore, dynamic light scattering used to determine the composition of the sample showed both monomodal and monodisperse rRET preparation, as showed in Fig. 3.1.6. Thus, the rRET prepared here can be used in crystallization experiments.

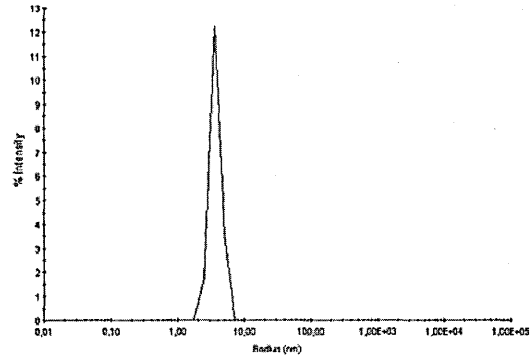

Figure 3.1.6 Graph of dynamic light scattering (Y axis % intensity, X axis radius nm). The peak indicates that rRET preparation is monodisperse and monomodal. rRET was used at concentration 5 mg/ml in 30mM TrisHCl pH 7.5, 150mM NaCl, 5mM DTT.

3.1.3.3 Enzymatic properties of rRET catalytic domain

In order to understand if rRET could be used also for the screening of small molecule inhibitor compounds identified by computational methods, the reaction conditions of *in vitro* phosphorylation and high salt inhibition upon rRET were determined. Fifty percent inhibition of rRET was observed at 100 mM NaCl. Thermal inactivation curves showed that rRET activity was reduced by 50% and 80% after 15 minutes at 30°C and 37°C, respectively. Complete inactivation was observed after 30 minutes at 37°C. The kinase reaction occurred in the presence of divalent cations, such as Mn^{++}, Mg^{++} and Co^{++} with Mg^{++} being preferred. Activity was optimal at pH values between 7.0 and 8.0.

The mechanism of rRET autophosphorylation was studied by determining the relationship between reaction rate and enzyme concentration. The data indicated that rRET autophosphorylation follows second-order kinetics. To set up a rapid and fairly selective assay of rRET activity, which is a prerequisite for the analysis and development of specific inhibitors, the following peptides were synthesized and used as substrates: aas 896-916 of the RET activation loop (SRDV**Y**EEDS**Y**VKRSQGRIPVK) containing the Y900 and Y905 autophosphorylation residues; the sequence ARDIYRASYYRKGGCAMLPVK derived from the activation loop of the oncogenic tyrosine kinase ALK (Anaplastic Lymphoma Kinase) and the N-terminal sequence MARTTSQLYDAVPIQSSVVL of PDK1 since the serine/threonine kinase PDK1 has been described to be phosphorylated at Tyr9 by RET/PTC oncogenes. rRET activity was tested on these three peptides and on the synthetic peptide poly(Glu_4Tyr). The time courses of peptide phosphorylation showed that poly(Glu_4Tyr) was the preferred substrate. rRET was, however, also active on both peptides derived from activation loops, displaying a higher phosphorylation rate toward the RET sequence. Calculated k_{cat} for RET and ALK peptide phosphorylation was 4.2 ± 0.2 and 1.1 ± 0.1 min^{-1}, respectively. In contrast to tyrosine kinase-derived peptides, PDK1 peptide was a poor substrate of rRET in our test. This finding suggests that the molecular recognition of PDK1 as a substrate by RET relies not only upon primary amino acid sequence, but is also based on additional specificity determinants dictated by the other regions of the intact protein (Figure 3.1.7).

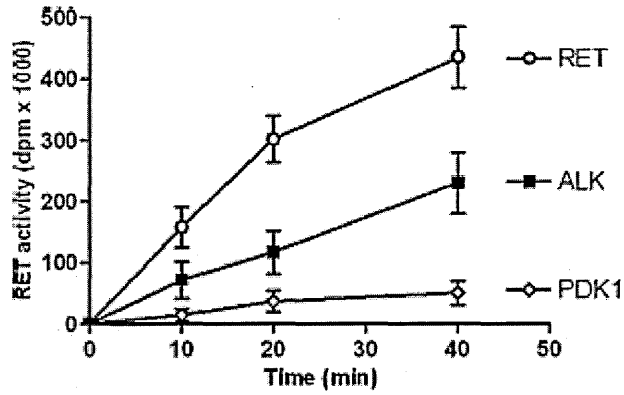

Figure 3.1.7 Time courses of peptide phosphorylation by rRET. Peptides (400 μM) were phosphorylated in a radioactive assay as previously described. Data points are presented as the mean ± standard deviation of three measurements.

Finally, the use of common inhibitors of tyrosine kinases or compounds active against RET, such as PP1 and PP2 demonstrated that rRET was inhibited with an IC_{50} similar to that reported in literature, 40 and 150 nM, respectively. Results from an experiment are shown below (Figure 3.1.8).

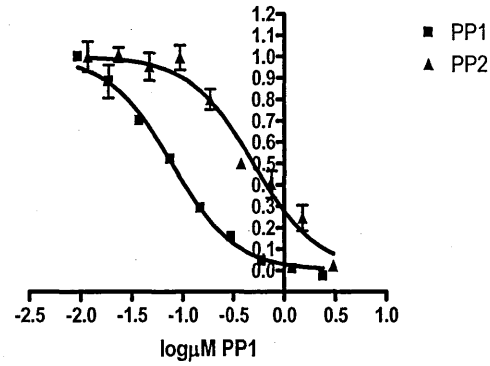

Figure 3.1.8 Inhibition curves of rRET in presence of PP1 and PP2. The IC_{50} obtained from ELISA assay, 40 nM for PP1 and 150nM for PP2 are consistent with the values reported in literature.

The conclusion was that rRET produced here was active and properly folded. The results obtained from the ELISA studies were reproducible and consistent with data

reported in literature. Thus the rRET produced here could be used in ELISA for studies into screening of small molecule inhibitors.

3.1.3.4 Expression of V804M mutant

It has been reported that the mutation V804M identified in some cases of sporadic MTC causes resistance to PP1 and ZD6474 [54]. This mutation occurs in the same position as in other tyrosine kinases, such as ABL T315I and EGFR T766M. In all cases the substitution of a threonine with a bulkier amino acid confers resistance to ATP binding site inhibitors. The mutant V804M (rRET 804) was produced in order to have another reagent with which test the effect of the inhibitor compounds. The procedure used for the expression and purification of this mutant protein, rRET 804, was the same as those used for rRET. rRET 804 was tested by ELISA in the presence of PP1 and staurosporine to verify its pharmacological properties. As shown in Figure 3.1.9 below, no inhibition of phosphorylation by rRET 804 was observed using PP1 while staurosporine, an all tyrosine kinase inhibitor, blocked phosphorylation.

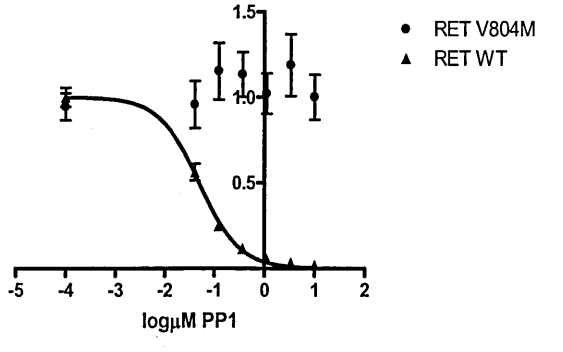

Figure 3.1.9 Inhibition curves of rRET and V804M rRET in presence of PP1. V804M rRET is resistant to PP1, while rRET is inhibited with the same IC_{50} as usual.

3.1.4 Discussion

The procedure of expression and purification of the recombinant protein rRET containing the catalytic domain of the tyrosine kinase receptor RET is described in the present Chapter. The use of Baculovirus system was necessary to obtain a correctly folded and active protein and this method is commonly utilized to synthesize recombinant proteins, in particular tyrosine kinases. The level of expression of the viral preparation is crucial to obtain a good yield of protein and it is, therefore, essential to optimize the conditions of infection in terms of number of cells and amount of virus. Another important aspect to improve the yield is the volume of lysis buffer used to resuspend the cells harvested after infection. I identified a compromise between the necessity of efficient cell lysis and the problem of overdilution of the recombinant protein. Furthermore, the number of cells loaded in the 26-XKcolumn for the anionic exchange chromatography is not directly related to the yield since it observed that , after a certain threshold, increasing the amount of loaded material does not lead to an significant increase of purified rRET.

The Ionic Exchange Chromatography (IEX) is performed at pH 6.5, although rRET has a calculated PI equal to 8. One possibility to account for this is that perhaps the basic amino acids are not exposed to the solvent and do not therefore interact with the resin. TrisHCl buffer was used for both for IEX and for the Immobilized Metal ion Affinity Chromatography (IMAC), because rRET precipitates in presence of $NaHPO_3$. As shown in silver nitrate-stained gel, the product after IMAC is 95% pure (Figure 3.4).

In order to perform crystallization tests, it was necessary to change the buffer containing the rRET (50mM TrisHCl pH 8, 250mM NaCl, 20mM β-mercaptoethanol, 80mM imidazole, glycerol 10%) with a more hypotonic buffer (20mM TrisHCl, 50mM

NaCl, 10mM β-mercaptoethanol) without imidazole and glycerol that could avoid rRET crystal formation. The results from dynamic light scattering indicate the absence of aggregates and a monodisperse distribution both of which are good theoretical start points for the crystallization studies.

During its *in vitro* characterization, rRET demonstrated autophosphorylation following second-order kinetics (rate increases linearly with the square of enzyme concentration). This result is consistent with an intermolecular event. It is known that RTKs like RET undergo activation upon homodimerization through cross-phosphorylation [115]. However, since our isolated kinase domain does not have any interaction interface and is present in solution as a monomer, the mechanism of its autophosphorylation is not obvious. However, the current data suggest that the intermolecular autophosphorylation mechanism is inherent in the catalytic domain and can occur independently of the other RET domains. Therefore, the recombinant kinase domain of RET is a good model of the full-length enzyme.

The rRET recombinant protein was considered to be suitable for the investigation of screening of small molecule inhibitors for RET. A few micro liters rRET per well were used to phosphorylate the peptide substrate using conditions described by Mologni et al [52]. The inhibition achieved in presence of PP1 and PP2 with the same IC_{50} values reported in literature [50, 51], confirmed that rRET produced here has pharmacological properties which are favorable for use by ELISA [114]. Moreover, the availability of the mutant recombinant protein, RET V804M, will be important to identify any inhibitors that are active on a mutated RET protein that is resistant to the common inhibitors. Finally, comparison of the experimental data of small-molecule compounds in the rRET and rRET V804M is important to validate the virtual models which were used as the rationale for the screening studies.

In summary, the rRET recombinant protein containing a kinase domain exhibits features which should enable it to be used in crystallization studies and to used to screen for kinase inhibitors screening in ELISA validated assay.

3.2 RET crystallization

3.2.1 Introduction

It is essential to know the three-dimensional architecture of the catalytic domain in order to analyse the mechanism of RET activation and how to efficiently inhibit it. In this section, I describe the recombinant proteins that have been used in the crystallization attempts. Collaborations were established with Prof. Zanotti's laboratory, in the Dept. of Chemistry at the University of Padova, to perform crystallization screening.

3.2.1.1 Principles of protein crystallization

To understand cellular processes, knowledge of the three dimensional structure of proteins, enzymes in particular, is crucial. Two techniques are widely used for the structural determination at atomic resolution: nuclear magnetic resonance (NMR) and X-ray diffraction of crystal. While NMR does not require crystals and provides more detailed information on the dynamics of the molecules, it can be used only for biopolymers with a molecular weight of less than 30 kDa. In contrast, X-ray crystallography can be applied to compounds with molecular weight up to at least 10^3 kDa. For proteins then X-ray diffraction is the principal method of choice.

Protein crystallization is a trial and error procedure in which the protein is slowly precipitated from a saturated of protein solution. An highly pure preparation of the protein is dissolved in a suitable solvent from which it must be precipitated in crystalline form. The solvent is usually water and buffer solution added by precipitating

agents such as ammonium sulphate and polyethylenglycol (PEG). The solution is brought to supersaturation and small aggregates are formed. To generate crystal from precipitates a energy barrier has to be passed and this step is easier at high level of supersaturation [116]. Precipitation of the protein can be achieved by adding salt (salting out) or removing salt (salting in). In the first approach, ions immobilize water thus increasing the effective concentration of the protein, while in the second the absence of solvent ions induces Coulomb attraction between opposite charges on different protein molecules. It is also possible to decrease the repulsive forces between proteins or increase attractive forces. Electrostatic forces are influenced by an organic solvent such as alcohol or by change in pH, while hydrophobic interactions increase with temperature [117].

The crystallization of a protein results from a multi-parameter problem in which the parameters are varied in the search for optimal crystallization conditions. The most common parameters include protein concentration, nature and concentration of precipitant, pH and temperature. An appropriate statistical design for crystallization screening is the factorial method in which a table is constructed with a number of values entered for each parameter [118]. After approximate crystallization conditions have been found, then these conditions can be optimised. Although other strategies can be followed [119], a large number of attempts must still be tried in all cases.

3.2.1.2 Crystallization technique

The vapour diffusion method is commonly used in crystallization attempts [117].

Supersaturation is reached by diffusion of the vapour from the drop that contains proteins to the precipitating solution or vice versa. Drops are prepared by mixing few

microliters (3-10μl) of protein solution with the same volume of precipitant solution, while precipitant partially fills the tray. In the 'hanging drop' method, the drop is positioned on a siliconized microscope glass cover slip and the slip is placed upside down over a depression in the tray which is filled by precipitant. In the 'sitting drop' method, then the drop is placed on a support in the tray. The latter technique is preferable if the protein solution has a low surface tension and it tends to spread over the cover slip in the hanging drop method. The crystallisation chamber is sealed with grease or oil and incubated at a controlled temperature till a crystal appears [120, 121]. However, the oldest and simplest methods used for protein crystallization is the 'batch technique [117]. The principle of this method is that the precipitating reagent is instantaneously added to the protein solution, suddenly bringing the solution to a state of high supersaturation and crystals grow gradually without further processing. Several automated systems for microbatch crystallization has been designed to evaluate a larger number of conditions using just a small amount of protein [122]. 1-2 μl drops of the protein solution and precipitant are suspended in oil that acts as sealant to prevent evaporation [123, 124]

3.2.1.3 Cryo-cooling of crystal

Once a crystal appears, then the drops must be cooled. The main reason for cooling protein crystals is to slow the destructive processes induced by X rays [125, 126]. Cooling the crystals from room temperature to a cryogenic temperature must occur suddenly because the water in the mother liquor and in the crystal must freeze to a vitreous structure in order to prevent the ice formation that would damage the protein crystal structure by expanding the water structure in its transition to crystalline ice

[127]. Cooling is accomplished by nitrogen gas, which is boiled off from liquid nitrogen or cooled in a heat exchanger. The crystal is then transferred to a solvent containing an anti-freeze such as glycerol, MPD, ethyleneglycol and low molecular weight PEG, to prevent ice formation in and around it completely. For data collection, the crystal is lifted from the cryoprotectant solution by a loop made from a thin fibre of rayon, nylon or glass and mounted in a metal capillary that can be fixed to the top of a goniometerhead for X rays diffraction [128].

3.2.1.4 X-ray diffraction

X rays are electromagnetic radiation with wave length of 10^{-7}-10^{-11} m. Electrons in the atoms are responsible for the diffraction; proteins consist predominantly of carbon, nitrogen and oxygen, elements which have only a relatively few electrons per atom, and have a low scattering power. Moreover, diffraction is a cooperative event between molecules in the crystal. In the case of larger molecules then there are fewer molecules in a crystal of the same size and the diffracted intensity is therefore lower. Protein diffraction therefore requires a high intensity source of X rays and a rotating anode tube or a synchrotron for very small size (< 0.1mm) crystals. The result of X rays diffraction is a pattern generated by constructive interference of diffracted waves. Mathematical software can produce the image from an electronic map [129].

3.2.1.5 Characterization of the crystal

The important parameters in the characterisation of a crystal are the diffraction limit, the space group and the number of protein molecule that are in the unit cell. The quality of

the crystal depends on the ordering of the molecules in the unit cell which is defined by the regular packing of the molecule in the crystal. Diffraction patterns with maximal observed resolution corresponding to a lattice spacing of 1-1.5 Å can be considered as of very high quality. However, most of the crystals cannot be regarded as a single crystal because the regular repetition of the unit cells is interrupted by lattice defects. In this case the diffraction pattern is the sum of several blocks with slightly different orientations. To recognize the space group to which the crystal belongs, one can observe the symmetry and the systematic absence in the pattern. Finally, the number of the molecules per unit cell can be estimated by the ratio of the unit cell volume and the molecular weight that for many crystals is between 1.7/3.5 $Å^3$/Da (Principles of Protein X-ray crystallography, Drenth).

In summary, X ray diffraction is a very informative technique with which one can obtain invaluable information concerning the exact relationship of the amino acids inside a protein. The result is a picture of the protein in an instant and an more in depth knowledge of protein dynamics derived from the resolution of several forms in different states. In the case of protein kinases, structures of non-phosphorylated and phosphorylated forms or complexes with small molecule inhibitors should clarify the mechanism of action of the kinase(s) and its regulation. The most important parameters to obtain a three-dimensional structure of the protein are the choice of correct construct and the identification of crystallization screening. In this field, good results are often associated to serendipity.

3.2.2 Materials and methods

3.2.2.1 Concentration

Vivaspin columns 5000 Da MWCO (molecular weight cut off) were used to concentrate rRET and to change the buffer. The sample was centrifuged in a swing out angle rotor at 4000 g until the final concentration of 5-8mg/ml was achieved. The recombinant protein sample was then added to 50mM TrisHCl pH8, 20mM NaCl, 10mM β-mercaptoethanol and concentrated again. A Bradford assay was used to quantify the protein after concentration.

Coomassie Brilliant Blue solution (Pierce) was used to quantify protein after concentration. With a curve of known amounts of BSA we determined the linear range to extrapolate the concentration of our preparation.

3.2.2.2 His tag cleavage

Enterokinase (Invitrogen) cleavage was optimised to remove the His tag from the rRET protein. The reaction was maintained at 30°C for 4 hours with 20U enzyme/mg of rRET. Enterokinase was removed by beads according to manufacturer's instructions (Invitrogen). The cleaved recombinant protein was purified by Nickel affinity chromatography and concentrated again.

3.2.2.3 Crystallization attempts

Crystallization attempts were performed in Prof. Zanotti's laboratory in the Department of Chemistry at the University of Padova and Hautmann Institute of Buffalo (USA). Both sitting and hanging drop methods were used in Italy while the microbatch method was used in the USA to investigate more than thousand conditions for crystallisation.

3.2.2.4 New constructs for the generation and purification of rRET

Modified constructs were obtained from wild-type RET plasmid by site-directed mutagenesis using the QuikChange kit (Stratagene), according to manufacturer's instructions, with the following mutagenic primers: for N-deletion construct (N-Del) sense, ATGGCTAGCATGACTGGTGGAATCCTGGAGGATCCAAAGTGG, and antisense, CCACTTTGGATCCTCCAGGATTCCACCAGTCATGCTAGCCAT; to remove the kinase insert sequence (Kid Long) were used:
sense CTTCCTCCGCGAGAGGCCGCCGGGCCCTCAGGGCG and
antisense CGCCCTGAGGGCCCGGCGGCCTCTCGCGGAGGAAG.
The construct with the N-terminal deletion and without kinase insert sequence (Kid short) was obtained from Kid Long plasmid by direct mutagenesis using N-deletion primers. Recombinant Baculoviruses were produced following the procedure described in the previous section. New rRET forms were purified with the same protocols used to obtain recombinant RET wild type protein consisting of anionic exchange chromatography and affinity chromatography.

3.2.3 Results

3.2.3.1 Large scale purification

As described above, rRET was produced in Sf9 cells infected with Baculovirus and purified with a two step procedure consisting of anionic exchange chromatography and Nickel affinity chromatography. Several purifications were performed to obtain sufficient amounts of recombinant proteins to start crystallization screening. The median yield from each purification was 1mg of rRET from 2 billion cells. All positive fractions were frozen at -80°C in the elution buffer following affinity chromatography. The 10% of glycerol acted as a crioprotector.

rRET diluted in a large volume (200ml) must be concentrated to a final volume of 4ml (50x) in order to obtain a final protein concentration of 2mg/ml. Concentration was performed by centrifugation in concentrator columns with 30 KDa as molecular weight cut off. The polyethylensulphone membrane avoided protein adhesion thus favouring the complete recovery of rRET. During the concentration step, the buffer was changed by diluting the preparation and re-concentrating it. Indeed, for crystallization attempts the ideal buffer contains low salts and 1% of glycerol as maximum. rRET was stored in small aliquots at 2mg/ml in 50mM TrisHCl pH 8, 20mM NaCl, 10mM β-mercaptoethanol at -80°C. Flash freezing in liquid nitrogen was used to minimize protein degradation.

3.2.3.2 First screenings in Padova and Buffalo

The first screening was carried out using His-tagged rRET, purified and concentrated, as previously described. An aliquot of rRET (2mg/ml) was further concentrated to 6.4mg/ml and tested by the sitting drop method in the presence of strong precipitant agents, such as ammonium sulphate $(NH_4)_2SO_4$, methyl-pentane-diol MPD 40%, 0.5M TrisHCl pH 7.5, poly-ethylen-glycol PEG400 40%, 0.5M TrisHCl pH 7.5. rRET precipitated in all conditions. Large scale screening of crystallization conditions by both sitting and hanging drop methods with commercial kits that allow to evaluate a wide range of different situations was started. rRET was tested in apo form or in presence of AMP-PNP, an ATP analog non-hydrolysable, or small molecule inhibitors such as ZD6474 and L6, The latter was a new chemical entity discovered by our group as RET inhibitor by molecular modeling.

The results are reported in table 3.2.

KIT	N	Conditions
structure screen I	48	
crystal screen II	40	RET incubated with AMP-PNP + MgCl2
Clear strategy screen I	22	precipitants pH 8.5
Clear strategy screen I	16	screen di pH 45.-5.5-6.5-7.5; RET incubated with L6
Clear strategy screen II	23	precipitants pH 6.5; RET incubated with L6
Clear strategy screen II	45	RET incubated with ZD6474
Precipitant PEG 3350	34	precipitants different pH and salt; RET incubated with ZD6474

TOTAL	**228**	

Table 3.2 Conditions of the crystallization screening performed in Padova

The best conditions identified from this preliminary screening were:

Na acetate + Na formate pH4.5 in the presence of ZD6474.

Unfortunately, the microcrystals obtained were too small for X-ray diffraction studies. Concurrently, we produced another 10mg of rRET to try the high throughput screening at Hauptman Woodward Institute of Buffalo (USA) [130]. The protein was concentrated to 8mg/ml and sent ready to use for crystallization analysis. 1573 different conditions were tested, without obtaining any crystals, but only multiple forms of precipitate.

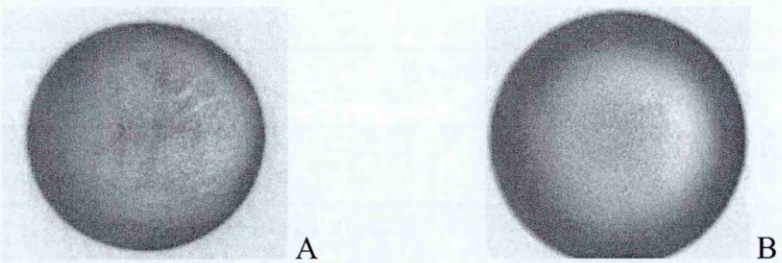

Figure 3.2.1 Examples of drop picture from high through put screening performed in Buffalo (USA); a picture of the drops were taken every week.

Figure A shows an example of light amorphous precipitate: here the protein precipitated without any ordered pattern probably because the supersaturation state occurred too quickly. Figure B shows the presence of a birefringent precipitate that may contain little microcrystals of proteins or salt crystals. Although the presence of precipitate, especially if non-amorphous or birefringent is a good starting point for crystal growth,

no crystal growth was observed after one month of incubation at 20°C. In other drops skin was observed: the skin is believed to be a layer of denaturated protein or caused by polyethylene glycol and its presence decreases the rate of supersaturation state and avoids crystal growth. Finally, some drops showed phase separation which generally occurs when organic solvent is added to highly concentrated salt solution and one of two solutes is insoluble in the other. The protein concentration is altered and becomes higher in the phase in which the protein is more soluble, subsequently giving rise to a high state of supersaturation. In some cases, unfortunately not in the current study, crystals can grow in boundary region that acts as nucleation catalyst ("The protein crystallization page" website).

3.2.3.3 Enterokinase cleavage optimisation and screening

During the first crystallization screening, the enterokinase cleavage was optimised to remove the His-tag from the N-terminal of rRET. Temperature, duration, salt concentration and amount of enzyme are the most important parameters for this reaction. Twenty units of enterokinase were used per milligram of rRET for 4 hours at 30°C. The rRET was previously diluted 1:5 (v/v) to decrease the salt concentration that could inhibit the enzyme. Thus, the final protocol consisted of two-step purification procedure, followed by enterokinase cleavage and a further affinity chromatography to remove uncleaved rRET. Partial cleavage caused a loss of 20% of protein that retained the His tag and eluted from Nickel column at 80mM imidazole as untreated rRET. By contrast, rRET without the His-tag eluted in the flow through fractions after washing the column. A typical example is shown in Figure 3.2.2 below Affinity column was performed using the conditions described in the previous section. Positive fractions

were pooled and concentrated again to obtain an optimal preparation for the crystallization screening.

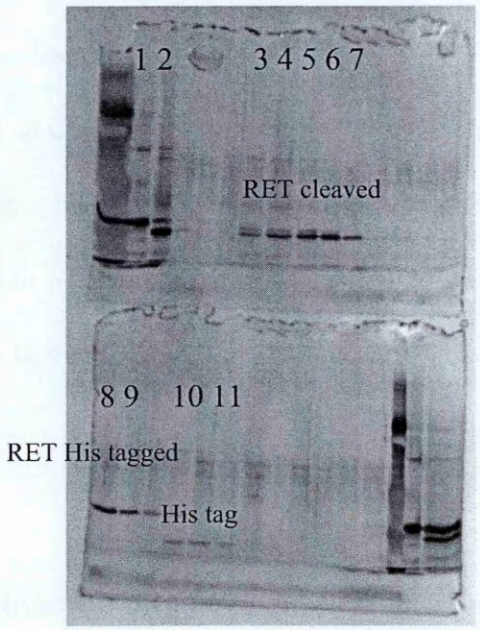

Figure 3.2.2 Silver stained gel of fractions from Nickel affinity chromatography. The first lane in upper gel is un-treated rRET, second lane is cleaved rRET, loaded in Nickel column; RET cleaved eluted in flow through fraction (3-7), while His tagged-RET eluted at 80mM Imidazole (8-9), as usual. In lanes 10 and 11 the removed His-tag is shown.

Some precipitate was present following concentration, probably because the solubility of the protein diminished in the absence of His-tag. Unfortunately, further crystallisation studies performed using this cleaved rRET protein were also unsuccessful.

3.2.3.4 New constructs

Analysis of the RET model revealed two disordered regions that could prevent crystallization: the N-terminal portion and the kinase insert which is a region between

the N and C lobes. The corresponding sequences were removed by mutagenesis from the complete RET sequence to obtain the following new constructs: NDEL was a form with a shorter N-terminal region, KID LONG was the construct without the kinase insert, while KID SHORT (derived by mutagenesis from the KID LONG plasmid), was represented the form without the kinase insert and with N-terminal deleted (Figure 3.2.3). The His tag was retained to allow the affinity chromatography of all the resulting recombinant proteins. The Baculovirus production protocol was the same as previously described for rRET.

NDEL

MPRGS*HHHHHH*GMAS(**MTGGQQMGRDLYDDDDKDRWIRPRDLQLVPMENQVSV DAFK)**ILEDPKWEFPRKNLVLGKTLGEGEFGKVVKATAFHLKGRAGYTTVAVKMLKE NASPSELRDLLSEFNVLKQVNHPHVIKLYGACSQDGPLLLIVEYAKYGSLRGFLRESRK VGPGYLGSGGSRNSSSLDHPDERALTMGDLISFAWQISQGMQYLAEMKLVHRDLAAR NILVAEGRKMKISDFGLSRDVYEEDSYVKRSQGRIPVKWMAIESLFDHIYTTQSDVWSF GVLLWEIVTLGGNPYPGIPPERLFNLLKTGHRMERPDNCSEEMYRLMLQCWKQEPDKR PVFADISKDLEKMMVKRRDYLDLAAV

KID LONG

MPRGS*HHHHHH*GMASMTGGQQMGRDLYDDDDKDRWIRPRDLQLVPMENQVSVDAF KILEDPKWEFPRKNLVLGKTLGEGEFGKVVKATAFHLKGRAGYTTVAVKMLKENASP SELRDLLSEFNVLKQVNHPHVIKLYGACSQDGPLLLIVEYAKYGSLRGFLRES(**RKVGP GYLGSGGSRNSSSLDHPDERALT)**MGDLISFAWQISQGMQYLAEMKLVHRDLAARNI LVAEGRKMKISDFGLSRDVYEEDSYVKRSQGRIPVKWMAIESLFDHIYTTQSDVWSFG

VLLWEIVTLGGNPYPGIPPERLFNLLKTGHRMERPDNCSEEMYRLMLQCWKQEPDKRP

VFADISKDLEKMMVKRRDYLDLAAV

KID SHORT

MPRGS*HHHHHH*GMAS**(MTGGQQMGRDLYDDDDKDRWIRPRDLQLVPMENQVSV**

DAFK)ILEDPKWEFPRKNLVLGKTLGEGEFGKVVKATAFHLKGRAGYTTVAVKMLKE

NASPSELRDLLSEFNVLKQVNHPHVIKLYGACSQDGPLLLIVEYAKYGSLRGFLRES**(RK**

VGPGYLGSGGSRNSSSLDHPDERALT)MGDLISFAWQISQGMQYLAEMKLVHRDLAA

RNILVAEGRKMKISDFGLSRDVYEEDSYVKRSQGRIPVKWMAIESLFDHIYTTQSDVWS

FGVLLWEIVTLGGNPYPGIPPERLFNLLKTGHRMERPDNCSEEMYRLMLQCWKQEPDK

RPVFADISKDLEKMMVKRRDYLDLAAV

Figure 3.2.3 Sequence of rRET in which deleted portions were labelled in bold. In N-DEL construct 41 amino acids (between parenthesis) were removed. In KID LONG construct the kinase insert sequence (in bold, underlined) was eliminated, while in KID SHORT both N-terminal portion and kinase insert were removed.

In both the NDEL and KID SHORT constructs the RET sequence started 11 amino acids later than rRET and immediately after His tag sequence. The Enterokinase cleavage site was removed and the constructs retained His tag in the crystallization tests. In some cases the presence of this tag favoured the solubility of the protein and slowed down the rate with which the supersaturation state was reached. In KID LONG and KID SHORT the kinase insert, a loop between N-lobe and C-lobe that confers mobility to the lobes, was removed. All the mutated RET forms were tested by ELISA assay to evaluate their activity and verify that deletion did not interfere with the catalytic properties of the protein. The evidence of regular kinase activity of the new constructs indicated the proper folding of these proteins.

Sufficient amounts of recombinant proteins were produced to perform crystallization screening for all KID LONG, NDEL and, lastly, KID SHORT.

3.2.3.5 Kid Long crystallization screening and microcrystals

KID LONG protein was biochemically characterized by gel filtration to verify the correct molecular weight and the absence of aggregated forms. The elution buffer was 30mM TrisHCl pH 8, 300mM NaCl, 1mM DTT. As shown in figure 3.2.4 the protein molecular weight was 39KDa, as expected, and was present as monomer.

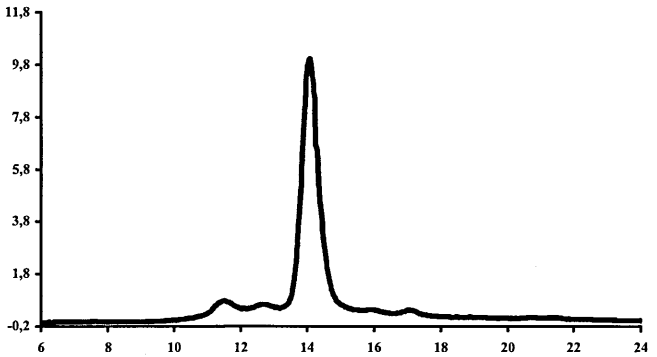

Figure 3.2.4 Chromatogram of analytical gel filtration of KID LONG

Crystallization screening was performed using both cleaved and His-tagged proteins. The presence of an Enterokinase cleavage site made it possible to remove the His-Tag thus producing two different proteins to test their different solubilities.

The Enterokinase reaction was performed at 4°C overnight since the absence of the kinase insert could increase precipitate formation. Cleaved protein was recovered by NiNTA resin in a batch purification.

Microcrystals were obtained with KID LONG cleaved in presence of 0.1M NaCl, 0.1M Bicine pH 9, 30% PEG 550, ZD6474. These conditions were reproducible and microcrystals from drop containing birefringent precipitate were obtained in repeat experiments

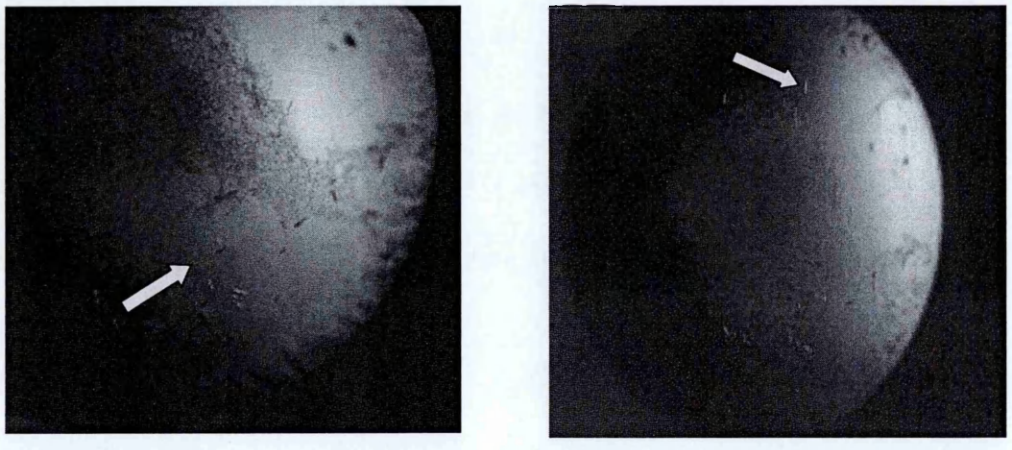

Figure 3.2.5 Microcrystals of KID LONG; arrows indicate crystals

Unfortunately, these crystals were too small to undergo X rays diffraction and no subsequent attempts to grow crystals were made of KID LONG.

The NDEL and KID SHORT recombinant proteins did not crystallize under any conditions including the promising conditions identified for KID LONG.

3.2.4 Discussion

In this part of my thesis I tried to crystallize the kinase domain of rRET. The work was performed in collaboration with prof. Zanotti's lab, I was mainly responsible for the production of protein suitable for crystallization experiments. The first screening was performed with His-tagged rRET using commercial kits. Several methods were used, such as hanging and sitting drop methods. Crystallization tests were performed without or in presence of small molecules compounds, such as ZD6474, L6 (a small molecule inhibitor identified by molecular modelling as RET inhibitor) and AMPNP. The presence of small molecule inhibitors preferentially stabilizes the kinase domain in one conformation [10, 15, 17], theoretically favouring the crystal growth. Concurrently, high throughput screening at Hauptman Woodward Institute of Buffalo (USA) was performed. In this case, the microbatch method was used. A large amount of conditions were screened without obtaining any suitable crystal conditions. Furthermore, enterokinase cleavage was optimized to remove the his-tag form the C-terminal. Temperature, salt concentration and amount of the enzyme were the most important parameters to control. Although the cleavage was partial and some precipitate was observed during the reaction, some crystallization drops were prepared. Also in this case crystals did not grow. New constructs were designed to produce other forms of rRET. N-terminal region was shorted by removing amino acids belonging to the vector and the first 11 amino acids of RET kinase domain. Furthermore, the kinase insert, a link region between C-lobe and N-lobe, was deleted to obtain another form: this loop could be flexible and could disturb the crystallization process, in other kinases for example FLT3R this region was eliminated [131]. Finally, rRET without the kinase insert and the N-terminal region was produced. The modifications did not alter the biochemical

properties of rRET, as NDEL, KID LONG and KID SHORT retained the catalytic activity. All the new constructs were used in crystallization screening. The best results were obtained with KID LONG, but the microcrystals did not grow enough to be diffracted.

RET structure has been published in 2006 August by Knowles et al. [132]. Construct encompasses between 705 and 1013 amino acids, this sequence is similar but shorter than our rRET, in particular 6 amino acids at the N-terminal and 7 at C-terminal have been removed. Sometimes, few differences in construct determine the outcome of crystallization experiments. The conditions of crystallization are: for un-phosphorylated RET and phosphorylated RET 1.5ul of protein (3mg/ml) mixed to 1ul of reservoir solution (2M sodium formate + 0.1M sodium citrate pH5.5), for PP1-RET 1ul of protein (1.5mg/ml) mixed to 1ul of 2.8M sodium formate + 0.1M sodium acetate pH4.5 + 0.1M lithium chloride, finally for ZD6474-RET 1.5ul of protein (3mg/ml) mixed to 1ul of 2.2M sodium formate, 0.1M sodium acetate pH4.5.

Our best conditions, identified in the first screening with rRET un-cleaved, were very similar to that used for un-phosphorylated-RET and phosphorylated-RET.

RET kinase domain adopts the characteristic protein kinase fold, consisting of a smaller N-lobe (713-805) and larger C-lobe (812-1013) connected by a hinge/linker (806-811). The relative position of N and C-lobes is similar in both phosphorylated and not-phosphorylated forms. Residues 705 to 711 of RET juxtamembrane region are present in RET kinase domain structure and generate a portion of N-terminal helix (αN) that connects to β1 strand of the kinase domain via loop 712-714. Helix αN packs against and tethers the functionally important αC helix through apolar contacts around F709 and F776.

The RET kinase domain conformation seems to be independent of the phosphorylation state of the activation loop and suggests that the activation loop exhibits no major auto-inhibitory effect either in binding ATP or substrate.

RET has been crystallized as head to tail dimer: the first contact area involves residues N^{763} ASP S^{767} prior the αC helix, interacting with the p+3 pocket and specifically M918; these residues are in extended conformation which masks the substrate-binding site of the second molecule. The second adjacent contact area in the dimer is the αN interacting with he side chains of F924 and F961 and with Q910 and H926.

Some activating mutations, such as M918T, P766S and E768/A919 map close to dimer contact region altering the regulatory component. These data confirm the model in which RET is present as dimer in the cellular membrane, GDNF/GFRα complex binds it and promotes conformational changes required for full kinase activity. Otherwise, trans-inhibition can be overcome during the recruitment in lipid raft and the formation of signalling complex [133].

It's not completely clear why RET fusion proteins that represent cytoplasmatic dimer form of RET are constitutively active in PTCs. An hypothesis could be that fusion partners maintain RET kinase domain close enough to accomplish phosphorylation in tyrosines important for signal transduction, such as Y1062, but quite far to be not trans inhibited. Further studies are necessary to well characterize RET regulation.

3.3 RET inhibition by SU5416

3.3.1 Introduction

The rRET recombinant protein produced as described is suitable for use screening studies to identify small molecule inhibitors of RET protein. In particular, it was used to screen members of the 2-indolinone derivative family. This part of my PhD project shows the inhibition of RET signalling by new compound -SU5416- in both *in vitro* and *in vivo* models.

3.3.1.1 Enzymatic kinetics

An enzymatic reaction is defined the conversion of substrate to a final product mediated by a protein that acts as catalyst; the formation of the complex enzyme-substrate is an equilibrium that is not perturbed by product formation. An equilibrium reaction for this is given below.

$$E+S \underset{k_{-1}}{\overset{k_1}{\rightleftharpoons}} ES \xrightarrow{k_2} E+P$$

In which E represents the enzyme, S is the substrate and P corresponds to the product. k_1 and k_{-1} are equilibrium constants that regulate the association between enzyme and substrate, while k_2 is the dissociation constant of E+P complex.

The main parameters that regulate the kinetics of the reaction are the Vmax and Km (Michaelis Menten constant): Vmax is the maximum rate at high substrate concentration

(close to saturation) while Km is a constant derived from the ratio between $(k_{-1}+k_2)/k_1$. Km is not an equilibrium constant, but represents one kinetic constant and its physical significance can be determined only when all k_1 k_{-1} k_2 are known. The ratio k_{-1}/k_1 indicates the affinity of the enzyme for the substrate, thus when $k_2 << k_{-1}$, Km defines the affinity of the enzyme.

In the presence of a reversible inhibitor then the reaction rate is decreased. Several mechanisms of inhibition are defined from the Michaelis Menten equation, such as competitive, non competitive and un-competitive inhibition.

A competitive inhibitor is a compound that binds the enzyme and avoids the formation of substrate-enzyme complex. This interaction determines an increased Km without modifying the Vmax. The inhibition can be overcome by increasing the amount of the substrate in reaction because the inhibitor does not alter the affinity of free enzyme for it; only the complex enzyme-inhibitor has no affinity for the substrate. Otherwise, the binding of one non-competitive inhibitor to the enzyme does not interfere with the formation of the complex substrate-enzyme, and both inhibitor and substrate can interact with the enzyme at the same time giving rise to the complex inhibitor-substrate-enzyme. This complex is unable to generate the final product and the Vmax of the reaction decreases. Finally, an un-competitive enzyme has affinity only for the complex substrate-enzyme and its binding blocks the reaction. Both Vmax and Km are decreased in presence of the inhibitor.

In a phosphorylation reaction, the kinase binds ATP to transfer a γ phosphate group onto tyrosine residues that act as a substrate. Small molecule inhibitors can interact with several portions of protein kinase, as previously described. Thus, understanding the modality of inhibition is very important to characterize an inhibitory compound.

3.3.1.2 The 2-indolinone family

SU5416 belongs to the 2-indolinone family, a class of compounds identified initially as FGFR1 inhibitors. Mohammadi et al. [17] evaluated the activity of SU4984 and SU5402 (other 2-indolinone family members) on FGFR1 in *in vitro* autophosphorylation assays. Using purified kinase domains, an IC_{50} of 10 to 20μM was obtained while using NIH3T3 cells stimulated by acidic FGF an IC_{50} 20 to 40μM was found. IC_{50} is defined as the inhibitor concentration that blocks the 50% of the enzymatic activity. Only SU4986 blocked the activity also of PDGFR and IRK when tested in the same cellular assay under the stimulation of PDGF and insulin respectively. In contrast, SU5402 showed higher specificity for FGFR (B). X ray diffraction of FGFR in complex with 2-indolinone derivatives demonstrated that both SU5402 and SU4986 bind to the ATP-binding pocket: the oxindole residue occupying the same position as the ATP adenine and adds two hydrogen bonds to the protein backbone in the hinge region. Numerous hydrophobic residues contribute to the stabilization of the interaction. Moreover, SU4986 (A) makes an oxygen aromatic contact with the carbonyl oxygen of A564. The piperazine ring has a Van der Waals interaction with G567, a highly conserved residue, while the terminal formyl group is disordered. All these interactions do not confer specificity for FGFR because they involve residues common to most protein tyrosine kinases. Conversely, SU5402 makes an intramolecular hydrogen bond between the pyrrole ring and O-2 of the oxindole residue and the methyl group of the pyrrole ring has a Van der Waals interaction with G567. Moreover, the carboxylethyl group forms a hydrogen bond with N568, (probably involved in ATP binding), and the oxindole binding pocket is capped by F489 in the nucleotide binding loop. This region is well ordered only in the crystal SU5402-FGFR1. Thus, SU5204 showed higher specificity because of the bond with N568 and the

stabilization of the nucleotide binding loop. In both PDGFR and IRK, N568 is substituted by aspartic acid which is unable to form any hydrogen bond with the SU5204, thus that results completely inactive; otherwise, VEGFR that has aspargine residues in the same position, is efficiently inhibited by SU5402. The following graft shows the interactions described above.

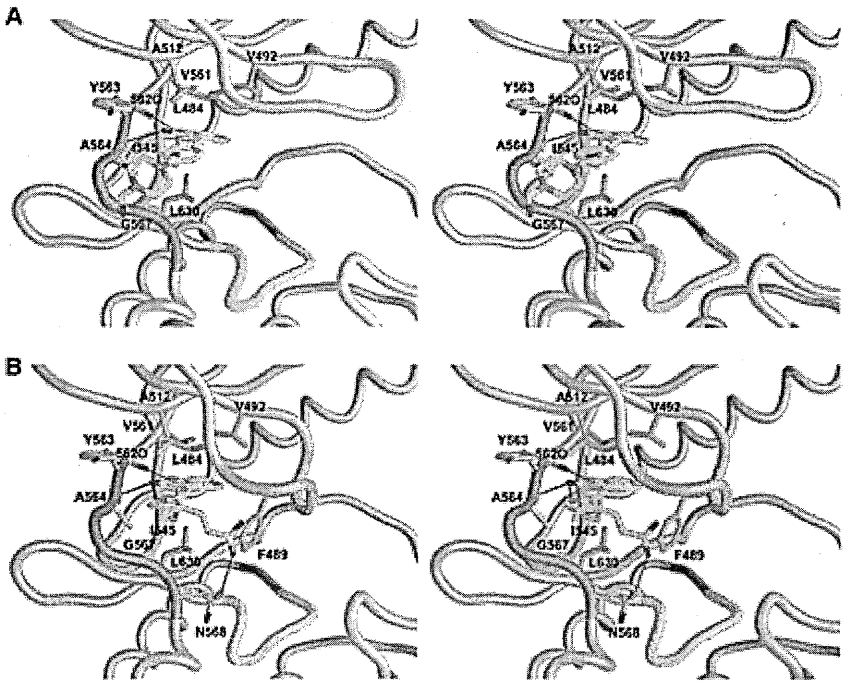

Further studies have been carried out on members of the SUGEN family, indicating an important role of this class as anti-angiogenic agents [134]. In particular, SU5416 (Semaxinib) showed inhibitory activity against the c-KIT and FLT3 tyrosine kinases besides to those against VEGFR [135-137]. It has been used in phase I clinical trials for the treatment of metastatic colorectal cancer targeting VEGFR and phase II trials for AML targeting c-KIT [138]. In this study SU5416 was administered to c-Kit-positive patients, who were resistant to conventional therapies for acute myeloid leukaemia (AML). Eight of 42 patients achieved a morphological or partial response, without showing major side effects: the main toxicities being nausea, headache and bone pain.

Strong levels of c-Kit negatively affected the response, while a positive correlation was identified with high VEGFR expression levels, suggesting that the positive effects of SU5416 were mediated by its anti-angiogenic properties and not by the direct growth inhibition of leukemic blasts.

3.3.2 Materials and methods

3.3.2.1 Cell cultures

All cell culture media were supplemented with 100 U/ml penicillin, 100 µg/ml gentamicin, and 2 mM Gln. The murine pro-B cell line Ba/F3 was maintained in RPMI medium with 10% fetal bovine serum (FBS), with CHO-conditioned supernatant as a source of IL-3. Three Ba/F3-derived cell lines expressing RET/PTC2 (here after referred to as Ba/PTC), NMP/ALK (Ba/NA, [139]) and BCR/ABL (Ba/BA, [140]) were generated following successful transfection cells with the corresponding fusion cDNA and the selection of stable transfectants using 1 mg/ml G418. These cells were kept in RPMI plus 10% FBS without IL-3. TPC-1, and NPA (human papillary thyroid carcinoma cell line, harbouring RET/PTC1 and B-RAF V600E, respectively) were grown in Dulbecco's modified Eagle's medium (DMEM) containing 10% FBS. Parental NIH-3T3 and NIH-3T3 cells stably transfected with RET/PTC2 (NIH-PTC2) and RETV804M mutant (NIH-V804M) were cultured in DMEM with 10% (parental cells) or 5% FBS. The insect cell line Sf9 was kept at 27 °C in SF900-II medium (Invitrogen) with 10% FBS and 0.1% Pluronic F-68.

3.3.2.2 Antibodies and inhibitors

Antibodies were used in western blotting according to recommended dilutions. Anti-HisG antibody (Invitrogen) is directed against the 6xhistidine tag followed by a glycine. Anti-RET (C-19, Santa Cruz Biotechnology, Santa Cruz, CA, USA) recognizes the short isoform of wild-type RET; anti-phospho-RET (recognizing phosphotyrosine 905

of wild-type RET), anti-phospho-JNK1/2 (which detects active diphosphorylated (Thr183/Tyr185) JNK1 and JNK2) and anti-JNK1/2 antibodies were from Cell Signaling Technology (Danvers, MA, USA). Anti-phosphotyrosine (4G10) was purchased from Upstate Biotechnology (Charlottes-ville, VA, USA); anti-ERK1/2 and anti-phospho-ERK1/2 (Thr183/Tyr185) were from Sigma; anti-p21/WAF1 (Ab-1) and anti-p27 (C-19)-G antibodies were bought from Merck Biosciences (Darmstadt, Germany) and Santa Cruz Biotechnology respectively.

SU5416 was purchased from Calbiochem, dissolved in dimethyl sulfoxide (DMSO), aliquoted and stored at –20 °C until used.

3.3.2.3 Proliferation assay and growth curve

Serial dilutions of kinase inhibitor were prepared in cell culture medium with 1% FBS in 96-well plates. Cells were then resuspended in 1% FBS medium and added to the plate at 10^4cells/well. Cell proliferation was measured at 72 h using the tritiated-thymidine incorporation assay as described previous [141]. Each data point was done in triplicate.

For growth curves, Ba/F3 and Ba/PTC cells were seeded (10^5/well) in 24-well plates in triplicate and treated with DMSO or various concentrations of SU5416. The cells were counted using a Trypan Blue exclusion assay every second day, diluted to keep them in logarithmic growth phase and fresh inhibitor was added.

3.3.2.4 Western blot analysis of cell extracts

Ba/PTC cells were grown overnight in 1% FBS and treated with SU5416 or DMSO for 4 h. They were then washed with PBS and lysed in 1 x Laemmli buffer (62.5 mM Tris–HCl, pH 6.8, 2% SDS, 10% glycerol, and 0.3 M ß-mercaptoethanol). Total lysates corresponding to 3 x 10^5 cells were loaded on SDS-PAGE, transferred to nitrocellulose membrane and probed with anti-RET and anti-phospho-RET antibodies.

TPC-1 cells (6 x 10^6) were seeded in 100 mm cell culture dishes, grown overnight in 1% FBS and treated with SU5416 or DMSO. Cell lysates were prepared after washing with PBS, by scraping the cells in lysis buffer (25 mM TrisHCl, pH 7.9, 150 mM NaCl, 1% NP-40, 1 mM EDTA, 2 mM EGTA, 10 mM NaF, 1 mM Na3VO4, 1 mM DTT, 1 mM PMSF, 1 µg/ml leupeptin and aprotinin) and incubating for 40 min on ice. The lysates were then centrifuged for 30 min at 13 000 r.p.m. at 4 °C and the total protein content of the supernatants was measured by the Bradford assay. Equal amounts (100 µg) of total protein were loaded on SDS-PAGE and analyzed by western blotting using phospho-specific antibodies.

3.3.2.5 Soft-agar growth assay

NIH-PTC-L cells were seeded in six-well plates at 1 x 10^4 cells/well in a medium containing 0.33% low melting agar (type VII, Sigma) and either DMSO or 20 µM SU5416, on a layer of 0.5% agar, as described [40]. Fresh inhibitor was added every 3 days to the top layer. The colonies were counted after 15 days.

3.3.2.6 Cell-cycle analysis

Cells were seeded in six-well plates at a density of 2 x 10^5/well and treated with inhibitor or DMSO. Cells were harvested at 24, 48, and 72 h after treatment, washed with PBS and fixed in 70% ethanol at –20 °C. The samples were then centrifuged and resuspended in PBS containing 50 μg/ml propidium iodide and 100 μg/ml RNase A, incubated at 37 °C for 30 min and analyzed by FACScan flow cytometer (Beckton Dickinson, Franklin Lakes, NJ, USA).

3.3.2.7 ATP competition assay

Increasing doses of ATP (0.011–2.4 mM) were incubated with rRET in the presence of DMSO, or 0.05, 0.25, and 1.25 μM SU5416, and an ELISA kinase assay was performed as previously described [52]. ATP binding curves were then calculated for each inhibitor concentration and plotted using the Lineweaver–Burke method.

3.3.2.8 *In vivo* target modulation

Female CD-1 nu/nu mice (7–9 weeks old) were supplied by Charles River (Calco, Como, Italy) and kept under standard laboratory conditions according to the guidelines of the Istituto Nazionale Tumori (INT), Milan, Italy. All animal studies were approved by the Ethics Committee for Animal Experimentation of INT. Mice were implanted subcutaneously with NIH-PTC cells (10^6 cells/mouse). When the tumours were measurable, the mice received an acute intraperitioneal dose of 50 mg/kg SU5416 in 60 μl DMSO, or DMSO alone. Mice were sacrificed 6 h after treatment and their tumours resected and snap frozen on liquid nitrogen. Tumour mass was minced in lysis buffer

and lysates were then prepared as described earlier. Equal amounts of total protein were loaded on 8% SDS-PAGE and visualized by western blot with anti-RET and anti-phospho-RET antibodies.

3.3.2.9 Molecular modelling

A model of the tertiary structure of the RET tyrosine kinase domain in an active conformation was built by homology modelling, using the phosphorylated active insulin receptor kinase domain (Protein Data Bank entry, 1IR3 [PDB]) as a template. The amino acid sequence similarity between the RET and IRK domains is 57%. The model was refined using AMBER 6 software for computing molecular dynamic simulations. The model of V804M mutant RET was built by changing Val-804 of wild-type RET model into a methionine; local side chain minimization was then performed with the Tripos force field and Powell method, with a convergence criterion of 0.05 kcal/mol, using Sybyl 7.0 (Anonymous). The binding mode of SU5416 to wild-type and V804M mutant RET was evaluated by molecular docking, using the GOLD algorithm (Tripos Inc., St. Louis, MO, USA).

3.3.2.10 Inhibitor specificity profiling

Radioactive kinase assays were performed at room temperature in the presence of substrate peptides, $[^{33}P]$ATP, and 10 μM SU5416, using recombinant kinases obtained from various expression systems. Procedures for purification and assay of 30 of the 52 kinases have been determined [142, 143]. The other enzymes will be described elsewhere. Kinase assays were performed using ATP concentrations close to the Km

value for each kinase. All protein kinases were grouped accordingly into three categories, namely 5, 20, and 50 μM ATP.

3.3.2.11 Statistical analysis

Data were always generated in triplicate and mean ± S.D. is reported on graphs. Dose–response curves were normalized over the DMSO control and analyzed by non-linear regression using Graph Pad PRISM 4.0 software. IC_{50} data are reported as the global fitting of at least three independent experiments, with 95% confidence interval (CI).

3.3.3 Results

3.3.3.1 SU5416 inhibits RET kinase activity *in vitro*

A series of compounds sharing a 2-indolinone core structure was identified by molecular modelling as possible candidates for producing RET inhibition. These compounds were in an *in vitro* ELISA-based kinase assay (ref. 3.2.2.12), using the recombinant enzyme and an exogenous peptide as a substrate, as previously described, in order to confirm the computational results. The results described in Chapter 3.2 demonstrated that rRET could be inhibited by small molecule compounds and used as reagent in the inhibitors screening. The peptide SRDVYEEDSYVKRSQGRIPVK derived from the RET activation loop was phosphorylated on tyrosine during the kinase reaction. In presence of the inhibitors, the block of rRET kinase activity was observed and quantified using the colorimetric reaction.

The results reported in Table 3.2.1 are the IC_{50} values of 2-Indolinone derivatives tested:

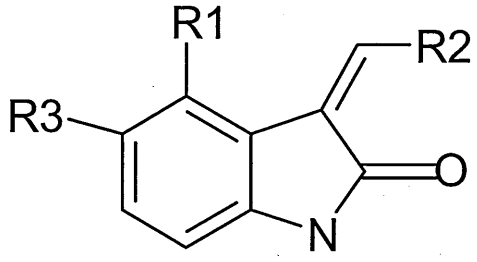

Compound	R1	R2	R3	RET IC50
A	CH3	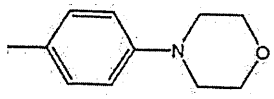	-	100

B	CH3	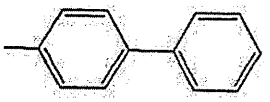	-	23
1	CH3	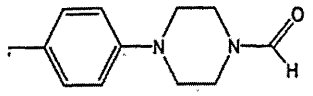	-	3,7
SU4984	-	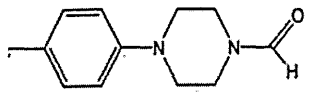	-	1,1
C	CH3	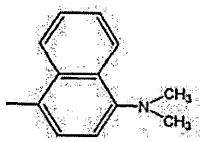	-	0,21
MAZ51	-	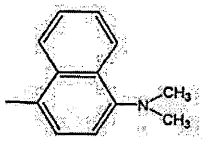	-	45
A2	-	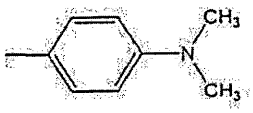	-	>100
A3	-	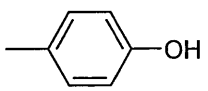	-	2,3
RPI-1	-	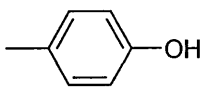	OCH3	28
3	-	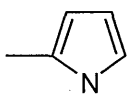	-	0,46
SU5416	-	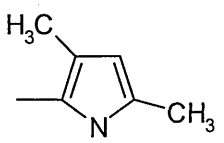	-	0,17
SU6656	-	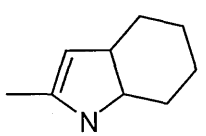	$SO_2N(CH_3)_2$	0,77

SU5614	-	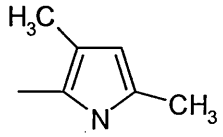	Cl	1
VEGFR2KI-II (676485)	-	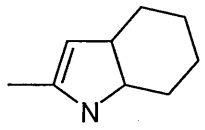	Br	1,74
VEGFR2KI-I (676480)	-	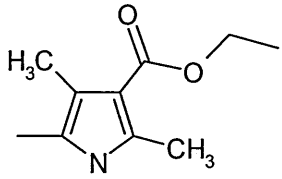	-	0,76
SU9516	-	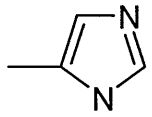	OCH3	1,57
SU11248	-	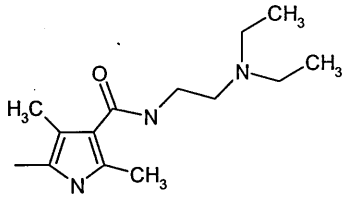	F	1,3
PM0	-	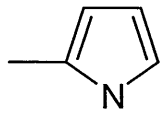	CH3	>30
PM01	-	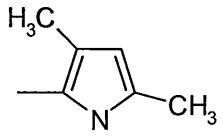	CH3	8
AM0	-	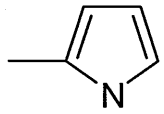	NH2	0,3
AM06	-	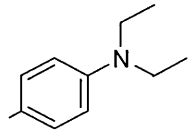	NH2	1,1
AM07	-	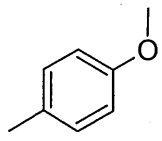	NH2	7,5

AM07u	-	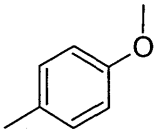	NH2	0,7

Table 3.2.1 2-indolinone compounds screened in ELISA assay; R1, R2, R3 represent the substitutions of 2-indolinone core. For each compound IC_{50} on RET kinase has been reported.

We focussed our attention on SU5416 because seemed to be the most promising compound of all of those screened.

SU5416

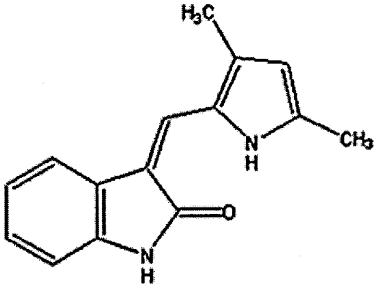

Figure 3.2.1 Chemical structure of SU5416

SU5416 inhibited RET with an IC_{50} of 170 nM, using 300 μM ATP in ELISA assay (Figure 3.2.2 A) It also showed a similar degree of inhibition on FLT-3 kinase, a well-known target in the same assay, but was much less active against the ABL and ALK kinases. An autophosphorylation assay of rRET was performed in order to confirm the data. Significant inhibition was seen at only 0.1 μM, supporting the finding that SU5416 is a RET inhibitor (Figure 3.2.2 B). The same membrane was stripped and developed with anti-HisG antibody to confirm that similar amounts of protein have been loaded (Figure 3.2.2 B).

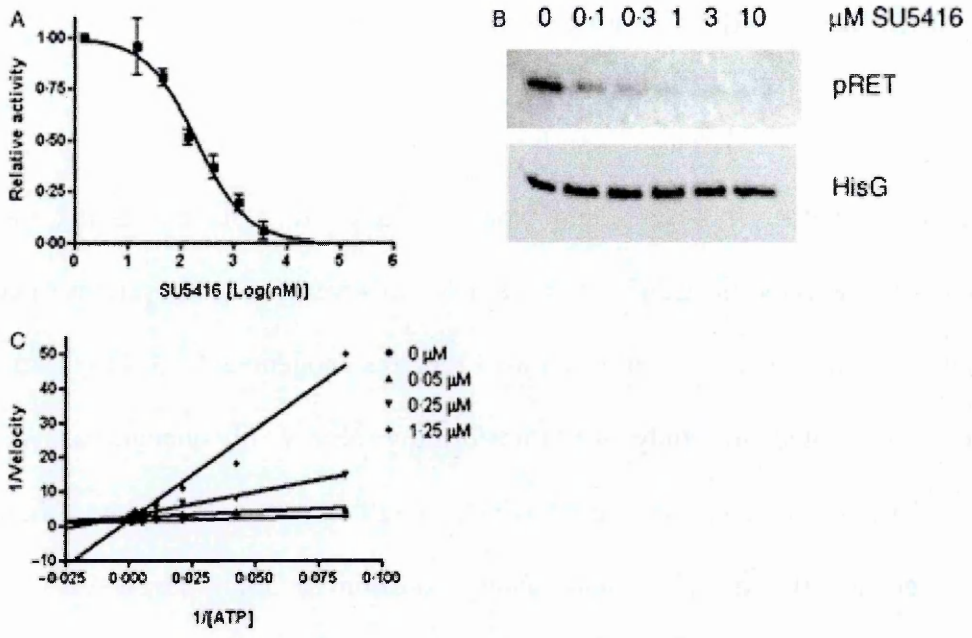

Figure 3.3.2 rRET inhibition by SU5416: (A) ELISA assay; (B) autophosphorylation assay developed by anti-phosphotyrosine-905 Western blotting (upper panel); anti-HisG western blot is shown in the lower panel as a loading control. (C) Lineweaver-Burke plot of competition of SU5416 with ATP .

To determine the mechanism of inhibition, an ATP competition assay was performed, based on the ELISA kinase assay. The ATP dose–response curves in the presence of different inhibitor concentrations showed that the Vmax was not altered by the compound, whereas the Km for ATP increased with increasing inhibitor concentration. Similarly, dose–response experiments performed at different ATP doses indicated that the IC_{50} of the compound increased progressively from 0.05 µM (at 11 µM ATP) to over 6 µM (with 3 mM ATP): all these data supported an ATP-competitive behaviour, in agreement with virtual docking data which showed that SU5416 binds within the ATP-binding pocket (ref. 3.3.3.5) The calculated Ki of compound SU5416 for RET was 13 nM.

3.3.3.2 Inhibition of RET-mediated transformation

Having established SU5416 as a good inhibitor of RET in cell-free conditions, I sought to determine whether the compound would be toxic to cells expressing the RET oncogene. The activity of SU5416 was evaluated in several cellular systems to confirm the results. The murine pro-B cell line Ba/F3 requires exogenous IL-3 for growth and is commonly exploited to study the transforming ability of oncogenes. A stably transfected Ba/F3 clone expressing RET/PTC2 (Ba/PTC) was established. These cells grow independently of IL-3 and show constitutive high levels of tyrosine-phosphorylated proteins. Treatment with 2 μM PP1 significantly blocked the growth of the Ba/PTCs thus validating the assay. The addition of SU5416 blocked the proliferation of Ba/PTC cells in a dose-dependent manner, with an IC_{50} of 7.9 μM (95% CI, 6.8–9.1 μM), while sparing parental Ba/F3 cells. Results are shown in Figure 3.3.3 A-B The observed proliferation arrest correlated with a strong inhibition of RET/PTC2 phosphorylation, as shown by the anti-phospho-RET western blot of total lysates (figure 3.3.3 C). Densitometric analysis of phosphorylated bands revealed an IC_{50} of approximately 5 μM, consistent with proliferation data. The RET expression level was not affected by the treatment. In line with the results obtained in ELISA, the treatment with SU5416 only marginally affected the proliferation of NPM/ALK- and BCR/ABL-transfected Ba/F3 cells, which showed IC_{50} values between 30 and 40 μM.

Finally, a time-course experiment was carried out by exposing Ba/F3 and Ba/PTC cells to SU5416 for 10 days. The growth of Ba/PTC cells was progressively delayed with increasing SU5416 concentrations, while Ba/F3 cells were not affected. Results are showed in figure 3.3.3 D.

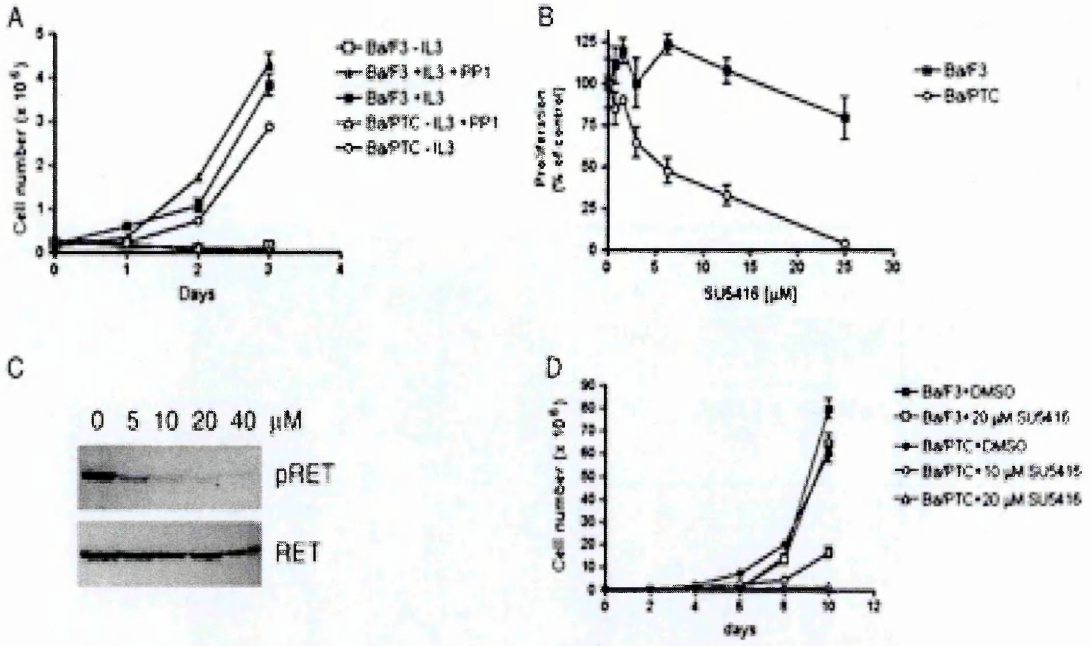

Figure 3.3.3 (A) Growth curves of Ba/F3 parental cells and RET/PTC2 stable transfectants Ba/PTC, with and without IL-3 and PP1. (B) Dose-response curves of SU5416 in a ^{3}H-thymidine uptake assay of Ba/F3 and Ba/PTC cells. DMSO-treated controls are set as 100%. (C) Analysis of Ba/PTC total lysates, after 4 hours treatment with SU5416 at the indicated concentrations. D) Time-course of Ba/F3 and Ba/PTCcells without (black symbols) and with different SU5416 doses.

Another cellular model frequently used for oncogene studies is represented by NIH-3T3 murine fibroblasts. The expression of RET/PTC oncogenes induces anchorage-independent growth [50] and morphological changes in NIH-3T3 cells. Moreover, while the parental NIH-3T3 cells grow as a monolayer, RET/PTC-transfected cells are not inhibited by cell contact and form foci. Inhibition of RET kinase activity restores the parental phenotype [64]. We treated NIH-PTC2 cells with 10 μM SU5416, causing complete RET inactivation, as shown by the lack of activation loop phosphorylation (Figure 3.3.4 A). After 48 h of SU5416 treatment, we observed that the morphology of cells reverted to a flattened, non-dense appearance (Figure 3.3.4 D), similar to parental cells shown in figure 3.3.4 B, indicating blockage of RET tyrosine kinase signalling. By contrast, DMSO-treated cells maintained a transformed phenotype (Figure 3.3.4 C). NIH-PTC2 cells treated with SU5416 were no longer able to grow in soft agar medium,

or form transformation foci (Figure 3.3.4 E-F-G). These data suggest that SU5416 is able to abrogate the transforming potential of the RET/PTC2 oncogene.

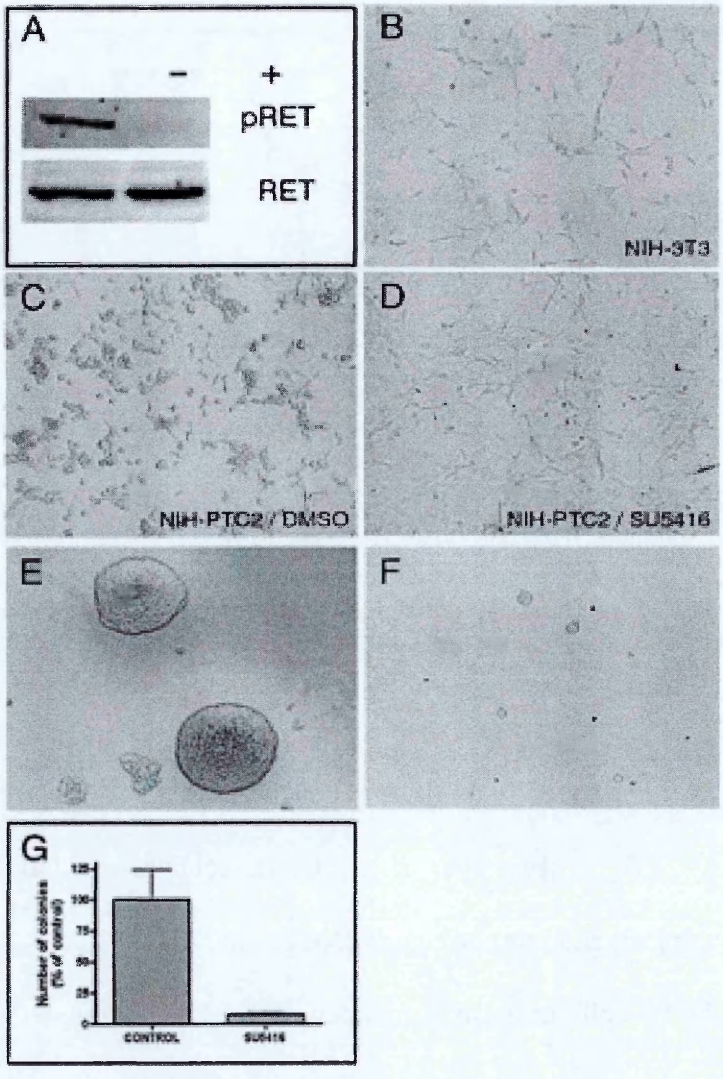

Figure 3.3.4 (A) Cells were treated with DMSO (-) or 10 μM SU5416 (+) for 4 hours and lysed. Total lysates were run on SDS-PAGE and probed with anti-phosphoRET^{Y905} (top panel) and anti-RET (bottom panel) antibodies. Photographs of parental NIH-3T3 cells (B) and NIH-PTC2 cells treated with DMSO (C) or 10 μM SU5416 (D) for 48 hours. (E-G) NIH-PTC2 cells were seeded in soft agar medium without (E) or with 20 μM SU5416 (F). After two weeks, large colonies were counted and photographed. Percent number of colonies is reported in (G). All pictures were taken at the same magnification.

The previous results were obtained from transfected cell lines and so it was necessary to confirm them in human cell lines expressing RET/PTC fusion proteins: these systems, established from human tumours, demonstrating more physiological similarity to human

PTCs. TPC-1 cells are derived from PTC and express the RET/PTC1 fusion kinase. The proliferation of TPC-1 cells was inhibited in the presence of SU5416, with an IC_{50} of 2.7 μM (95% CI, 2.3–3.2 μM). In contrast, NPA, a RET-negative papillary carcinoma cell line carrying the V600E B-Raf mutation, was much more resistant to the treatment showing 50% inhibition at 40 μM (Figure 3.3.5 A). The proliferative block of TPC-1 cells correlated at the molecular level with a complete shut off of RET/PTC1 Tyr-905 phosphorylation, after 8 h treatment (Figure 3.3.5 B). Tyr-905 (numbering refers to wild-type RET) is a main switch of RET catalytic activity. As SU5416 induced the inactivation of RET/PTC1 kinase, an investigation was carried out into whether the downstream signalling pathways were affected by the treatment. RET oncogenes have been shown to activate a number of proliferative and anti-apoptotic signals, including the RAS/ERK and the JNK pathways, as reported in previous section (ref 1.3.1.3). In TPC-1 cells treated with SU5416 for 36 h, a reduction of both ERK1/2 and JNK1/2 phosphorylation was observed, concomitantly with a block of RET/PTC1 phosphorylation (Figure 3.3.5 C). The relative phosphorylation inhibition of p44 and p42 ERK was 90 and 75% respectively, as determined by densitometric analysis of the bands. The phospho-JNK signal in treated cells was reduced by 60%.

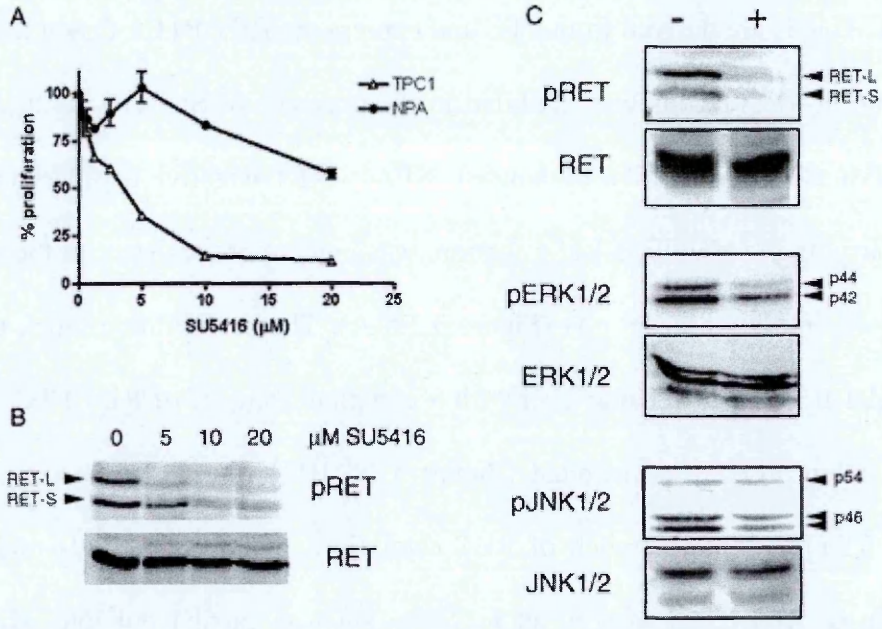

Figure 3.3.5 (A) Effect of SU5416 on the proliferation rate of TPC-1 and NPA cells. (B) Dose-dependent inhibition of RET phosphorylation in TPC-1 cells. Both RET/PTC1 isoforms are detected by the antibody. Total RET is shown below for loading control.(C) TPC-1 cells were treated for 36 hours with DMSO (-) or 25 μM SU5416 (+) and lysates probed with the indicated phospho-specific and total protein antibodies.

3.3.3.3 *In vivo* modulation of RET autophosphorylation

To determine whether SU5416 is able to block RET activity *in vivo*, nude mice were inoculated subcutaneously with NIH-PTC cells. These cells grow as a xenograft with high efficiency [40] and formed palpable tumours within 10 days. At day 14 after implantation, tumour-bearing mice were treated with either a single dose of inhibitor, or vehicle alone, for 6 h. Western blot analysis of the resected tumours showed inhibition of RET autophosphorylation on Tyr 905 in treated animals, when compared to control mice (Figure 3.3.6). RET protein levels were left unaffected by the treatment. This result indicated that RET catalytic activity was shut down in the tumours and confirmed SU5416 as a potent RET inhibitor.

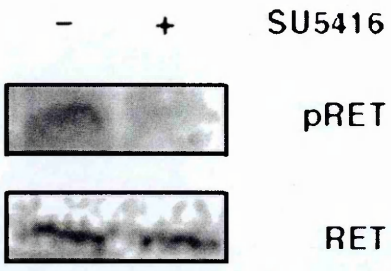

Figure 3.3.6 Western blot analysis performed on tumor lysates, using anti-phospho-RET (top panel) or anti-RET (bottom panel) antibodies.

3.3.3.4 Activity of SU5416 on mutant RET

The sensitivity of tyrosine kinases to different classes of inhibitors appears to be modulated by a key residue regulating access to the ATP-binding site, named the "gate-keeper residue". The corresponding amino acid in wild-type RET is a valine, which is small enough to accommodate inhibitors within the ATP pocket, as demonstrated in diffracted structure described above. However, disease-associated mutations at Val-804 confer resistance to inhibition by PP1, PP2, and ZD6474 [54]. A V804M rRET protein, was used in the current study to investigate the inhibitory effects of SU5416. Surprisingly, SU5416 did not inhibit the mutant RETV804M recombinant protein, 50% inhibition was not reached at concentrations up to 30 μM. In contrast, SU4984, the compound that inhibited FGFR1 V561M mutant [55], blocked both wt RET and RETV804M with similar IC_{50}, namely, 1.3 vs 2.6 μM (Figure 3.3.7 B). The growth of mutant RETV804M-expressing NIH-V804M cells was not affected by SU5416 up to 10 μM, thus confirming that SU5416 is incapable of blocking V804M-substituted RET kinase. In keeping with this result, phosphorylation of RETV804M was not inhibited in these cells. (Figure 3.3.7 C)

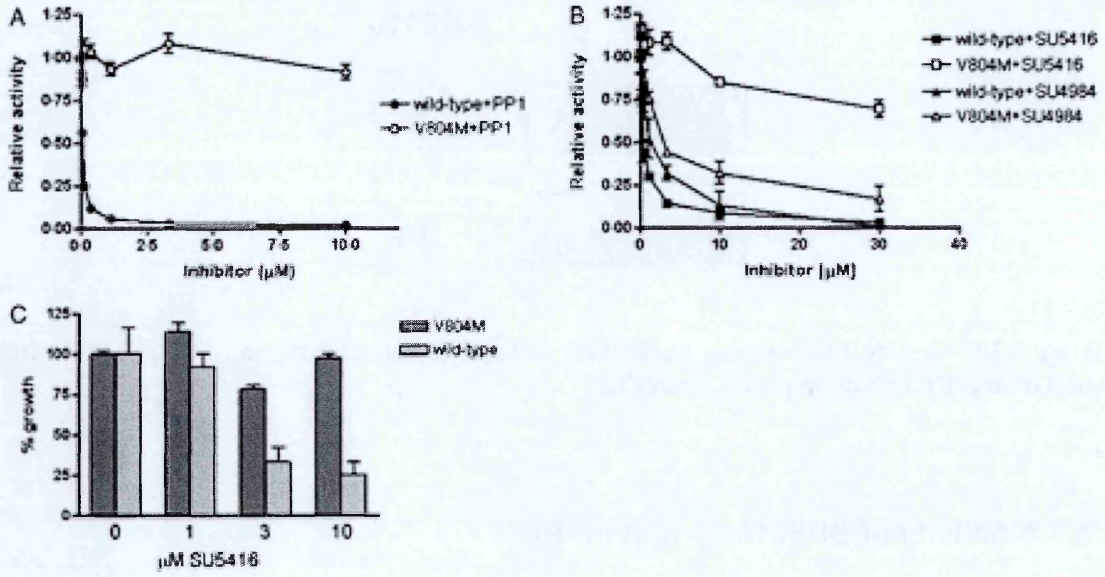

Figure 3.3.7 (A-B) ELISA kinase assay showing dose-response curves of wild-type RET and RET^{V804M} incubated with PP1 (A) or with SU5416 and the related compound SU4984 (B). (C) NIH-PTC2 (wild-type) and NIH-V804M cells were treated with increasing doses of SU5416 for 72h and counted.

3.3.3.5 Molecular modelling

To explain this unexpected result, a computational model of the active RET kinase using the insulin receptor kinase as a template was generated in our lab. Molecular docking of SU4984 within the ATP-binding site of RET revealed an orientation of this compound that corresponded very well with the one observed in the crystal structure of the inhibitor in complex with FGFR1 kinase [17]: this is in keeping with the high degree of similarity between the FGFR1 and RET molecules. The oxindole core is positioned at the same region as the adenine ring of ATP and makes two hydrogen bonds with the backbone of the RET hinge region. The carbonyl oxygen of E805 interacts with the indolinone nitrogen, while the amide nitrogen of A807 is in contact with the oxygen atom of the inhibitor, in exactly the same corresponding positions of FGFR1. In addition, several hydrophobic residues surround the cavity in which the inhibitor binds, thus contributing to the stabilization of compound binding. The C3 substituent points

towards the outside of the pocket. Docking of SU5416 showed a similar binding mode, with two hydrogen bonds with the protein backbone. When docked onto mutant RETV804M, SU5416 could not bind in the same way, because of a clash with M804. The software did find a docking solution, but the inhibitor was flipped to 180° with respect to wild-type docking, losing both hydrogen bonds. This may explain the resistance to inhibition. The docking of inhibitor SU4984, instead, was only partially affected by the mutation. The compound is slightly pushed outwards because of the presence of the bulkier methionine but, while it loses one H-bond (with E805), this is compensated for a new interaction between Y806 and the N1 of the piperazine ring. The conservation of one interaction with the hinge region and the establishment of a new interaction by the phenyl–piperazinyl moiety of SU4984 suggest that its activity on RET mutant kinase should not be significantly reduced (Figure 3.3.8).

Figure 3.3.8 (A) Compound SU4984 from the crystal structure of the complex FGFR1-SU4984 (1AGW) (C, magenta; O, red; N, blue) and from GOLD calculation (C, green; O, red; N, blue) superimposed on the model of RET. The nucleotide binding loop (yellow), the DFG motif (blue), the activation loop (orange) and the hinge region (red) of RET are indicated. Figure generated by Sybyl 7.0 [144]. (B-E) Schematic representation of SU5416 interactions with models of RET^{wt} (B) and RET^{V804M} (C) and SU4984 interactions with RET^{wt} (D) and RET^{V804M} (E). Residues forming Van der Waals contacts are indicated; those involved in H-bonding are shown in ball-and-stick representation. H-bonds are shown as dotted lines with distance given in Ångström. Figures generated by LIGPLOT [145].

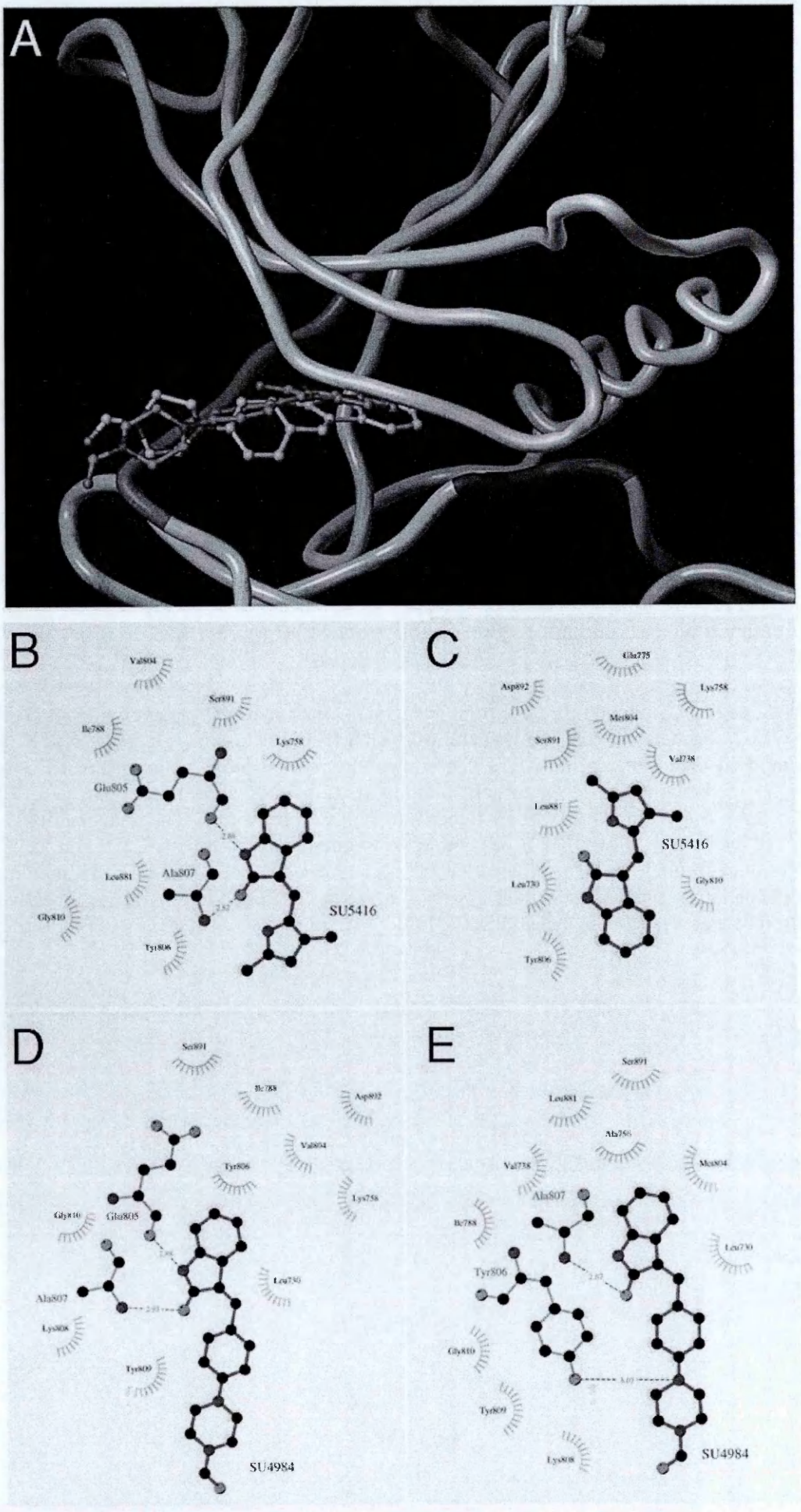
A
B
Val804
Ser891
Ile788
Lys758
Glu805
Leu881
Ala807
Gly810
Tyr806
SU5416
C
Glu775
Asp892
Lys758
Met804
Ser891
Val738
Leu881
SU5416
Leu730
Gly810
Tyr806
D
Ser891
Ile788
Asp892
Val804
Tyr806
Lys758
Gly810
Glu805
Ala807
Leu730
Lys808
Tyr809
SU4984
E
Ser891
Leu881
Ala756
Val738
Met804
Ala807
Ile788
Leu730
Tyr806
Gly810
Tyr809
Lys808
SU4984

3.3.3.6 Specificity of SU5416

SU5416 was discovered as a VEGFR2 inhibitor, with some activity against PDGFR but no inhibition of EGFR, HER2, and IGF1R [146]. It was later shown to inhibit FLT-3 and c-Kit tyrosine kinases at nanomolar concentrations [135], as well as c-Src, MET, FGFR1, and Zap70 at micromolar doses [135, 147]. As for several other kinase inhibitors, initial assumption of selectivity was due to limited experimental testing. Therefore, the specificity profile of SU5416 was investigated further by analysing its inhibitory activity on a panel of 52 available protein kinases belonging to different classes, at 10 μM inhibitor, a concentration that causes 97% inhibition the activity of RET kinase. In order to perform this experiment SU5416 was sent to Prof. Cohen's lab in the MRC protein phosphorylation unit, School of life science, at the University of Dundee (United Kingdom). As reported in Table 3.3.2, c-Src was inhibited by approximately 50%, in line with previous reports, while Src-related Lck was 70% inhibited. In addition, we found four serine/threonine kinases that showed less than 10% residual activity in the presence of the inhibitor, phosphorylase kinase (PHK), the checkpoint kinase Chk2 [148], the centromere-associated kinase Aurora B, which is often over-expressed in cancer cells [149], and mammalian Ste20-like kinase 2 (MST2), a pro-apoptotic factor [150]. Four other kinases (MAPKAP-K1a and 1b, SGK, and p70S6K) were substantially (>80%) but not completely inhibited by 10 μM SU5416.

Protein kinase	Activity (% of control)	Protein kinase	Activity (% of control)
AMPK	43 ± 8	MSK1	38 ± 4
Aurora B	5 ± 2	MST2	6 ± 1
CAMK-1	67 ± 2	NEK2a	55 ± 1
CDK2/cyclin A	92 ± 5	NEK6	91 ± 8
CHK1	29 ± 6	NEK7	88 ± 3
CHK2	7 ± 2	p70 S6K	19 ± 1
CK1	21 ± 4	PDK1	58 ± 6
CK2	81 ± 8	PHK	4 ± 0
CSK	95 ± 6	PIM2	94 ± 2
DYRK1a	50 ± 2	PKA	78 ± 1
EFK2	80 ± 1	PKBΔph	81 ± 1
ERK8	55 ± 3	PKBb	89 ± 1
GSK3b	85 ± 5	PKCa	99 ± 7
IKKb	100 ± 6	PKD1	43 ± 0
JNK/SAPK1c	86 ± 2	PLK1	85 ± 8
JNK3	75 ± 1	PRAK	66 ± 4
Lck	27 ± 5	PRK2	47 ± 1
MAPK2/ERK2	73 ± 1	ROCK-II	59 ± 2
MAPKAP-K1a	12 ± 3	SAPK2a/p38	73 ± 0
MAPKAP-K1b	16 ± 4	SAPK2b/p38ß2	86 ± 3
MAPKAP-K2	103 ± 2	SAPK3/p38g	78 ± 2
MAPKAP-K3	80 ± 7	SAPK4/p38d	70 ± 7
MARK3	31 ± 2	SGK	14 ± 4
MKK1	23 ± 2	smMLCK	23 ± 4
MNK1	78 ± 0	Src	51 ± 4
MNK2	92 ± 1	SRPK1	68 ± 2

Table 3.3.2 Specificity activity of SU5416 in a wide range of protein kinases

3.3.4 Discussion

In a preliminary screening of potential RET inhibitors, it was noted that a couple of indolinone compounds showed good inhibition *in vitro*, but poor activity in cell culture. This was largely due to insolubility of the compounds. It was, therefore, decided to test other SUGEN compounds since they share the same oxindole scaffold. Particular attention was focussed on SU5416 because it seemed promising in computational modelling and it had already been demonstrated to possess good inhibitory properties *in vivo*. SU5416 inhibited RET in cell-free kinase assays at nanomolar doses, comparable to the IC_{50} values reported for Flt-3 and c-Kit [151]. Our assay also confirmed that SU5416 to be a potent inhibitor of Flt-3, while it blocked ALK and ABL kinases only at micromolar concentrations. Selectivity of this compound had also been reported by previous studies. Sun et al described SU5416 to be inactive against a number of other kinases, such as EGFR, Her-2, IGF-1R, and weakly inhibited PDGFR [147] and c-Kit [135]. A related molecule, RPI-1, has antitumor activity against thyroid carcinoma in mice [70, 71]. In molecular modelling studies, SU5416 docked in the RET active site, in the same position occupied by other indolinone compounds in crystallisation studies with the related tyrosine kinase, FGFR1. In view of its potency and selectivity and its good pharmacokinetics, and the fact that it is amenable to chemical modifications, the results described in this thesis indicate that SU5416 may be a good lead structure for new, more selective RET inhibitors.

Inhibition of RET by SU5416 was obtained in various model systems, including IL-3-dependent cells, murine fibroblasts and human PTC cells. The growth of RET/PTC-1-expressing TPC-1 cells was selectively growth-inhibited compared to the RET-negative PTC cell line NPA, originating from the same cell type as TPC-1 but carry a B-Raf

mutation as the primary oncogenic lesion. This result indicated that growth inhibition induced by SU5416 is indeed mediated by RET. Involvement of the VEGFRs can be excluded because NPA cells express these receptors and were not affected by SU5416. The compound was toxic to NPA control cells only at high concentrations, possibly because of the non-specific inhibition of other proliferative pathways. Also, the use of stably transfected cell lines, such as the NIH and Ba/F3 expressing i.e. RET/PTC2, helped to define the role of RET oncogene in mediating SU5416 biological effects. Since both parental and transfected cells are genetically identical with the exception of the transgene, the growth arrest observed solely in the latter provides support that RET is the relevant target. Blockage of RET autophosphorylation was observed in TPC-1 cells as early as 8 hours and was followed by reduced signalling through the ERK and JNK pathways. The RAS/RAF/ERK1/2 pathway is known to be activated by RET both in transfectants and in human thyroid carcinoma cell lines, through docking of Shc adaptor proteins to tyrosine-1062 [39, 152]. JNK1/2 MAPKs are normally involved in stress response and induction of apoptosis [153]. In thyroid tissue, activation of JNKs is instead induced by growth stimuli [154, 155]. Indeed, thyroid carcinoma cells are reported to express high levels of activated JNK, both via Dok-1 phosphorylation and through activation of the small GTPase Cdc42 [156]. Our results confirmed the role of these pathways in cellular proliferation, rather than in apoptosis process. Indeed, the inhibition of RET blocked the cellular growth in dose-dependent manner but did not result in apoptosis in TPC-1 cells. This is in agreement with previous reports which showed little or no evidence of cell death after block of oncogenic RET activity [50, 64]. Either these cells are somewhat resistant to apoptosis and need longer exposure to drugs in order to induce programmed cell death, or the oncogenic activity of RET/PTC is mainly exerted by a growth advantage rather than increased survival. Indeed, a multi-

step model of thyroid carcinoma is emerging where RET is a very early event that requires secondary events (such as the loss of p53 expression) to establish full-blown aggressive carcinoma [157]. Cell cycle arrest induced by SU5416 coincided with a significant up-regulation of the CDK inhibitor protein p27, in line with a previous report [158]. Surprisingly, p21 expression was instead down-modulated. The same result was obtained in two independent experiments, using different antibodies. Although we cannot exclude that this effect may be due to unspecific toxicity of the compound, few cases have been described where p21 repression, rather than induction, correlates with cell cycle arrest [159, 160].

Activating mutations at valine-804 of RET kinase domain occur both in sporadic and in familial MTC with aggressive behaviour and are sometimes associated with a second RET mutation. RET^{V804} mutants show resistance to the kinase inhibitors PP1 and ZD6474 [54]. The valine 804 represents the "gate-keeper" residue in the RET kinase domain and, as reported in the Introduction section, the mutations at this position cause resistance to small molecule inhibitors. Replacement of Tyr-315 in ABL by bulkier residues, such as isoleucine, causes resistance to Imatinib. Similarly, PP1 is unable to inhibit c-SrcT341M kinase, or oncogenic v-Src, which carries an isoleucine at the corresponding position [53]. The same phenomenon was observed also for EGFR, FGFR, and PDGFR [55]. On the other hand, changing Phe-691 to a smaller threonine rendered the FLT-3 kinase sensitive to Imatinib [161]. In contrast, three indolinone compounds were found to be insensitive to mutations of the gate-keeper amino acid, suggesting that this class of inhibitors may represent an exception to the rule [55]. The possibility that RET mutant V804M was inhibited by SU5416 was investigated. Using SU5416, no significant inhibition at concentrations that give almost 100% block of wild-type RET activity was detected. This result was in contrast with the proposed

property of indolinone compounds of entering kinases carrying bulky gatekeeper residues [55]. In their work, Blencke et al. [55] showed that three such compounds inhibited wild-type and mutant kinases with similar potency, although at rather high doses. In the current study, however, SU5416 did not alter RET^{V804M} activity even at 30 μM, showing that not all indolinones behave in a similar inhibitory fashion. SU4984, a compound that showed activity on mutant FGFR1 [147] was used as a control in the current study. This inhibitor belongs to the same series of compounds as SU5416, developed by Sun et al [146]. It has 1-log reduced potency against RET, compared to SU5416, possibly because it exists predominantly as the inactive *E* isomer (referring to the configuration of the C-3 substituent). Unlike SU5416, compound SU4984 was able to inhibit mutant RET, as it could be predicted by published results [55]. A possible reason to account for this difference between the two compounds was provided by the molecular modelling study. This demonstrated that, while SU5416 loses hydrogen interactions in RET^{V804M}, SU4984 does not and establishes a new H-bond, Y806. However, it should be noted that Y806 is thought to be phosphorylated in fully activated RET [162]. It is unknown at present whether the enzyme used in the current assay is phosphorylated on this particular residue. Should this be the case, then the interaction would take place only when the piperazine nitrogen is protonated.

Finally, the activity of compound SU5416 on a large panel of protein kinases is described. New targets of SU5416 were identified, including some serine/threonine kinases, unrelated to known target tyrosine kinases. This is of interest, not only for biochemical and biological studies on the newly identified targets, but also as a *caveat* for cell-based studies focused on known targets. In this study, biological effects were always correlated to RET inactivation. Although the possibility that the observations

described here are at least partially due to off-target effects cannot be disregarded, the *in vitro* data support the notion that RET is a direct target of SU5416.

In conclusion, we have shown that SU5416 is a potent fairly selective inhibitor of RET catalytic activity in biochemical and cellular assays and may represent a good starting structure in the search of a selective RET inhibitor, even if it does not inhibit RET^{V804M}.

3.4 Target validation of B-RAF and PLX4032 characterization

3.4.1 Introduction

In this section I analysed the role of B-RAF in cell growth and survival in melanoma and thyroid cancer cells. I used RNA interference (RNAi) technology to validate B-RAF as a potential therapeutic target and characterised a new small molecule inhibitor that was selectively active against this protein.

3.4.1.1 siRNA principles

RNAi is a gene-regulatory mechanism triggered by dsRNAs. Small interfering RNAs (siRNAs) consist of RNA duplexes of 21-23nt in length that are base paired with 2-nt 3' overhangs, whose antisense strand is complementary to target mRNA. siRNAs mimic the intermediates of the natural processing of longer double-stranded RNA triggered by RNAse III enzymes, such as Dicer, which, together with other components of the RNAi machinery, specifically recognize an siRNA duplex and selectively incorporate one of the siRNA strands into RISCs (RNA-induced silencing complex). The RISC includes the catalytic endonuclease-containing complex which is ultimately responsible for the strong gene-knock down effect. The antisense strand to the targeted mRNA is often referred to as the guide strand while its base-paired sense strand is named the passenger strand, which is destroyed upon the incorporation of the guide strand into RISC. The catalytic RISC recognizes mRNAs containing perfect, or near perfect, complementary sequences and cleaves the mRNA at the site precisely 10nt upstream of the nucleotide opposite the 5'-most nucleotide of the guide strand. The mRNA fragments are

subsequently degraded by cellular nucleases, resulting in knockdown of the expression of the corresponding gene.

3.4.1.2 siRNA selection

In order to exploit RNAi as a tool for gene silencing, a number of variables has to be considered for the generation of effective siRNAs.

Although the selection of siRNA against a gene of interest starts with an annotated target mRNA sequence, including its 5'-3' untranslated regions (UTRs), splice, polymorphic and allelic variant, the coding sequence remains the most commonly targeted [163]. Several algorithms have been developed in recent years that rely on the intrinsic sequence and stability features of functional siRNAs [164, 165]. Following selection, each candidate siRNA is examined for similarity to all other mRNA transcripts that might unintentionally be targeted at a genome-wide level. It has been noted that structurally symmetric but primary sequence-asymmetric siRNAs, from which the target mRNA complementary guide strand has been generated, demonstrate a great propensity to be assembled into the RISC than the passenger strand, and show improved efficacy and specificity [166]. Most of the functional siRNAs have a low to medium G+C content ranging between 30-55%. Indeed, too low a G+C content may destabilize the siRNA duplexes and reduce the affinity for target mRNA binding, while too high a G+C content may avoid RISC loading or cleavage-product release [165]. Additionally, stable duplexes without internal repeats or palindromes are the better silencers [167].

Single nucleotide positional preferences into the siRNA sequences have been identified, namely, U or A at position 10, C or G at position 19 and/or A+U richness between position 1 and 7 [168]. These features correlate with the rule of thermodynamic

asymmetry and the preferred nucleotides on the indicated positions may contribute to the bias for the selection of antisense strand, for example, A or U at position 10 may promote the catalytic RISC mediated passenger strand and substrate cleavage [168].

Each strand of the siRNA duplex, once assembled into the RISC, can guide the recognition of fully or partially complementary target mRNAs, named as on and off targets, respectively. Off targets can share contiguous and centrally located sequence complementarity over more than half of the siRNA sequence somewhere within the mRNA sequence [169], as well as show solely 6 or 7 nucleotides of perfect match preferentially in the 3'UTRs with position 2-7 and 2-8 of the guide siRNA [170]. To enforce the specificity, the current strategy is to select siRNAs in which the strand entering in RISC has some mismatches to all undesired target mRNAs [168].

3.4.1.3 Inducible systems

RNAi has the potential to permit the down-regulation of virtually any gene. It is important in many circumstances that this knockdown is externally controllable, for example, to examine the role of certain protein in human pathology. In this case, the effectors of the knockdown can be either short hairpin RNA (shRNA) produced from RNA polymerase III promoters or micro RNA (miRNA)-based shRNA expressed from Pol II promoters [171]. Pol III promoters are ideally suited for the production of shRNAs, as they produce RNA transcripts that lack the polyadenylation tail and have a well-defined transcriptional start site. Repression of an shRNA driven by Pol III promoter can be achieved by placing an *Escherichia Coli* Tet operator (*tetO*) sequence upstream of the transcription start site to interfere with the function of the TATA box through the recruitment of the tetracycline repressor (*tetR*). In absence of the drug, *tetR* binds to *tetO* and the production of shRNA is suppressed. Upon addition of tetracycline

or doxycycline, repression is relieved by sequestration of tetR [172-174]. This was the system of choice used in my work. An inducible system was necessary to produce stably transfected cell lines. In these models, the silencing of B-RAF was modulated and its role in cellular context was evaluated also in long term treatment. Doxycycline was not toxic and did not induce aberrant responses in cells. Furthermore, a shRNA under control of *TetO* was previously used to validate B-RAF in melanoma cell lines [173], thus this system could be efficiently applied also to thyroid model.

Another inducible system is based on the Kruppel associated box (KRAB) domain found in many zinc-finger proteins and that can silence both pol II and pol III promoters by triggering heterochromatin formation. When tethered to specific DNA regions within the context of chimeric proteins, KRAB can induce a general silencing of transcription within up to 3 kilobases from its binding site. When KRAB is fused to the *tetR* DNA binding domain, the resulting tTRKRAB chimeric protein allows for the doxycycline-mediated control of any promoter placed nearby *tetO* sequences, in either tet-on and tet-off configurations depending on the *tetR* version used [175].

The major advantages of pol III promoter- based conditional systems are their demonstrated high activity in most cell types, both *in vitro* and *in vivo*, the small size of the expression cassettes and the robust levels of knockdown achieved with shRNA. One limitation, however, is their lack of tissue-specificity. In contrast, the pol II-based production of miRNA-based shRNA allow tissue-specific knockdown and should be fully amenable to exogenous control, for instance with the tet-KRAB system. Nevertheless, pol II promoter-based systems require that the transcript be processed by the enzyme Drosha to produce shRNA before Dicer-mediated processing yields siRNA, thus adding a level of complexity that may be detrimental in some settings [175].

3.4.2 Materials and methods

3.4.2.1 Cell cultures

Four cancer cell lines were used in this study: the malignant melanoma cell line A375, the anaplastic thyroid carcinoma cell line ARO, the NPA cell line established from a poorly differentiated thyroid carcinoma and the PTC-derived cell line TPC1. A375 were grown in RPMI-1640, other cell lines in DMEM; all media were supplemented with 10% fetal bovine serum (Sigma South America origin), 2mmol/L L-glutamine, 100 units/ml penicillin-streptomycin (Sigma) and 100units/ml gentamycin.

3.4.2.2 Inducible siRNA

To generate the anti-BRAF shRNA construct, the following oligonucleotides were used:

BRAF shRNA-1 (sense)

5'gatccccAGAATTGGATCTGGATCATTTCAAGAGAATGATCCAGATCCAATTC

Tttttggaaa-3',

BRAF shRNA-1 (antisense)

5'tttccaaaaaAGAATTGGATCTGGATCATTCTCTTGAAATGATCCAGATCCAATT

CTggggatc-3' [176].

This sequence was cloned in pTer + vector using Hind III and Bgl II restriction enzymes. The system described by van der Wetering et al. [172] was used. In this system the pCDNA6TR vector encodes for the *Tet repressor* that binds the *TetON operon* in pTER vector; in the presence of doxycycline, the *Tet repressor* leaves the *TetON operon* allowing shRNA expression. A375 and ARO cells were transfected using

the Ca_2PO_4 method firstly with the pCDNA6TR vector and selected with 4μg/ml blasticidin (Sigma Aldrich). Briefly, 3 $x10^5$ cells were seeded in 2 ml of medium in six-multiwell plates (60% confluence). On the following day, the cells were transfected with 1μg of DNA and incubated at 37°C for 8 hours. The medium was then removed, the cells washed with PBS 1X, treated with 1ml of 70% glycerol for one minute and then washed twice again with PBS 1X. The selection procedure was started 72 hours after transfection. Limiting dilutions were performed and each clone was screened by a Luciferase assay (Stop and Glo®, Promega), following the manufacturer's protocol, to evaluate the ratio between induction by doxycycline and repression in absence of the drug. Positive clones were then transfected with the second vector (pTer-BRAF-shRNA-1) and selected with 600μg/ml zeocin (Invitrogen). Stably transfected cell lines were cultured in the appropriate medium, adding blasticidin and zeocin every two passages.

3.4.2.3 Western blot and inhibitors

We seeded 3x 10^5 cells in 2 ml of medium in six-multiwell plate and harvested them after 72 and 96 hours of treatment with doxycycline 1mg/ml or PLX4032 at the indicated doses. Cells were directly lysated in Laemmli buffer and boiled. Western blot was performed with the procedure described before. Antibodies were used in western blotting according to recommended dilutions. Anti-B-RAF (C19) was purchased from Santa Cruz Biotechnology (Santa Cruz, CA, USA), anti-phospho-MEK1/2 (Ser 217-221), anti-MEK1/2, anti-phospho-AKT (Ser473), anti-AKT, anti-p27Kip 1 were from Cell Signalling Technology (Danvers, MA, USA), anti-BCL_{XL} (7B2.5) was from Upstate Biotechnology (Charlottes-ville, VA, USA), anti-$p21^{CIP/WAF}$ was purchased

from New England Biolabs (UK), anti-NIS (clone 2.2) was from Chemicon International (Temecula, CA, USA) and anti-actin from Sigma .

PLX4032 was kindly provided from Plexxikon (Berkeley, CA, USA). The compound was dissolved in DMSO and stored at -20°C until used.

3.4.2.4 Proliferation assay

Serial dilutions of kinase inhibitor were prepared in cell culture medium with 5% FBS in 96-well plates. Cells were then resuspended in 5% FBS medium and added to the plate at 10^4cells/well. Cell proliferation was measured at 72 h using the tritiated-thymidine incorporation assay as described previously [141]. Each data point was done in triplicate.

3.4.2.5 Cell-cycle analysis and apoptosis

Cells were seeded in six-well plates at a density of 2 x 10^5/well and treated with inhibitor or vehicle (DMSO). Cells were harvested at 72 h and 96 h after treatment, washed with PBS and fixed in 70% ethanol at –20 °C over night. The samples were then centrifuged and resuspended in PBS containing 50 µg/ml propidium iodide and 100 µg/ml RNase A, incubated at 37 °C for 30 min and analyzed by FACScan flow cytometer (Beckton Dickinson, Franklin Lakes, NJ, USA).

Annexin V binding assay was performed following manufacturer's protocol (Promega).

3.4.2.6 Adenovirus infection

Adenoviruses were kindly provided by dr Carlo Gaetano (Istituto dermopatico dell'Immacolata, Rome, Italy) [177]. Experiments were performed by plating 3 $x10^5$ cells in 2 ml of appropriate medium with PLX4032 added at the indicated doses. After 24 h the virus was diluted in 1 ml of medium containing 2% FBS, and cells were infected cells by incubation with the diluted virus for 2 h at 37°C. The viral suspension was then removed, fresh medium added and the cells were cultured for 72 h or 96 h. The infection efficiency was evaluated by measuring the fluorescence from green fluorescence protein (present in adenoviral construct as marker of the infection) (GFP) using a FACScan flow cytometer (Beckton Dickinson, Franklin Lakes, NJ, USA).

3.4.2.7 Statistical analysis

Data were always generated in triplicate and mean ± S.D. is reported on the graphs. Dose–response curves were normalized over the vehicle control and analysed by non-linear regression using Graph Pad PRISM 4.0 software. IC_{50} data are reported as the global fitting of at least three independent experiments, with 95% confidence interval (CI).

3.4.3 Results

3.4.3.1 B-Raf validation

An inducible siRNA under control of doxycycline was established to validate B-Raf as a target for a therapeutic intervention. The ARO cell line, derived from anaplastic thyroid carcinoma, was used as the test model. These cells are heterozygous for a B-RAF mutation (V600E/wt B-RAF) and also carry an inactivating mutation on the hemizigous p53 allele [178]. As described above, ARO cells were transfected with two plasmids: the first encoding for the Tet Repressor protein while the second one encodes for the siRNA sequence. After the first transfection, those clones that showed the highest luciferase expression in presence of doxycycline and the strongest repression in absence of the compound were selected. The selection was performed using a luciferase assay and only those clones with induction/inhibition ratio of more than 3 were considered for further culture. Since siRNA is an autocatalytic system, the control of the repression in absence of doxycycline was more important than the induction. After the second transfection, the silencing of the B-RAF protein and the consequent downregulation of downstream pathways were evaluated after 72h or 96h of treatment with doxycycline (1μg/ml). In particular, the effects on MEK phosphorylation (the direct substrate of B-RAF in the MAPK pathway) were studied. The stably transfected A375 malignant melanoma cell line, homozygous for B-RAF mutation (V600E/V600E) and p53 wild type was used as a control. The efficient siRNA silencing of B-RAF on this cell line has recently been published [173].

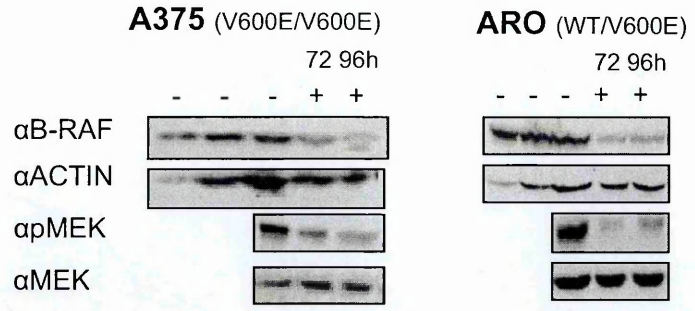

Figure 3.4.1 Down-regulation of B-RAF protein by siRNA after 72 or 96 hours of doxycyclin treatment, in melanoma (A375) and anaplastic thyroid carcinoma (ARO) cell lines. Dilutions of untreated cells (-) lysates were loaded in order to evaluate the silencing (from left to right: 5, 10, 15 µl); 15 µl of treated cells (+) lysates were loaded. MEK1/2 phosphorylation was inhibited in correspondence of B-RAF modulation. Anti-actin and anti-MEK1/2 immunoblotting are shown as loading controls.

From Figure 3.4.1 it can be seen that B-RAF was silenced by >70% in both cell lines after 72 hours compared to untreated controls. A further decrease in expression levels was observed by prolonging the treatment till 96h. MEK phosphorylation was also down-regulated in correlation with the reduced levels of B-RAF. No changes in MEK were, however, detected.

Cell growth was delayed in the ARO cell line and arrested in the A375 melanoma cell line in comparison with un-treated cells (Figure 3.4.2) and cells transfected only with the first plasmid (not shown). Furthermore, cell cycle analyses showed an important increase the number of cells in the subG1 fraction in the A375 cell line with a consequent decrease in G1 population and an increase in G2/M, suggesting increased apoptosis and mitotic block. In contrast, only the G2/M fraction significantly decreased in the ARO cells, suggesting a decrease rate in cell proliferation. These experiments were accomplished with 96h treatment at the indicated dose of doxycycline. The induction of the apoptotic process in melanoma in consequence to B-RAF silencing was previously observed [173, 179]. In anaplastic thyroid carcinoma B-RAF/MAPK pathway was likely to comprise main survival mechanisms [180].

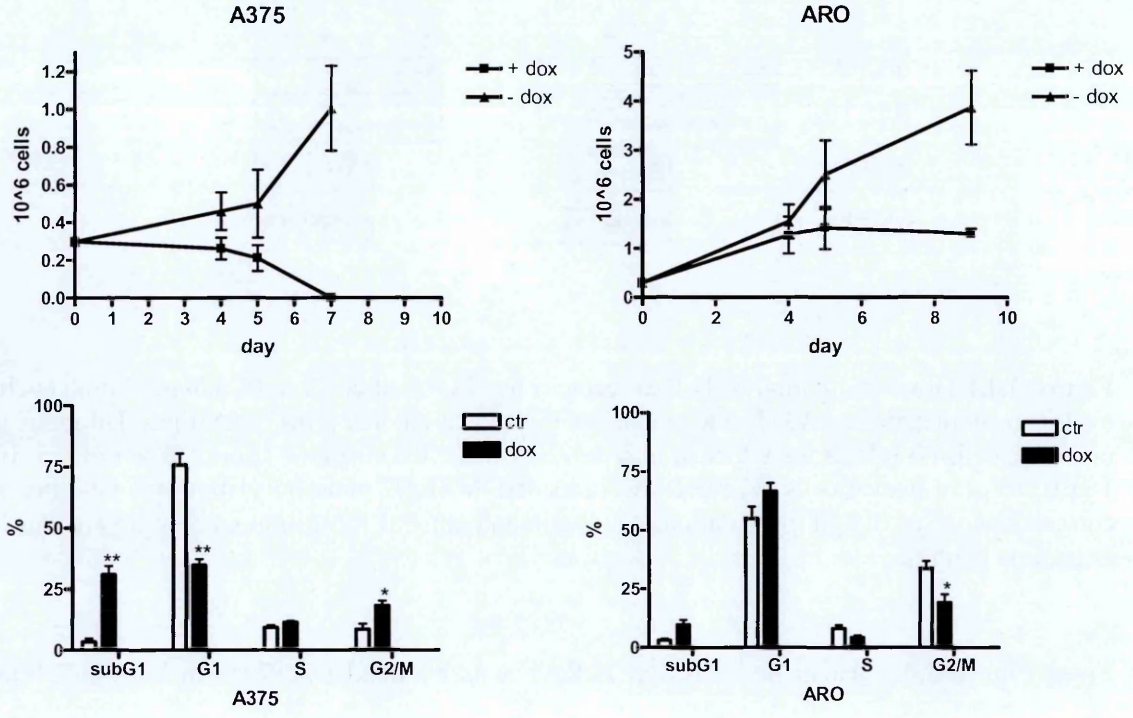

Figure 3.4.2 Biological effects of B-RAF silencing: (A) growth curves of A375 and ARO cell lines in absence or presence of doxycycline; cells were treated and counted by Trypan Blue Exclusion assay. Doxycycline-treated A375 cells were all dead at day 7. For ARO cells, the treatment continued till day 9 in order to evaluate the effect in the differentiation process. (B) cell cycle analysis of A375 and ARO cells after 96h of shRNA induction. An increase in subG1 and decrease in G1 fractions is evident in melanoma cells, while ARO cell line showed a decrease in the G2/M peak; * = $p < 0.01$; ** $p < 0.001$

One possible explanation to the delay in the growth of ARO cells could be the restoration of differentiation [86, 181]. To investigate this, the levels of expression of Sodium Iodide Simporter (NIS) after 8 days treatment were analysed using Western blotting. The appearance of NIS is a mark of the re-differentiation process [182, 183]. NIS is responsible to iodide uptake in normal thyrocytes and radioactive iodide in targeted therapies against differentiated thyroid cancer [184, 185]. Re-expression of the NIS pump, if correctly located at membrane level, makes I^{131} therapy possible also in tumours that have lost this protein [182, 183, 186, 187].

As shown in figure 3.4.3, the expression of NIS was inversely correlated to B-RAF silencing. The presence of NIS was observed only after long-term treatment, probably because the cells need several days to adapt to a lack of the proliferative and dedifferentiating stimulus of B-RAF.

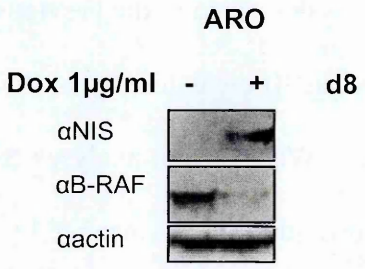

Figure 3.4.3 Western blot of total lysate after long term treatment with doxycycline. NIS and B-RAF expression was evaluated, anti-actin is the loading control.

In summary, these results provide evidence that B-RAF could be considered as a possible target for small molecule inhibitors in thyroid carcinoma. Its down-regulation induces re-differentiation and decrease in cell growth, even if doesn't determine apoptotic death in thyroid carcinoma. In contrast, apoptosis was observed in melanoma model, as expected [173].

3.4.3.2 PLX4032 characterization

Since we validated B-RAF as a potential target in thyroid carcinoma cell lines, the biochemical characterization of a new BRAF inhibitor, PLX4032, was undertaken. PLX4032 was recently developed by Plexxikon for the treatment of malignant melanoma and other malignancies with BRAF hyperactivation. This compound was tested on three thyroid carcinoma cell lines and on the A375 melanoma cell line. The ARO cell line previously characterized by siRNA as anaplastic thyroid carcinoma

model, the NPA cell line derived from poorly differentiated thyroid carcinoma and the TPC1 cell line established from a well differentiated papillary carcinoma were studied. A study of cell lines derived from different staged tumours should enable the characterization of the inhibitor to be obtained. From a genetic point of view, NPA presents homozygous V600E B-RAF and p53 mutated [96], while TPC1 carries the RET-PTC1 translocation [188], as described in the previous section.

Dose- response curves indicated an efficient activity of PLX4032 in all cellular systems investigated at micromolar doses. Western blot analyses confirmed the inhibitory block on MEK phosphorylation in dose-dependent manner by PLX4032 and, therefore, a possible involvement of the MAPK pathway in cellular growth control [189]. Time course experiments showed that B-RAF inhibition started after 4 hours of treatment and continued for 24 hours (data not shown). As expected, in ^{3}H-Thymidine proliferation assay, the IC_{50} value was lower in the A375 cell line, while both the ARO and NPA cells demonstrated similar level of inhibition It is interesting to note that the IC_{50} of ARO cells doubled that of NPA. One explanation to account for this is that PLX4032 is more potent against V600E B-RAF and the ARO and NPA cell lines are heterozygous and homozygous for this molecule, respectively. The TPC1 cell line showed a 50 fold higher IC_{50} value, probably due to numerous signalling pathways activated by the RET/PTC in addition to those of the RAF-MEK-ERK pathway [37, 40, 190].

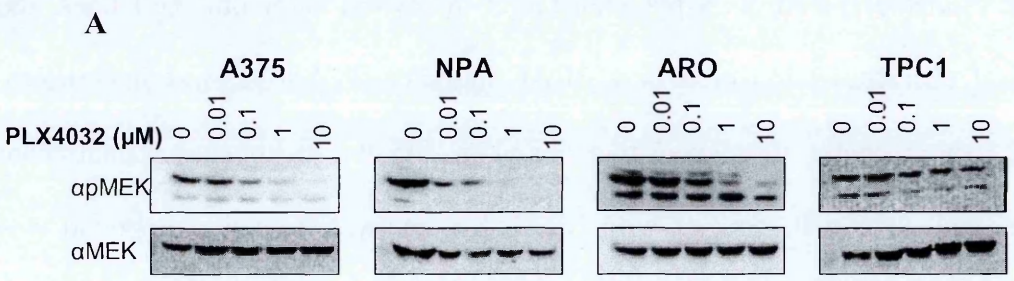

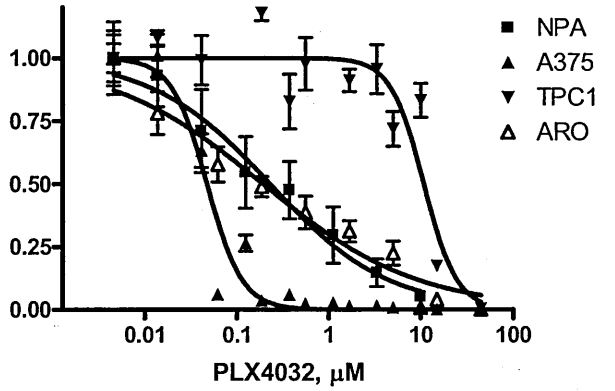

	EC50 (μM)	95% CI
A375	0.0472	0.04058 to 0.05448
NPA	0.1260	0.07350 to 0.2159
ARO	0.2051	0.1295 to 0.3250
TPC1	9.982	1.854 to 53.75

Figure 3.4.4 B-RAF inhibition by PLX4032: (A) effects of B-RAF inhibition on phosphorylation of its direct substrate, MEK1/2. Anti-MEK1/2 western blot demonstrated that PLX4032 did not interfere with the expression levels of the protein and did not induce MEK degradation. (B) Relative proliferation of the indicated cell lines in the presencev. of increasing concentrations of PLX4032. The IC_{50} value (calculated as the dose that caused 50% inhibition) for each cell line is reported in the table.

The cell cycle was analysed using two different methods: propidium iodide staining and annexin V binding assay. In the first assay, the DNA content in relation to its subcellular localisation is evaluated in fixed cells [191]. In the second case, annexin specifically binds to phosphaditylserine when it's exposed on the outer layer of the cellular membrane; this phenomenon usually occurs during the apoptotic process [192]. The concomitant coloration with propidium that recognizes non-viable cells and FITC-annexin V allows the discrimination between intact, early and late apoptotic cells. Both experiments were quantified and analysed by flow cytometry. The Annexin V assay is more sensitive than propidium staining and allows the distinction of early apoptotic cells belonging to the G1 fraction.

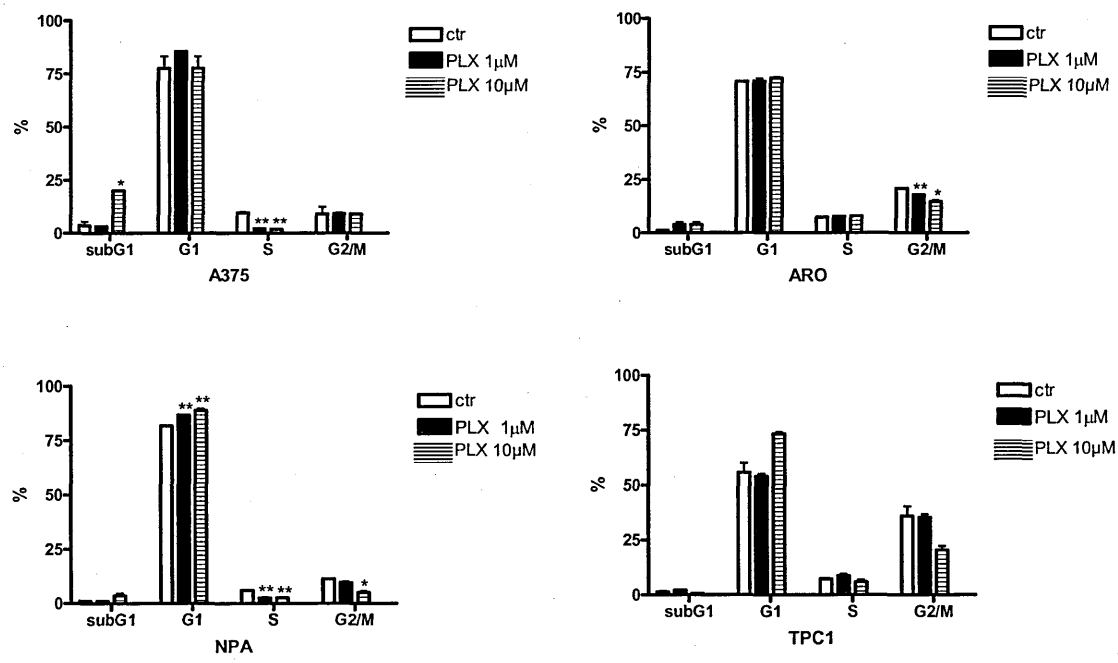

Figure 3.4.5 Cell cycle analysis with propidium iodide staining after 96h treatment with 0, 1, 10μM PLX4032 * = $p < 0.01$; ** $p < 0.001$

As expected, on contrast to the three thyroid derived cell lines, the A375 melanoma cell line showed a significant apoptosis at a concentration of 10μM PLX4032. A reduction of the G2/M fraction of the ARO cells was observed while the NPA cell line showed an arrest in G1 and a less important decrease in S and G2/M phases. PLX4032 did not affect the TPC1 cell cycle.

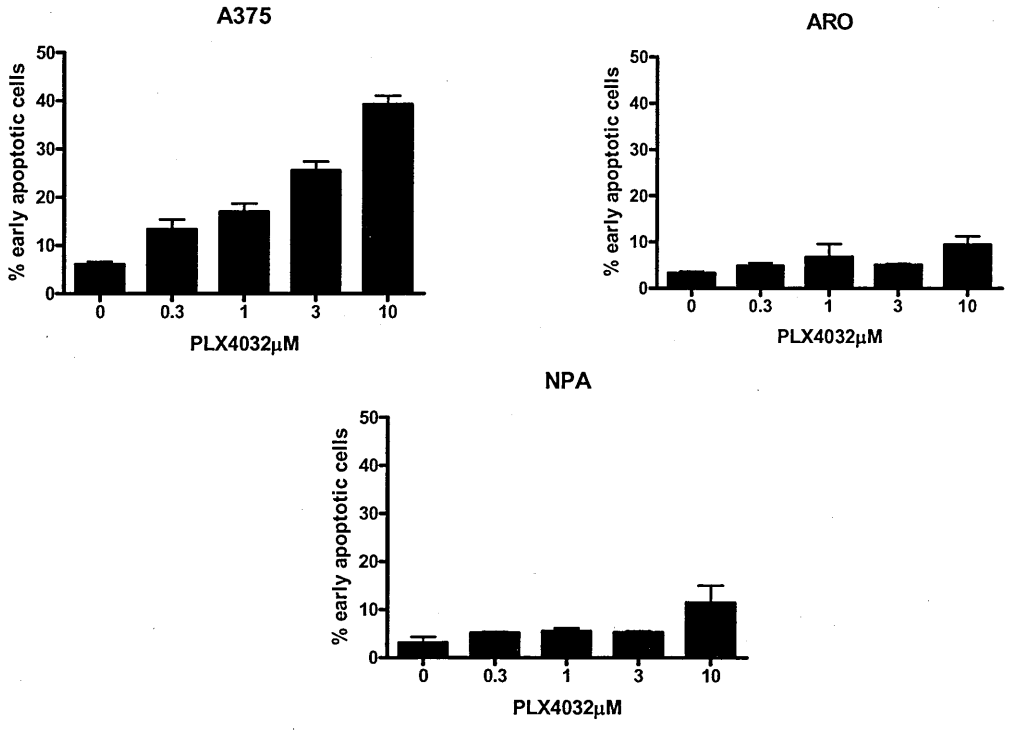

Figure 3.4.6 Effects of PLX4032 on cell cycle: Annexin V binding assay was used to determine the percentage of early apoptotic cells in all cell lines after 96h of treatment. A375 underwent apoptosis in a dose-dependent manner, while in thyroid carcinoma cell lines no significant apoptosis was observed even at high doses.

The apoptotic cell percentage increased in both of the A375 and NPA cell lines at 10μM PLX4032 whereas no significant variation was detected in the ARO cells (Figure 3.4.6). One possible explanation to account for this difference is that the ARO lines is derived from more un-differentiated tumour stage [178] and it is therefore probably that they possess additional chromosomal mutations that are not present in NPA. These results obtained on the thyroid cell lines are consistent with that recently reported using other B-RAF inhibitors [193].

The inhibition of MAPK signalling by a down-regulation of B-RAF or by using a chemical block of its enzymatic activity resulted in the same consequence in terms of cell growth and alterations in cell cycle in the present study. We could conclude that

PLX4032 was specific for B-RAF used at high doses and was prevalently potent on B-RAF mutated cell lines because of its inability to inhibit the RET-positive cell line.

3.4.3.3 Comparison between melanoma and thyroid carcinoma cell lines

It was important to investigate the reasons for the different behaviour observed between melanoma and thyroid carcinoma cell lines, in particular the A375 and ARO cells showed a significantly different response to B-RAF inhibition. It was hypothesized that there the involvement of other cell signalling pathway, as well as alteration(s) in anti-apoptotic factors expression levels or cell cycle regulators siRNA experiments were therefore performed in order to ensure that the effects observed were related only to silence of B-RAF.

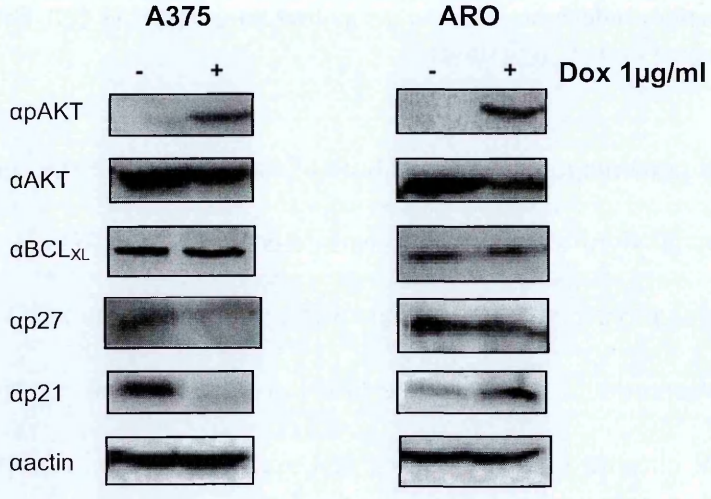

Figure 3.4.7 Western blot analysis of total cell lysate after treatment with doxycycline for 96h. Decreased B-RAF expression levels have been shown in figure 3.4.1 Anti- actin blot is the loading control.

B-RAF down-regulation has been showed in fig. 3.4.7 and the same lysates were used in Western blotting studies to investigate the expression of other signalling molecules involved in apoptotic/proliferation pathways.

Intriguingly, an increased phosphorylation of AKT protein was observed in both cell lines, when the MAPK pathway was switched off (Figure 3.4.7). A possible explanation is that the cells may have attempted to activate pathways that may be redundant in the presence of B-RAF. No differences were observed in BCL_{XL} or BCL2 levels (data not shown) and the activation of this anti-apoptotic pathway could be excluded in the thyroid cell lines. In contrast, differences in p21 expression, but not p27 was detected. The A375 melanoma cell line down-regulated p21 in response to B-RAF silencing, while up-regulation of p21 was present in the ARO thyroid cells. Similar results were obtained in PLX4032-treated cells (Figure 3.4.8) thus demonstrating that the changes in p21 expression were not due to non-specific effects of doxycycline or a side-effect of shRNA.

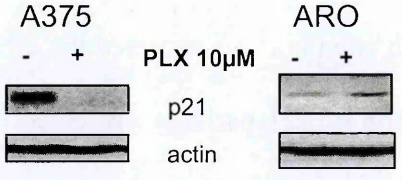

Figure 3.4.8 Western blot of anti-p21 of total lysate of PLX treated cells: p21 was down-regulated in the A375 cell line, while it was up-regulated in ARO cells. The correspondent inhibition of B-RAF has been showed in fig. 3.4.4 A. Anti actin was blotted as loading control.

To evaluate the role of p21 in the resistance to apoptosis resistance two Adenovirus vectors were used: one encodes for p21 to restore p21 levels in A375, the other one encodes for an antisense p21 to knock down the protein in ARO cell line. Cells were transfected by the relevant Adenovirus and also simultaneously treated with PLX4032.

The use of this small molecule inhibitor resulted in an immediate block of B-RAF activity with its consequent change in p21 levels. The effects on cell cycle were analysed using propidium iodide staining and flow cytometry. Annexin V assay could not be used because Adenoviruses contained green fluorescence protein gene, which prevents analysis using FITC-Annexin V.

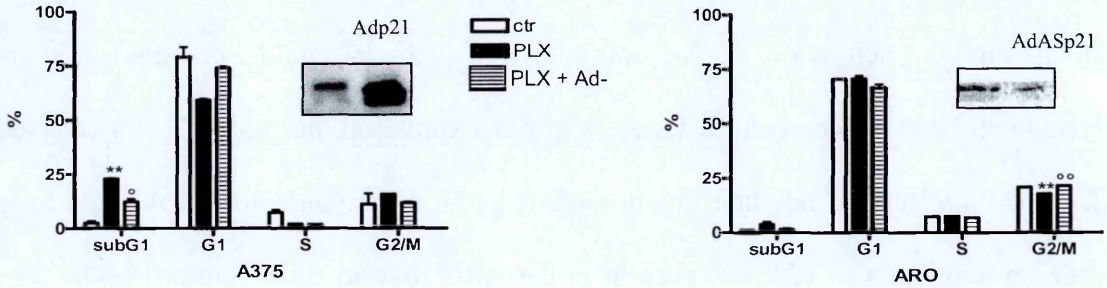

Figure 3.4.9 Role of p21CIP/WAF modulation in cell cycle: p21 expression was up-regulated and down-regulated by Adenoviral vector in A375 and ARO, respectively. Concomitant treatment with PLX4032 was performed. Protection from apoptosis was observed in the melanoma cell line, while in thyroid carcinoma no effect on programmed cell death was obtained. In both cases, p21 expression was modulated as expected (insets). * = $p < 0.01$; ** $p < 0.001$

As shown in figure 3.4.9, both adenoviruses reversed the effects of B-RAF inhibition. In the case of A375, re-expression of p21 partially protected from apoptosis, while in the ARO cells, the G2/M fraction increased at the same level of un-treated cells. No evidence of apoptosis in ARO cells was observed in several experiments, thus confirming the natural resistance of this cell line to undergo to apoptotic process. A relationship was further confirmed between B-RAF and p21 expression. The silencing of B-RAF resulted in a lack of p21 regulation and the restoration of normal apoptotic process in melanoma cells or proliferation arrest in anaplastic thryroid carcinoma cells.

3.4.4 Discussion

In this part of the project, I focussed my attention on the MAPK signalling pathway that is one of downstream pathways activated by RET in thyroid carcinomas. In particular, I was interested on understanding the role of B-RAF in this pathology and verifying if it could be a possible target for selective therapy with small molecule inhibitors. As previously described, B-RAF is often mutated in PTC and this alteration is related to the un-differentiated status of the tumour. An inducible siRNA was established to silence B-RAF expression in the ARO cell line under control of doxycycline [172]. The presence of a stably transfected cell line makes it possible to perform long term treatments without losing silencing efficiency. The melanoma A375 cell lines was recently used as a model to validate B-RAF expression in melanoma [173] using the same system and construct used in the current study. siRNA efficiently worked in both cell lines, silencing B-RAF protein within 96h and down-regulating the MAPK pathway. RAF-MEK1/2-ERK1/2 cascade regulates the progression through G1 to DNA synthesising S-phase, in melanoma [194], while in thyroid cancer recent evidences rely on RAS and G2/M checkpoint, indicating a main involvement of MAPK pathway in this cell cycle phase [195]. In long-term treatment, the restoration of NIS expression indicative of the restoration of differentiation properties of the cell was achieved [183]. Since B-RAF V600E expression induces dedifferentiation in the PCCl3 rat thyroid cell line with a significant decrease in NIS expression within 6 days [86], the data presented here demonstrated NIS expression with the same timing, thus indicating that B-RAF plays an important role in this process. Furthermore, the transient expression of B-RAF V600E in differentiated PCCl3 cell line impairs both NIS expression and its targeting to membrane, probably because of interference of B-RAF with TSH-mediated response

[196]. The induction of re-differentiation could be the first step to strictly control and block anaplastic tumour growth.

We characterised one new compound in the three following PTC cell lines: ARO, NPA and TPC1. PLX4032 showed submicromolar IC_{50} against all cell lines that carry B-RAF mutation and a 50 fold higher value against TPC1 that present the RET/PTC1 fusion protein. Such discrepancy in effect can be related to the multiplicity of signalling pathways that are activated by RET [37, 40]. A decrease in MEK phosphorylation indicated that the proliferation arrest was due to the MAPK pathway inhibition and the doses of PLX4032 necessary to block MEK phosphorylation were consistent with the IC_{50}. Cell cycle analysis was performed by treating cells with either 1 or 10μM PLX4032 in two distinct assays. The A375 cell lines showed high level of apoptosis, as expected from previous results obtaining with inducible siRNA, while two thyroid cell lines, ARO and NPA, demonstrated only G1 arrest and a little apoptosis at the highest dose or a decrease in G2/M phase in NPA and ARO cells, respectively. In contrast the TPC1 cells were not perturbed by the treatment. Similar results were recently published by Ouyang et al. [193] using a isoquinoline compound that showed at 10μM impaired progression into S and G2-M and caused an G0-G1 arrest, without inducing apoptosis. Possible studies were performed in the present study to account for the differences in behaviour observed between the melanoma and thyroid carcinoma cell lines, in particular in ARO cells. We used siRNA inducible system to exclude any side effects related to the non-specificity of PLX4032. No activation of alternative survival pathways, such as the AKT pathway, nor anti-apoptotic factors were preferentially observed in any cell line. In contrast, changes of p21 were noted in the melanoma and thyroid carcinoma cell lines, while p27 levels didn't change. These results obtained using siRNA were confirmed using a small molecule inhibitor in order to exclude in this

case side effects due to siRNA or doxycycline. Changes in p21 expression have been previously described in tumour cells. It has been reported that p21 up-regulation is related to resistance to drug induced apoptosis and cells that are unable to up-regulate p21 die [197]. Moreover, in anaplastic thyroid carcinoma growth arrest induced by PPARγ activation is mediated by the up-regulation of p21 [198]. p21 up-regulation also makes cells more sensitive to paclitaxel treatment [198]. The effects of adenovirally transduced p21 expression, induced after treatment with PLX4032, in A375 and ARO cells were studied in order to verify its role in apoptosis protection. The reversion in B-RAF inhibition effects was observed in both cell lines. A possible relationship between p21 expression level and B-RAF inhibition was suggested: the A375 cells that underwent apoptosis in the absence of a B-RAF proliferative stimulus were partially protected from death, while in ARO cells that had showed a delay in cellular growth the decreased level of G2/M was reverted.

Taken together, these data confirmed the important role of B-RAF in cancer thyroid de-differentiation, and open up the possibility of a restoration of a differentiated status of the tumour cells through the use of small molecule inhibitors. The PLX4032 compound showed high efficiency and specificity against the B-RAF mutated cell lines, but not against RET/PTC positive cell lines, supporting the importance of directly targeting the oncogenic protein. p21 regulation by B-RAF through MEK-ERK pathway provides a possible molecular explanation of different effects of B-RAF inhibition in cell lines analysed.

4 CONCLUSION

This PhD project analysed the involvement of the receptor tyrosine kinase RET in PTC. The study utilised biochemical and biological techniques to determine the biological role of RET- dependent signalling in cancer. In particular, I focussed my attention on the characterization of new small molecules inhibitors that could selectively block RET pathway.

The first goal of my work was the production of a suitable reagent to perform structural and pharmacological studies. rRET was produced using the Baculovirus system and purified using a procedure optimised by myself. This protein showed biochemical and physical characteristics that were compatible with the further analyses that were desired. Indeed, the recombinant catalytic domain of rRET showed the same properties of the full length protein present in an *in vitro* cellular system and in the cells of cancer patients. No discrepancies between the rRET and full length RET activity in crystallization attempts and in inhibitor screening were observed in the current project.

Knowledge of the three-dimensional structure of the RET catalytic domain represents the most important starting point to identify a specific inhibitor. Several attempts with different constructs were made at crystallisation but no crystals were obtained that were suitable for X-ray diffraction studies. Some experiments were performed in two independent institutes (University of Padova and Hauptmann Institute in Buffalo) in order to optimise the possibility of a successful outcome. Fortunately for the advance of my project, the RET structure was very recently solved by another group. The availability of such a detailed model will be invaluable for the identification of new selective inhibitory compounds and for exploring new binding sites rather than the ATP-binding pocket. Our molecular modelling was based on sequence similarity and

was constantly improved using data from inhibitor screening. Indeed, the positive and negative results from my *in vitro* experiments made it possible to adjust the model. The positions of the amino acids that virtually bind the inhibitors can be modified in relation to IC_{50} experimentally determined. The work described in this thesis resulted in the identification of an efficient class of RET inhibitor, the further study of which resulted in the identification of a good molecule, SU5416, that was feasible for clinical further studies in PTC. SU5416 demonstrated an efficient and selective inhibition of RET, both in *in vitro* and *in vivo* systems. Cell based experiments showed a favourable solubility and *in vivo* data suggested that its bio-availability is compatible with exigencies of clinical application. Furthermore, ongoing clinical trials against other cancers indicate favourable pharmaco-kinetic properties of this 2-indolinone derivative. The administration of this drug in PTC patients could be reasonable.

The second target validated in this PhD project was identification of the serine/threonine kinase B-RAF. B-RAF is downstream to RET in the MAPK pathway and is often mutated in PTC. The selective targeting of B-RAF could therefore provide an opportunity to treat both RET and B-RAF positive PTC. The results presented here demonstrated that B-RAF could be a good target in poorly differentiated papillary carcinoma and in anaplastic carcinoma because of its involvement in the de-differentiation process. We promoted growth arrest and the acquisition of a differentiated status by blocking B-RAF kinase activity. Two different strategies, siRNA and a small molecule inhibitor, were employed to achieve these results to exclude any doubt relied to methodological non-specific effects. However, RET positive cell growth was inhibited only at high doses of compound, suggesting the necessity to directly act against the mutated protein in order to achieve a cellular response. The complex interaction existing between the various cellular signalling pathways allows

raises the possibility that cells can overcome a single pathway block, and so are able to adapt to the lack of an oncogenic signal. Moreover, several mechanism can be controlled by the same pathway in different cell lines. Evidence to this latter point was obtained from my comparison between melanoma and anaplastic thyroid carcinoma cell lines, in which the inhibition of B-RAF-MEK1/2-ERK1/2 had completely different consequences on cell cycle. Nevertheless, these effects were mediated by p21 regulation, the presence of this same protein in both cell lines indicating a common set of control factors. Improved knowledge of the various signalling pathways in cellular systems associated with analyses of patient biopsy tissues would be invaluable in the identification of new targets for selective treatment. Moreover, it would be possible to exploit the wide spectrum of one small molecule compound on cells to obtain major effects *in vivo*: for instance, SU5416 acts as anti-proliferative agent by blocking RET and as anti-angiogenic by inhibiting VEGFR. This dual mechanism could improve the efficiency of the therapy, with minimal side-effects.

This work has proposed the rational identification of RET and B-RAF inhibitors by analysing their signalling pathway. These results raise the possibility that PTC could be treated effectively with small molecule inhibitors, as is the case for other cancers, such as chronic myeloid leukaemia, which are linked to oncogenic tyrosine kinases.

5 BIBLIOGRAPHY

1. Manning, G., et al., *The protein kinase complement of the human genome.* Science, 2002. **298**(5600): p. 1912-34.
2. Manning, G., et al., *Evolution of protein kinase signaling from yeast to man.* Trends Biochem Sci, 2002. **27**(10): p. 514-20.
3. Spring, J., *Genome duplication strikes back.* Nat Genet, 2002. **31**(2): p. 128-9.
4. Knighton, D.R., et al., *Crystal structure of the catalytic subunit of cyclic adenosine monophosphate-dependent protein kinase.* Science, 1991. **253**(5018): p. 407-14.
5. Johnson, L.N., M.E. Noble, and D.J. Owen, *Active and inactive protein kinases: structural basis for regulation.* Cell, 1996. **85**(2): p. 149-58.
6. Jeffrey, P.D., et al., *Mechanism of CDK activation revealed by the structure of a cyclinA-CDK2 complex.* Nature, 1995. **376**(6538): p. 313-20.
7. Xu, W., S.C. Harrison, and M.J. Eck, *Three-dimensional structure of the tyrosine kinase c-Src.* Nature, 1997. **385**(6617): p. 595-602.
8. Sicheri, F. and J. Kuriyan, *Structures of Src-family tyrosine kinases.* Curr Opin Struct Biol, 1997. **7**(6): p. 777-85.
9. Hubbard, S.R., et al., *Crystal structure of the tyrosine kinase domain of the human insulin receptor.* Nature, 1994. **372**(6508): p. 746-54.
10. Hubbard, S.R., *Crystal structure of the activated insulin receptor tyrosine kinase in complex with peptide substrate and ATP analog.* Embo J, 1997. **16**(18): p. 5572-81.
11. Zhang, X., et al., *An allosteric mechanism for activation of the kinase domain of epidermal growth factor receptor.* Cell, 2006. **125**(6): p. 1137-49.
12. Levitzki, A., *Protein kinase inhibitors as a therapeutic modality.* Acc Chem Res, 2003. **36**(6): p. 462-9.
13. Noble, M.E., J.A. Endicott, and L.N. Johnson, *Protein kinase inhibitors: insights into drug design from structure.* Science, 2004. **303**(5665): p. 1800-5.
14. Schindler, T., et al., *Structural mechanism for STI-571 inhibition of abelson tyrosine kinase.* Science, 2000. **289**(5486): p. 1938-42.
15. Nagar, B., et al., *Crystal structures of the kinase domain of c-Abl in complex with the small molecule inhibitors PD173955 and imatinib (STI-571).* Cancer Res, 2002. **62**(15): p. 4236-43.
16. Fitzgerald, C.E., et al., *Structural basis for p38alpha MAP kinase quinazolinone and pyridol-pyrimidine inhibitor specificity.* Nat Struct Biol, 2003. **10**(9): p. 764-9.
17. Mohammadi, M., et al., *Structures of the tyrosine kinase domain of fibroblast growth factor receptor in complex with inhibitors.* Science, 1997. **276**(5314): p. 955-60.
18. Cho, H.S., et al., *Structure of the extracellular region of HER2 alone and in complex with the Herceptin Fab.* Nature, 2003. **421**(6924): p. 756-60.
19. Gorre, M.E. and C.L. Sawyers, *Molecular mechanisms of resistance to STI571 in chronic myeloid leukemia.* Curr Opin Hematol, 2002. **9**(4): p. 303-7.
20. Shah, N.P., et al., *Overriding imatinib resistance with a novel ABL kinase inhibitor.* Science, 2004. **305**(5682): p. 399-401.
21. Baselga, J., *Targeting tyrosine kinases in cancer: the second wave.* Science, 2006. **312**(5777): p. 1175-8.

22. Sheils, O., *Molecular classification and biomarker discovery in papillary thyroid carcinoma.* Expert Rev Mol Diagn, 2005. **5**(6): p. 927-46.
23. Gimm, O., *Thyroid cancer.* Cancer Lett, 2001. **163**(2): p. 143-56.
24. Antonelli, A., et al., *Epidemiologic and clinical evaluation of thyroid cancer in children from the Gomel region (Belarus).* World J Surg, 1996. **20**(7): p. 867-71.
25. Verga, U., et al., *The role of radiopharmaceuticals MIBG and (V) DMSA in the diagnosis of medullary thyroid carcinoma.* Henry Ford Hosp Med J, 1989. **37**(3-4): p. 175-7.
26. Lips, C.J., et al., *Clinical screening as compared with DNA analysis in families with multiple endocrine neoplasia type 2A.* N Engl J Med, 1994. **331**(13): p. 828-35.
27. Drosten, M. and B.M. Putzer, *Gene therapeutic approaches for medullary thyroid carcinoma treatment.* J Mol Med, 2003. **81**(7): p. 411-9.
28. Fagin, J.A., *Minireview: branded from the start-distinct oncogenic initiating events may determine tumor fate in the thyroid.* Mol Endocrinol, 2002. **16**(5): p. 903-11.
29. Takahashi, M., *The GDNF/RET signaling pathway and human diseases.* Cytokine Growth Factor Rev, 2001. **12**(4): p. 361-73.
30. Sozzi, G., et al., *Refined localization to contiguous regions on chromosome 10q of the two genes (H4 and RET) that form the oncogenic sequence PTC.* Oncogene, 1991. **6**(2): p. 339-42.
31. Santoro, M., et al., *Molecular characterization of RET/PTC3; a novel rearranged version of the RETproto-oncogene in a human thyroid papillary carcinoma.* Oncogene, 1994. **9**(2): p. 509-16.
32. Heinlein, C.A., et al., *Identification of ARA70 as a ligand-enhanced coactivator for the peroxisome proliferator-activated receptor gamma.* J Biol Chem, 1999. **274**(23): p. 16147-52.
33. Jhiang, S.M., *The RET proto-oncogene in human cancers.* Oncogene, 2000. **19**(49): p. 5590-7.
34. Bongarzone, I., et al., *Molecular characterization of a thyroid tumor-specific transforming sequence formed by the fusion of ret tyrosine kinase and the regulatory subunit RI alpha of cyclic AMP-dependent protein kinase A.* Mol Cell Biol, 1993. **13**(1): p. 358-66.
35. Salassidis, K., et al., *Translocation t(10;14)(q11.2:q22.1) fusing the kinetin to the RET gene creates a novel rearranged form (PTC8) of the RET proto-oncogene in radiation-induced childhood papillary thyroid carcinoma.* Cancer Res, 2000. **60**(11): p. 2786-9.
36. Miyagi, E., et al., *Chronic expression of RET/PTC 3 enhances basal and insulin-stimulated PI3 kinase/AKT signaling and increases IRS-2 expression in FRTL-5 thyroid cells.* Mol Carcinog, 2004. **41**(2): p. 98-107.
37. De Falco, V., et al., *RAI(ShcC/N-Shc)-dependent recruitment of GAB 1 to RET oncoproteins potentiates PI 3-K signalling in thyroid tumors.* Oncogene, 2005. **24**(41): p. 6303-13.
38. Puxeddu, E., et al., *Microsomal prostaglandin E2 synthase-1 is induced by conditional expression of RET/PTC in thyroid PCCL3 cells through the activation of the MEK-ERK pathway.* J Biol Chem, 2003. **278**(52): p. 52131-8.
39. Knauf, J.A., et al., *RET/PTC-induced dedifferentiation of thyroid cells is mediated through Y1062 signaling through SHC-RAS-MAP kinase.* Oncogene, 2003. **22**(28): p. 4406-12.

40. Borrello, M.G., et al., *The full oncogenic activity of Ret/ptc2 depends on tyrosine 539, a docking site for phospholipase Cgamma.* Mol Cell Biol, 1996. **16**(5): p. 2151-63.
41. Mercalli, E., et al., *Key role of Shc signaling in the transforming pathway triggered by Ret/ptc2 oncoprotein.* Oncogene, 2001. **20**(27): p. 3475-85.
42. Besset, V., R.P. Scott, and C.F. Ibanez, *Signaling complexes and protein-protein interactions involved in the activation of the Ras and phosphatidylinositol 3-kinase pathways by the c-Ret receptor tyrosine kinase.* J Biol Chem, 2000. **275**(50): p. 39159-66.
43. Panta, G.R., et al., *Direct phosphorylation of proliferative and survival pathway proteins by RET.* Surgery, 2005. **138**(2): p. 269-74.
44. Viglietto, G., et al., *RET/PTC oncogene activation is an early event in thyroid carcinogenesis.* Oncogene, 1995. **11**(6): p. 1207-10.
45. Jhiang, S.M., et al., *Targeted expression of the ret/PTC1 oncogene induces papillary thyroid carcinomas.* Endocrinology, 1996. **137**(1): p. 375-8.
46. Powell, D.J., Jr., et al., *The RET/PTC3 oncogene: metastatic solid-type papillary carcinomas in murine thyroids.* Cancer Res, 1998. **58**(23): p. 5523-8.
47. Santoro, M., et al., *Activation of RET as a dominant transforming gene by germline mutations of MEN2A and MEN2B.* Science, 1995. **267**(5196): p. 381-3.
48. Asai, N., et al., *Mechanism of activation of the ret proto-oncogene by multiple endocrine neoplasia 2A mutations.* Mol Cell Biol, 1995. **15**(3): p. 1613-9.
49. Schindler, T., et al., *Crystal structure of Hck in complex with a Src family-selective tyrosine kinase inhibitor.* Mol Cell, 1999. **3**(5): p. 639-48.
50. Carlomagno, F., et al., *The kinase inhibitor PP1 blocks tumorigenesis induced by RET oncogenes.* Cancer Res, 2002. **62**(4): p. 1077-82.
51. Carlomagno, F., et al., *Efficient inhibition of RET/papillary thyroid carcinoma oncogenic kinases by 4-amino-5-(4-chloro-phenyl)-7-(t-butyl)pyrazolo[3,4-d]pyrimidine (PP2).* J Clin Endocrinol Metab, 2003. **88**(4): p. 1897-902.
52. Mologni, L., et al., *Expression, purification, and inhibition of human RET tyrosine kinase.* Protein Expr Purif, 2005. **41**(1): p. 177-85.
53. Liu, Y., et al., *Structural basis for selective inhibition of Src family kinases by PP1.* Chem Biol, 1999. **6**(9): p. 671-8.
54. Carlomagno, F., et al., *Disease associated mutations at valine 804 in the RET receptor tyrosine kinase confer resistance to selective kinase inhibitors.* Oncogene, 2004. **23**(36): p. 6056-63.
55. Blencke, S., et al., *Characterization of a conserved structural determinant controlling protein kinase sensitivity to selective inhibitors.* Chem Biol, 2004. **11**(5): p. 691-701.
56. Waltenberger, J., et al., *A dual inhibitor of platelet-derived growth factor beta-receptor and Src kinase activity potently interferes with motogenic and mitogenic responses to PDGF in vascular smooth muscle cells. A novel candidate for prevention of vascular remodeling.* Circ Res, 1999. **85**(1): p. 12-22.
57. Ryan, A.J. and S.R. Wedge, *ZD6474--a novel inhibitor of VEGFR and EGFR tyrosine kinase activity.* Br J Cancer, 2005. **92 Suppl 1**: p. S6-13.
58. Wedge, S.R., et al., *ZD6474 inhibits vascular endothelial growth factor signaling, angiogenesis, and tumor growth following oral administration.* Cancer Res, 2002. **62**(16): p. 4645-55.
59. Ciardiello, F., et al., *Antitumor effects of ZD6474, a small molecule vascular endothelial growth factor receptor tyrosine kinase inhibitor, with additional*

activity against epidermal growth factor receptor tyrosine kinase. Clin Cancer Res, 2003. **9**(4): p. 1546-56.

60. McCarty, M.F., et al., *ZD6474, a vascular endothelial growth factor receptor tyrosine kinase inhibitor with additional activity against epidermal growth factor receptor tyrosine kinase, inhibits orthotopic growth and angiogenesis of gastric cancer.* Mol Cancer Ther, 2004. **3**(9): p. 1041-8.
61. Holden, S.N., et al., *Clinical evaluation of ZD6474, an orally active inhibitor of VEGF and EGF receptor signaling, in patients with solid, malignant tumors.* Ann Oncol, 2005. **16**(8): p. 1391-7.
62. Heymach, J.V., *ZD6474--clinical experience to date.* Br J Cancer, 2005. **92 Suppl 1**: p. S14-20.
63. Lee, D., *Phase II data with ZD6474, a small-molecule kinase inhibitor of epidermal growth factor receptor and vascular endothelial growth factor receptor, in previously treated advanced non-small-cell lung cancer.* Clin Lung Cancer, 2005. **7**(2): p. 89-91.
64. Carlomagno, F., et al., *ZD6474, an orally available inhibitor of KDR tyrosine kinase activity, efficiently blocks oncogenic RET kinases.* Cancer Res, 2002. **62**(24): p. 7284-90.
65. Vidal, M., et al., *ZD6474 suppresses oncogenic RET isoforms in a Drosophila model for type 2 multiple endocrine neoplasia syndromes and papillary thyroid carcinoma.* Cancer Res, 2005. **65**(9): p. 3538-41.
66. Strock, C.J., et al., *CEP-701 and CEP-751 inhibit constitutively activated RET tyrosine kinase activity and block medullary thyroid carcinoma cell growth.* Cancer Res, 2003. **63**(17): p. 5559-63.
67. Undevia, S.D., et al., *Phase I clinical trial of CEP-2563 dihydrochloride, a receptor tyrosine kinase inhibitor, in patients with refractory solid tumors.* Invest New Drugs, 2004. **22**(4): p. 449-58.
68. Smith, B.D., et al., *Single-agent CEP-701, a novel FLT3 inhibitor, shows biologic and clinical activity in patients with relapsed or refractory acute myeloid leukemia.* Blood, 2004. **103**(10): p. 3669-76.
69. Strock, C.J., et al., *Activity of irinotecan and the tyrosine kinase inhibitor CEP-751 in medullary thyroid cancer.* J Clin Endocrinol Metab, 2006. **91**(1): p. 79-84.
70. Lanzi, C., et al., *Inhibition of transforming activity of the ret/ptc1 oncoprotein by a 2-indolinone derivative.* Int J Cancer, 2000. **85**(3): p. 384-90.
71. Lanzi, C., et al., *Inactivation of Ret/Ptc1 oncoprotein and inhibition of papillary thyroid carcinoma cell proliferation by indolinone RPI-1.* Cell Mol Life Sci, 2003. **60**(7): p. 1449-59.
72. Lanzi, C., et al., *RET/PTC oncoproteins: molecular targets of new drugs.* Tumori, 2003. **89**(5): p. 520-2.
73. Arighi, E., et al., *Identification of Shc docking site on Ret tyrosine kinase.* Oncogene, 1997. **14**(7): p. 773-82.
74. Miozzo, M., et al., *Human TRK proto-oncogene maps to chromosome 1q32-q41.* Oncogene, 1990. **5**(9): p. 1411-4.
75. Greco, A., et al., *TRK-T1 is a novel oncogene formed by the fusion of TPR and TRK genes in human papillary thyroid carcinomas.* Oncogene, 1992. **7**(2): p. 237-42.
76. Greco, A., et al., *The DNA rearrangement that generates the TRK-T3 oncogene involves a novel gene on chromosome 3 whose product has a potential coiled-coil domain.* Mol Cell Biol, 1995. **15**(11): p. 6118-27.

77. Greco, A., et al., *Role of the TFG N-terminus and coiled-coil domain in the transforming activity of the thyroid TRK-T3 oncogene.* Oncogene, 1998. **16**(6): p. 809-16.
78. Beimfohr, C., et al., *NTRK1 re-arrangement in papillary thyroid carcinomas of children after the Chernobyl reactor accident.* Int J Cancer, 1999. **80**(6): p. 842-7.
79. Portella, G., et al., *Human N-ras, TRK-T1, and RET/PTC3 oncogenes, driven by a thyroglobulin promoter, differently affect the expression of differentiation markers and the proliferation of thyroid epithelial cells.* Oncol Res, 1999. **11**(9): p. 421-7.
80. Russell, J.P., et al., *The TRK-T1 fusion protein induces neoplastic transformation of thyroid epithelium.* Oncogene, 2000. **19**(50): p. 5729-35.
81. Boss, G.R., *cGMP-induced differentiation of the promyelocytic cell line HL-60.* Proc Natl Acad Sci U S A, 1989. **86**(18): p. 7174-8.
82. Saavedra, H.I., et al., *The RAS oncogene induces genomic instability in thyroid PCCL3 cells via the MAPK pathway.* Oncogene, 2000. **19**(34): p. 3948-54.
83. Missero, C., M.T. Pirro, and R. Di Lauro, *Multiple ras downstream pathways mediate functional repression of the homeobox gene product TTF-1.* Mol Cell Biol, 2000. **20**(8): p. 2783-93.
84. Wellbrock, C., M. Karasarides, and R. Marais, *The RAF proteins take centre stage.* Nat Rev Mol Cell Biol, 2004. **5**(11): p. 875-85.
85. Wan, P.T., et al., *Mechanism of activation of the RAF-ERK signaling pathway by oncogenic mutations of B-RAF.* Cell, 2004. **116**(6): p. 855-67.
86. Mitsutake, N., et al., *Conditional BRAFV600E expression induces DNA synthesis, apoptosis, dedifferentiation, and chromosomal instability in thyroid PCCL3 cells.* Cancer Res, 2005. **65**(6): p. 2465-73.
87. Ciampi, R., et al., *Oncogenic AKAP9-BRAF fusion is a novel mechanism of MAPK pathway activation in thyroid cancer.* J Clin Invest, 2005. **115**(1): p. 94-101.
88. Moretti, S., et al., *Biochemical and molecular characterization of the novel BRAF(V599Ins) mutation detected in a classic papillary thyroid carcinoma.* Oncogene, 2006. **25**(30): p. 4235-40.
89. Scarpino, S., et al., *Increased expression of Met protein is associated with up-regulation of hypoxia inducible factor-1 (HIF-1) in tumour cells in papillary carcinoma of the thyroid.* J Pathol, 2004. **202**(3): p. 352-8.
90. Christensen, J.G., J. Burrows, and R. Salgia, *c-Met as a target for human cancer and characterization of inhibitors for therapeutic intervention.* Cancer Lett, 2005. **225**(1): p. 1-26.
91. Dahia, P.L., et al., *Somatic deletions and mutations in the Cowden disease gene, PTEN, in sporadic thyroid tumors.* Cancer Res, 1997. **57**(21): p. 4710-3.
92. Adeniran, A.J., et al., *Correlation between genetic alterations and microscopic features, clinical manifestations, and prognostic characteristics of thyroid papillary carcinomas.* Am J Surg Pathol, 2006. **30**(2): p. 216-22.
93. Lima, J., et al., *BRAF mutations are not a major event in post-Chernobyl childhood thyroid carcinomas.* J Clin Endocrinol Metab, 2004. **89**(9): p. 4267-71.
94. Unger, K., et al., *Heterogeneity in the distribution of RET/PTC rearrangements within individual post-Chernobyl papillary thyroid carcinomas.* J Clin Endocrinol Metab, 2004. **89**(9): p. 4272-9.

95. Kumagai, A., et al., *Low frequency of BRAFT1796A mutations in childhood thyroid carcinomas.* J Clin Endocrinol Metab, 2004. **89**(9): p. 4280-4.
96. Nikiforova, M.N., et al., *BRAF mutations in thyroid tumors are restricted to papillary carcinomas and anaplastic or poorly differentiated carcinomas arising from papillary carcinomas.* J Clin Endocrinol Metab, 2003. **88**(11): p. 5399-404.
97. Oler, G., et al., *Investigation of BRAF mutation in a series of papillary thyroid carcinoma and matched-lymph node metastasis reveals a new mutation in metastasis.* Clin Endocrinol (Oxf), 2005. **62**(4): p. 509-11.
98. Garcia-Rostan, G., et al., *ras mutations are associated with aggressive tumor phenotypes and poor prognosis in thyroid cancer.* J Clin Oncol, 2003. **21**(17): p. 3226-35.
99. Nikiforov, Y.E., et al., *Solid variant of papillary thyroid carcinoma: incidence, clinical-pathologic characteristics, molecular analysis, and biologic behavior.* Am J Surg Pathol, 2001. **25**(12): p. 1478-84.
100. Possee, R.D., *Baculoviruses as expression vectors.* Curr Opin Biotechnol, 1997. **8**(5): p. 569-72.
101. Kitts, P.A. and R.D. Possee, *A method for producing recombinant baculovirus expression vectors at high frequency.* Biotechniques, 1993. **14**(5): p. 810-7.
102. Ernst, W.J., R.M. Grabherr, and H.W. Katinger, *Direct cloning into the Autographa californica nuclear polyhedrosis virus for generation of recombinant baculoviruses.* Nucleic Acids Res, 1994. **22**(14): p. 2855-6.
103. Luckow, V.A., et al., *Efficient generation of infectious recombinant baculoviruses by site-specific transposon-mediated insertion of foreign genes into a baculovirus genome propagated in Escherichia coli.* J Virol, 1993. **67**(8): p. 4566-79.
104. Luckow, V.A., *Baculovirus systems for the expression of human gene products.* Curr Opin Biotechnol, 1993. **4**(5): p. 564-72.
105. Boublik, Y., P. Di Bonito, and I.M. Jones, *Eukaryotic virus display: engineering the major surface glycoprotein of the Autographa californica nuclear polyhedrosis virus (AcNPV) for the presentation of foreign proteins on the virus surface.* Biotechnology (N Y), 1995. **13**(10): p. 1079-84.
106. Kost, T.A., J.P. Condreay, and D.L. Jarvis, *Baculovirus as versatile vectors for protein expression in insect and mammalian cells.* Nat Biotechnol, 2005. **23**(5): p. 567-75.
107. Hofmann, C., et al., *Efficient gene transfer into human hepatocytes by baculovirus vectors.* Proc Natl Acad Sci U S A, 1995. **92**(22): p. 10099-103.
108. Chen, Y.S., et al., *Purification and characterization of human prolyl dipeptidase DPP8 in Sf9 insect cells.* Protein Expr Purif, 2004. **35**(1): p. 142-6.
109. Ho, Y.C., et al., *Highly efficient baculovirus-mediated gene transfer into rat chondrocytes.* Biotechnol Bioeng, 2004. **88**(5): p. 643-51.
110. Fields, G.B. and R.L. Noble, *Solid phase peptide synthesis utilizing 9-fluorenylmethoxycarbonyl amino acids.* Int J Pept Protein Res, 1990. **35**(3): p. 161-214.
111. King, D.S., C.G. Fields, and G.B. Fields, *A cleavage method which minimizes side reactions following Fmoc solid phase peptide synthesis.* Int J Pept Protein Res, 1990. **36**(3): p. 255-66.
112. Brunati, A.M., et al., *Altered protein kinase activities of lymphoid cells transformed by Abelson and Moloney leukemia viruses.* FEBS Lett, 1986. **206**(1): p. 59-63.

113. Glass, D.B., et al., *Isolation of phosphorylated peptides and proteins on ion exchange papers.* Anal Biochem, 1978. **87**(2): p. 566-75.
114. Gunby, R.H., et al., *An enzyme-linked immunosorbent assay to screen for inhibitors of the oncogenic anaplastic lymphoma kinase.* Haematologica, 2005. **90**(7): p. 988-90.
115. Hubbard, S.R., *Protein tyrosine kinases: autoregulation and small-molecule inhibition.* Curr Opin Struct Biol, 2002. **12**(6): p. 735-41.
116. Drenth, J. and C. Haas, *Nucleation in protein crystallization.* Acta Crystallogr D Biol Crystallogr, 1998. **54**(Pt 5): p. 867-72.
117. Forsythe, E.L., D.L. Maxwell, and M. Pusey, *Vapor diffusion, nucleation rates and the reservoir to crystallization volume ratio.* Acta Crystallogr D Biol Crystallogr, 2002. **58**(Pt 10 Pt 1): p. 1601-5.
118. Gilliland, G.L. and J.E. Ladner, *Crystallization of biological macromolecules for X-ray diffraction studies.* Curr Opin Struct Biol, 1996. **6**(5): p. 595-603.
119. Gilliland, G.L., M. Tung, and J. Ladner, *The Biological Macromolecule Crystallization Database and NASA Protein Crystal Growth Archive.* J Res Natl Inst Stand Technol, 1996. **101**(3): p. 309-20.
120. Chayen, N.E., *Comparative studies of protein crystallization by vapour-diffusion and microbatch techniques.* Acta Crystallogr D Biol Crystallogr, 1998. **54**(Pt 1): p. 8-15.
121. Dunlop, K.V. and B. Hazes, *When less is more: a more efficient vapour-diffusion protocol.* Acta Crystallogr D Biol Crystallogr, 2003. **59**(Pt 10): p. 1797-800.
122. Bard, J., et al., *Automated systems for protein crystallization.* Methods, 2004. **34**(3): p. 329-47.
123. D'Arcy, A., A.M. Sweeney, and A. Haber, *Practical aspects of using the microbatch method in screening conditions for protein crystallization.* Methods, 2004. **34**(3): p. 323-8.
124. Chayen, N.E., *Methods for separating nucleation and growth in protein crystallisation.* Prog Biophys Mol Biol, 2005. **88**(3): p. 329-37.
125. Garman, E.F. and R.L. Owen, *Cryocooling and radiation damage in macromolecular crystallography.* Acta Crystallogr D Biol Crystallogr, 2006. **62**(Pt 1): p. 32-47.
126. Ravelli, R.B. and E.F. Garman, *Radiation damage in macromolecular cryocrystallography.* Curr Opin Struct Biol, 2006. **16**(5): p. 624-9.
127. Rubinson, K.A., et al., *Cryosalts: suppression of ice formation in macromolecular crystallography.* Acta Crystallogr D Biol Crystallogr, 2000. **56**(Pt 8): p. 996-1001.
128. Garman, E.F. and S.M. McSweeney, *Progress in research into radiation damage in cryo-cooled macromolecular crystals.* J Synchrotron Radiat, 2007. **14**(Pt 1): p. 1-3.
129. Hendrickson, W.A., *Determination of macromolecular structures from anomalous diffraction of synchrotron radiation.* Science, 1991. **254**(5028): p. 51-8.
130. Luft, J.R., et al., *A deliberate approach to screening for initial crystallization conditions of biological macromolecules.* J Struct Biol, 2003. **142**(1): p. 170-9.
131. Griffith, J., et al., *The structural basis for autoinhibition of FLT3 by the juxtamembrane domain.* Mol Cell, 2004. **13**(2): p. 169-78.
132. Knowles, P.P., et al., *Structure and chemical inhibition of the RET tyrosine kinase domain.* J Biol Chem, 2006. **281**(44): p. 33577-87.

133. Tansey, M.G., et al., *GFRalpha-mediated localization of RET to lipid rafts is required for effective downstream signaling, differentiation, and neuronal survival.* Neuron, 2000. **25**(3): p. 611-23.
134. Mendel, D.B., et al., *Development of SU5416, a selective small molecule inhibitor of VEGF receptor tyrosine kinase activity, as an anti-angiogenesis agent.* Anticancer Drug Des, 2000. **15**(1): p. 29-41.
135. Krystal, G.W., et al., *Indolinone tyrosine kinase inhibitors block Kit activation and growth of small cell lung cancer cells.* Cancer Res, 2001. **61**(9): p. 3660-8.
136. Yee, K.W., et al., *SU5416 and SU5614 inhibit kinase activity of wild-type and mutant FLT3 receptor tyrosine kinase.* Blood, 2002. **100**(8): p. 2941-9.
137. Shaheen, R.M., et al., *Antiangiogenic therapy targeting the tyrosine kinase receptor for vascular endothelial growth factor receptor inhibits the growth of colon cancer liver metastasis and induces tumor and endothelial cell apoptosis.* Cancer Res, 1999. **59**(21): p. 5412-6.
138. Fiedler, W., et al., *A phase 2 clinical study of SU5416 in patients with refractory acute myeloid leukemia.* Blood, 2003. **102**(8): p. 2763-7.
139. Coluccia, A.M., et al., *Bcl-XL down-regulation suppresses the tumorigenic potential of NPM/ALK in vitro and in vivo.* Blood, 2004. **103**(7): p. 2787-94.
140. Piazza, R.G., et al., *Evidence for D276G and L364I Bcr-Abl mutations in Ph+ leukaemic cells obtained from patients resistant to Imatinib.* Leukemia, 2005. **19**(1): p. 132-4.
141. Gambacorti-Passerini, C., et al., *Inhibition of the ABL kinase activity blocks the proliferation of BCR/ABL+ leukemic cells and induces apoptosis.* Blood Cells Mol Dis, 1997. **23**(3): p. 380-94.
142. Bain, J., et al., *The specificities of protein kinase inhibitors: an update.* Biochem J, 2003. **371**(Pt 1): p. 199-204.
143. Davies, S.P., et al., *Specificity and mechanism of action of some commonly used protein kinase inhibitors.* Biochem J, 2000. **351**(Pt 1): p. 95-105.
144. *SYBYL 7.0.* Tripos Inc., St. Louis, Missouri, USA.
145. Wallace, A., R. Laskowski, and J. Thornton, *LIGPLOT: a program to generate schematic diagrams of protein-ligand interactions.* Prot. Eng., 1995. **8**: p. 127-134.
146. Sun, L., et al., *Synthesis and biological evaluations of 3-substituted indolin-2-ones: a novel class of tyrosine kinase inhibitors that exhibit selectivity toward particular receptor tyrosine kinases.* J Med Chem, 1998. **41**(14): p. 2588-603.
147. Sun, L., et al., *Identification of substituted 3-[(4,5,6, 7-tetrahydro-1H-indol-2-yl)methylene]-1,3-dihydroindol-2-ones as growth factor receptor inhibitors for VEGF-R2 (Flk-1/KDR), FGF-R1, and PDGF-Rbeta tyrosine kinases.* J Med Chem, 2000. **43**(14): p. 2655-63.
148. Bartkova, J., et al., *Aberrations of the Chk2 tumour suppressor in advanced urinary bladder cancer.* Oncogene, 2004. **23**(52): p. 8545-51.
149. Kanda, A., et al., *Aurora-B/AIM-1 kinase activity is involved in Ras-mediated cell transformation.* Oncogene, 2005. **24**(49): p. 7266-72.
150. O'Neill, E.E., D. Matallanas, and W. Kolch, *Mammalian sterile 20-like kinases in tumor suppression: an emerging pathway.* Cancer Res, 2005. **65**(13): p. 5485-7.
151. Smolich, B.D., et al., *The antiangiogenic protein kinase inhibitors SU5416 and SU6668 inhibit the SCF receptor (c-kit) in a human myeloid leukemia cell line and in acute myeloid leukemia blasts.* Blood, 2001. **97**(5): p. 1413-21.

152. Borrello, M.G., et al., *The oncogenic versions of the Ret and Trk tyrosine kinases bind Shc and Grb2 adaptor proteins.* Oncogene, 1994. **9**(6): p. 1661-8.
153. Liu, J. and A. Lin, *Role of JNK activation in apoptosis: a double-edged sword.* Cell Res, 2005. **15**(1): p. 36-42.
154. Shklyaev, S.S., et al., *Transient activation of c-Jun NH2-terminal kinase by growth factors influences survival but not apoptosis of human thyrocytes.* Thyroid, 2001. **11**(7): p. 629-36.
155. Shklyaev, S.S., et al., *Involvement of wild-type p53 in radiation-induced c-Jun N-terminal kinase activation in human thyroid cells.* Anticancer Res, 2001. **21**(4A): p. 2569-75.
156. Murakami, H., et al., *Role of Dok1 in cell signaling mediated by RET tyrosine kinase.* J Biol Chem, 2002. **277**(36): p. 32781-90.
157. Powell Jr, D.J., et al., *Altered gene expression in immunogenic poorly differentiated thyroid carcinomas from RET/PTC3p53-/- mice.* Oncogene, 2001. **20**(25): p. 3235-46.
158. Vitagliano, D., et al., *Regulation of p27Kip1 protein levels contributes to mitogenic effects of the RET/PTC kinase in thyroid carcinoma cells.* Cancer Res., 2004. **64**(11): p. 3823-9.
159. Gartel, A.L. and S.K. Radhakrishnan, *Lost in transcription: p21 repression, mechanisms, and consequences.* Cancer Res., 2005. **65**(10): p. 3980-5.
160. Noseda, M., et al., *Notch activation induces endothelial cell cycle arrest and participates in contact inhibition: role of p21Cip1 repression.* Mol Cell Biol., 2004. **24**(20): p. 8813-22.
161. Bohmer, F.D., et al., *A single amino acid exchange inverts susceptibility of related receptor tyrosine kinases for the ATP site inhibitor STI-571.* J Biol Chem, 2003. **278**(7): p. 5148-55.
162. Kawamoto, Y., et al., *Identification of RET autophosphorylation sites by mass spectrometry.* J Biol Chem, 2004. **279**(14): p. 14213-24. Epub 2004 Jan 06.
163. Harborth, J., et al., *Sequence, chemical, and structural variation of small interfering RNAs and short hairpin RNAs and the effect on mammalian gene silencing.* Antisense Nucleic Acid Drug Dev, 2003. **13**(2): p. 83-105.
164. Yuan, B., et al., *siRNA Selection Server: an automated siRNA oligonucleotide prediction server.* Nucleic Acids Res, 2004. **32**(Web Server issue): p. W130-4.
165. Chalk, A.M., C. Wahlestedt, and E.L. Sonnhammer, *Improved and automated prediction of effective siRNA.* Biochem Biophys Res Commun, 2004. **319**(1): p. 264-74.
166. Khvorova, A., A. Reynolds, and S.D. Jayasena, *Functional siRNAs and miRNAs exhibit strand bias.* Cell, 2003. **115**(2): p. 209-16.
167. Patzel, V., et al., *Design of siRNAs producing unstructured guide-RNAs results in improved RNA interference efficiency.* Nat Biotechnol, 2005. **23**(11): p. 1440-4.
168. Pei, Y. and T. Tuschl, *On the art of identifying effective and specific siRNAs.* Nat Methods, 2006. **3**(9): p. 670-6.
169. Jackson, A.L., et al., *Expression profiling reveals off-target gene regulation by RNAi.* Nat Biotechnol, 2003. **21**(6): p. 635-7.
170. Jackson, A.L., et al., *Widespread siRNA "off-target" transcript silencing mediated by seed region sequence complementarity.* Rna, 2006. **12**(7): p. 1179-87.
171. Zeng, Y., X. Cai, and B.R. Cullen, *Use of RNA polymerase II to transcribe artificial microRNAs.* Methods Enzymol, 2005. **392**: p. 371-80.

172. van de Wetering, M., et al., *Specific inhibition of gene expression using a stably integrated, inducible small-interfering-RNA vector.* EMBO Rep, 2003. **4**(6): p. 609-15.
173. Hoeflich, K.P., et al., *Oncogenic BRAF is required for tumor growth and maintenance in melanoma models.* Cancer Res, 2006. **66**(2): p. 999-1006.
174. Matsukura, S., P.A. Jones, and D. Takai, *Establishment of conditional vectors for hairpin siRNA knockdowns.* Nucleic Acids Res, 2003. **31**(15): p. e77.
175. Wiznerowicz, M., J. Szulc, and D. Trono, *Tuning silence: conditional systems for RNA interference.* Nat Methods, 2006. **3**(9): p. 682-8.
176. Hingorani, S.R., et al., *Suppression of BRAF(V599E) in human melanoma abrogates transformation.* Cancer Res, 2003. **63**(17): p. 5198-202.
177. Mattiussi, S., et al., *p21(Waf1/Cip1/Sdi1) mediates shear stress-dependent antiapoptotic function.* Cardiovasc Res, 2004. **61**(4): p. 693-704.
178. Fagin, J.A., et al., *High prevalence of mutations of the p53 gene in poorly differentiated human thyroid carcinomas.* J Clin Invest, 1993. **91**(1): p. 179-84.
179. Karasarides, M., et al., *B-RAF is a therapeutic target in melanoma.* Oncogene, 2004. **23**(37): p. 6292-8.
180. Pushkarev, V.M., et al., *Molecular mechanisms of the effects of low concentrations of taxol in anaplastic thyroid cancer cells.* Endocrinology, 2004. **145**(7): p. 3143-52.
181. Demidem, A., et al., *Cystemustine induces redifferentiation of primary tumors and confers protection against secondary tumor growth in a melanoma murine model.* Cancer Res, 2001. **61**(5): p. 2294-300.
182. Catalano, M.G., et al., *Valproic acid induces apoptosis and cell cycle arrest in poorly differentiated thyroid cancer cells.* J Clin Endocrinol Metab, 2005. **90**(3): p. 1383-9.
183. Fortunati, N., et al., *Valproic acid induces the expression of the Na+/I-symporter and iodine uptake in poorly differentiated thyroid cancer cells.* J Clin Endocrinol Metab, 2004. **89**(2): p. 1006-9.
184. Dohan, O., et al., *The sodium/iodide Symporter (NIS): characterization, regulation, and medical significance.* Endocr Rev, 2003. **24**(1): p. 48-77.
185. Dadachova, E. and N. Carrasco, *The Na/I symporter (NIS): imaging and therapeutic applications.* Semin Nucl Med, 2004. **34**(1): p. 23-31.
186. Woodrum, D.T. and P.G. Gauger, *Role of 131I in the treatment of well differentiated thyroid cancer.* J Surg Oncol, 2005. **89**(3): p. 114-21.
187. Short, S.C., et al., *A phase II study using retinoids as redifferentiation agents to increase iodine uptake in metastatic thyroid cancer.* Clin Oncol (R Coll Radiol), 2004. **16**(8): p. 569-74.
188. Ishizaka, Y., et al., *cDNA cloning and characterization of ret activated in a human papillary thyroid carcinoma cell line.* Biochem Biophys Res Commun, 1990. **168**(2): p. 402-8.
189. Gollob, J.A., et al., *Role of Raf kinase in cancer: therapeutic potential of targeting the Raf/MEK/ERK signal transduction pathway.* Semin Oncol, 2006. **33**(4): p. 392-406.
190. Chiariello, M., et al., *Signalling of the Ret receptor tyrosine kinase through the c-Jun NH2-terminal protein kinases (JNKS): evidence for a divergence of the ERKs and JNKs pathways induced by Ret.* Oncogene, 1998. **16**(19): p. 2435-45.
191. Lecoeur, H., *Nuclear apoptosis detection by flow cytometry: influence of endogenous endonucleases.* Exp Cell Res, 2002. **277**(1): p. 1-14.

192. Schlegel, R.A. and P. Williamson, *Phosphatidylserine, a death knell.* Cell Death Differ, 2001. **8**(6): p. 551-63.
193. Ouyang, B., et al., *Inhibitors of Raf kinase activity block growth of thyroid cancer cells with RET/PTC or BRAF mutations in vitro and in vivo.* Clin Cancer Res, 2006. **12**(6): p. 1785-93.
194. Smalley, K.S., *A pivotal role for ERK in the oncogenic behaviour of malignant melanoma?* Int J Cancer, 2003. **104**(5): p. 527-32.
195. Knauf, J.A., et al., *Oncogenic RAS induces accelerated transition through G2/M and promotes defects in the G2 DNA damage and mitotic spindle checkpoints.* J Biol Chem, 2006. **281**(7): p. 3800-9.
196. Riesco-Eizaguirre, G., et al., *The oncogene BRAF V600E is associated with a high risk of recurrence and less differentiated papillary thyroid carcinoma due to the impairment of Na+/I- targeting to the membrane.* Endocr Relat Cancer, 2006. **13**(1): p. 257-69.
197. Gorospe, M., et al., *p21(Waf1/Cip1) protects against p53-mediated apoptosis of human melanoma cells.* Oncogene, 1997. **14**(8): p. 929-35.
198. Copland, M., et al., *Dasatinib (BMS-354825) targets an earlier progenitor population than imatinib in primary CML but does not eliminate the quiescent fraction.* Blood, 2006. **107**(11): p. 4532-9.

6 INDEX OF FIGURES

7 AKNOWLEDGEMENTS

I wish to thank all which contribute to this work.

I would like to thank Dr Tommaso Dragani and Dr Karen Pulford, my director of study and supervisor respectively, for all the suggestions that they gave me to improve my work. Their scientific contribution was essential for my professional education.

I whish to thank also Dr Carlo Gambacorti-Passerini, my supervisor at the University Milano-Bicocca, for the time that I spent in his lab.

Dr Elena Papinutto, Dr Nicola Pasquato and Prof. Giuseppe Zanotti (University of Padova, Italy) collaborated with me in the rRET crystallization project, by performing the crystallization screening.

Dr Loredana Cleris and Dr Franca Formelli (National Cancer Institute of Milano, Italy) helped me to set up the *in vivo* experiments to characterize the SU5416 compound.

Dr Jenny Bain (University of Dundee, United Kingdom) performed the "inhibitor specific profiling" of SU5416.

Dr Thomas Kuoni and Dr Roberta Rostagno produced the RET model and performed the virtual screenings.

I whish to thank Dr Domenico Delia and Silvia Grassi to give me the opportunity to accomplish my PhD at the National Cancer Institute of Milano.

Thank you also to my family, to Diego and all the people who contribute in different way to reach me this important result. In particular, I would like to thank: Luca, Miriam, Sara, Ros, Carmen, Vera, Rocco, Anna, Lucia, Barbara, Sara, Barbara.